Research Square

Preprints are preliminary reports that have not undergone peer review.
They should not be considered conclusive, used to inform clinical practice,
or referenced by the media as validated information.

Effects of end-slip restraints on two-layer beams with interlayer slip

Beatrice TRAVASONI

beatrice.travasoni@unife.it

University of Ferrara

Fabio MINGHINI

University of Ferrara

Nerio TULLINI

University of Ferrara

Research Article

Keywords:

Posted Date: November 2nd, 2026

DOI: https://doi.org/10.21203/rs.3.rs-10877444/v1

License: This work is licensed under a Creative Commons Attribution 4.0 International License.
Read Full License

Additional Declarations: No competing interests reported.

Effects of end-slip restraints on two-layer beams with interlayer slip

Beatrice TRAVASONI, Fabio MINGHINI, Nerio TULLINI

Engineering Department, University of Ferrara, Via Saragat 1, Ferrara, Italy

corresponding author e-mail: beatrice.travasoni@unife.it

ABSTRACT

Static analysis of two Euler-Bernoulli beams made of linearly elastic material interconnected by elastic shear connections is presented. In particular, the influence of equal end-slip restraints on the static behaviour of two-layer composite beams is investigated. A displacement-based variational formulation is adopted to derive the governing equations. Extended closed-form solutions including axial and transverse displacements, interlayer slip and internal stress resultants for cantilever and simply supported two-layer composite beams subjected to point forces and couples, as well as to uniformly distributed loads, are reported as supplementary material. End-slip restraints behave as stiffeners for the entire beam, reducing the interlayer slip.

Keywords: Euler-Bernoulli beams, Two-layer composite beams, Partial interaction, Interlayer slip, End-slip restraints, Closed-form solutions.

1. INTRODUCTION

Composite structural systems, realised by mechanically or adhesively connecting dissimilar materials, are widely employed in civil engineering as floor diaphragms and wall systems to bridge decks. Their global stiffness and load-carrying capacity depend on the interaction at the interface, typically ensured by mechanical connectors such as headed studs, nails or screws in steel–concrete and timber–concrete members [1–6], or by adhesive layers in timber–timber joints [7,8] and glass laminates [9–11]. The interface deformability governs the degree of composite action, and interlayer slip may become a governing kinematic variable. Design recommendations for specific applications, such as guidelines for externally bonded FRP strengthening systems [12], include simplified provisions to account for adhesive-layer deformability, thereby acknowledging the role of local slip in the global response. For mechanically jointed timber-based composite members, simplified design procedures such as the γ-method [13,14] are also commonly adopted to account for partial interaction through an effective stiffness.

A very stiff interface involves full interaction, so allowing the application of classical elastic theory to the two-layer system considered as a whole, whereas deformable interface leads to partial interaction with non-negligible interlayer slip, which must be explicitly considered in the analysis [15–17]. In practical solutions, localised devices are frequently introduced at the member edges or ends (e.g., anchorage systems, end plates, edge restraints) to limit slip and increase stiffness [18]. Nevertheless, the structural implications of such localised restraints – especially when combined with distributed interface compliance – remain not fully quantified. Experimental evidence is available for several composite systems, including steel–concrete [1–3], timber–steel or timber–concrete [5,6], timber–timber [7,8] and laminated glass composites [9–11]. Notably, tests on steel–concrete composite slabs with end anchorage only indicate that end-slip restraints can significantly affect the load–deflection response, the development of interface slip, and the ultimate load, even when no discrete shear connectors are distributed along the span [19, 20]. These findings imply that models neglecting slip and boundary conditions may yield non-conservative estimates of stiffness

and stress distributions, particularly for partially interacting members with semi-rigid end restraints. Similar sensitivity has been reported for FRP-plated beams, where adhesive deformability and anchorage conditions markedly influence the global response [18,21]. Overall, these observations motivate analytical models capable of representing distributed and localised interaction mechanisms within a single consistent framework.

Closed-form solutions represent a key analytical tool for partially composite beams because they provide exact expressions for deflections, interlayer slip and internal forces without requiring any numerical discretisation. The theoretical basis of partial interaction was first established by Newmark et al. [15, 16] for steel–concrete T-beams under concentrated loading and was later adapted to timber members by McCutcheon [17]. In timber engineering, the γ-method adopted in Annex B of Eurocode 5 is derived from the exact solution to the problem of a simply supported composite beam under a sinusoidally distributed lateral load. This solution is expressed in terms of an effective bending stiffness via the γ-factor [13,14], as corroborated by subsequent studies [22]. Later contributions by Girhammar [23–25] extended the framework to additional loading conditions (including uniformly distributed loads) and second-order effects, while Challamel and Girhammar [26, 27] addressed boundary-layer phenomena and proposed variationally based formulations for the stability of partially composite beam–columns, including axial and shear contributions.

Subsequent studies further broadened the applicability to additional boundary conditions and loading schemes. For simply supported members, closed-form solutions have been progressively established for load cases of direct relevance to both design and experimental characterisation, including uniformly distributed loads [28–31], concentrated load at midspan [28,32], and four-point bending tests [29, 33]. The more general case of a concentrated load applied at an arbitrary position along the beam span was originally addressed by Newmark et al. [15,16]. Further extensions cover additional boundary conditions, such as propped and fixed-end restraints [34]. Approximate strategies were also proposed. Xu and Chen [35] developed a Ritz-based variational approach for multiple support and loading conditions. Peng et al. [36] derived analytical expressions for

multilayer systems, but their approach is restricted to layers with identical properties and is therefore not representative of heterogeneous composite members. Complementary investigations focused on interfacial stress transfer in plated beams: Smith and Teng [21] analysed interfacial stress distributions and highlighted the role of bond-slip behaviour, which has contributed to design-oriented approaches for FRP-strengthened members [12]. In timber engineering, related modelling needs also arise in cross-laminated timber (CLT) panels, where the shear deformability of transverse layers is non-negligible; simplified stiffness evaluations often adopt γ-method-based formulations and show close agreement with shear-deformation-based laminate theories for CLT and CLT–concrete members. In this context, applications to the interpretation of four-point bending tests [37–39] were also reported. Several examples highlight that layered members may require an explicit representation of shear-deformable interlayers with non-negligible thickness, overcoming the assumption of zero-thickness interface common to many applications. In the field of laminated glass, analytical models have been extended to take account of interlayer thickness for simple static schemes, including simply supported beams [40,41].

Most existing formulations idealise the interface as a continuous shear connection and therefore neglect the contribution of concentrated restraints that may act at the member ends. In practice, such boundary devices, typically introduced through anchorage systems or edge restraints to control slip and enhance stiffness, cannot be represented by models based on distributed compliance alone. To overcome this limitation, Gjelsvik [42] proposed the analogue beam method, whereby shear deformation is concentrated within a fictitious compliant layer reproducing the relative slip between the connected components. This approach was later refined by Betti and Gjelsvik [43] and extended to static and free–vibration analysis by Ellakany and Tablia [44], enabling the inclusion of end-slip restraints within a numerical framework. More recently, Sun et al. [18] investigated FRP-plated reinforced concrete beams and reported significant differences in terms of interface slip between configurations relying solely on end anchorage and those employing distributed bonding or combined systems. These evidences indicate that composite beams with concentrated anchorages,

albeit considered as infinitely rigid, may not capture the behaviour of distributed or combined connection systems, and motivates analytical formulations capable of representing both distributed and localised interaction mechanisms within a unified framework. In the limiting case of infinitely rigid end restraints, the axial stress distribution in the plated layer may reduce, for specific configurations, to the analytical solution proposed by He and Liu [45] for unbonded tendons anchored at the ends. This highlights the importance of treating end-restraints by means of rigorous analytical models.

Existing models typically idealise boundary behaviour through two limiting cases: either the beam ends are free to slip or the relative displacement is fully restrained, while intermediate end-restraint stiffness is rarely addressed in closed form. Zhang et al. [46] extended this formulation by introducing end-slip and rotational restraints, and demonstrated their impact on global deflection and interlayer slip. In their model, the end-spring stiffness terms appear with opposite signs, consistently reflecting the relative displacement of the two layers. Nevertheless, the resulting solution is expressed as an approximate series (via Stokes' transformation) and is restricted to simply supported members under basic loading schemes.

Despite these contributions, available formulations either provide approximate series solutions or remain confined to simplified loading and boundary conditions. A further open aspect concerns the accurate representation of end effects, which is particularly relevant for composite systems with imperfect bonding. Elasticity-based analyses [47–50], including the classical treatment by Timoshenko and Goodier [49] and subsequent developments for multilayered configurations [48,50], show that localised stress concentrations decay over a characteristic length governed by the connection stiffness. This length scale controls the spatial extent of boundary-layer phenomena and may significantly influence the response in the vicinity of restraints.

The above considerations motivate the need for an exact analytical formulation capable of consistently combining distributed interaction and localised restraints within a unified variational framework, which is the objective of the present work.

In this paper, a closed-form formulation for two-layer composite beams featuring both distributed shear connection and finite-stiffness end-slip restraints is derived. The governing system of differential equations is obtained variationally, and solved analytically by applying Cramer's rule to its matrix form following the approach outlined by Ayres [51]. Then, exact solutions are derived for cantilever and simply supported schemes under concentrated forces, uniformly distributed loads, and end couples, providing explicit expressions for displacement fields, interlayer slip, and internal stress resultants. The formulation is further extended to include a non-negligible interlayer thickness, provided that geometric and mechanical parameters are consistently defined to account for interlayer deformability. In addition to the general case, the present study also investigates configurations where the connection is concentrated at the beam ends only. A parametric investigation quantifies the influence of end-restraint stiffness on the global response and its interaction with distributed connection stiffness. In addition, a loading configuration that suppresses boundary-layer effects [26] is identified and discussed. The accuracy of the proposed formulation is assessed through comparison with existing analytical models available for special cases. Detailed closed-form expressions are provided as supplementary material to this paper.

2. BASIC ASSUMPTIONS

With reference to the two-layer beam with zero-thickness interface shown in Fig. 26, the axial displacements of the centroids of layers 1 and 2 are denoted by $u_1(x)$ and $u_2(x)$, respectively, whereas $v(x)$ represents the sectional vertical displacement. Each layer is modelled by using the Euler–Bernoulli beam theory, which assumes that cross-sections remain plane and perpendicular to longitudinal layer axis, allowing for ignoring shear deformation. This classical assumption, appropriate for slender members, has been widely adopted to the analysis of composite beams with partial interaction [15, 16, 23–25]. Accordingly, the axial displacement within each layer is expressed as follow:

$$u^{(i)}(x,y) = u_i(x) - (y - y_i)\, v'(x) \qquad \text{for } i = 1, 2 \tag{1}$$

where the prime denotes a derivative with respect to axial coordinate x and y_i is the centroidal coordinate of the i-th layer. The relative slip at the interface is defined as:

$$u_s(x) = u_2(x) - u_1(x) + d_0 v'(x) \tag{2}$$

where $d_0 = d_1 + d_2$ is the distance between the centroids of the two layers and d_i ($i = 1, 2$) that of centroid of the i-th layer to the interface. The cross-section of the two-layer beam is shown in Fig. 27, where $d_{1,\infty}$ and $d_{2,\infty}$ represent the distances from each layer centroid to the centroid of the fully composite section characterized by zero interlayer slip. Denoting with A_i and E_i ($i = 1, 2$) cross-section area and Young's modulus of layer i, respectively, these parameters may be wrtitten as:

$$d_{1,\infty} = d_0 \frac{E_2 A_2}{E_1 A_1 + E_2 A_2}, \qquad d_{2,\infty} = d_0 \frac{E_1 A_1}{E_1 A_1 + E_2 A_2} \tag{3}$$

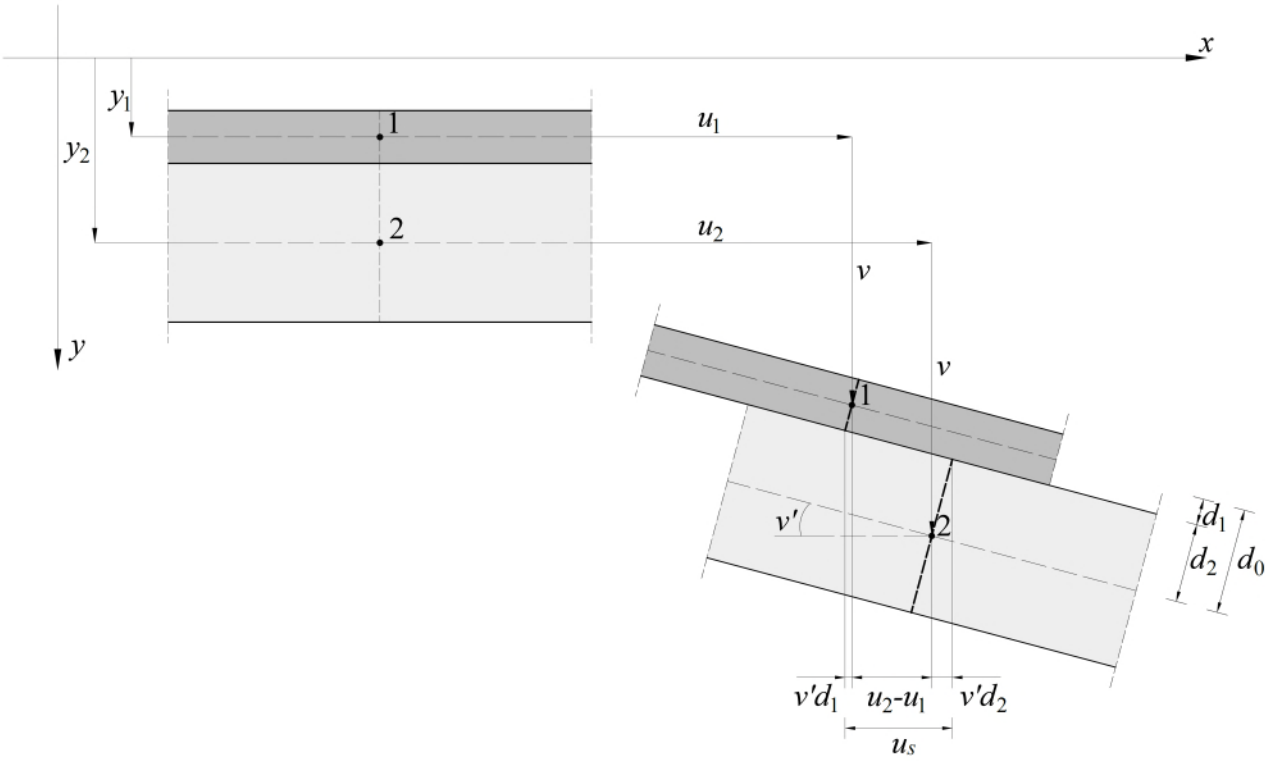


Fig. 1. Kinematic representation of a two-layer composite beam segment with zero-thickness interface.

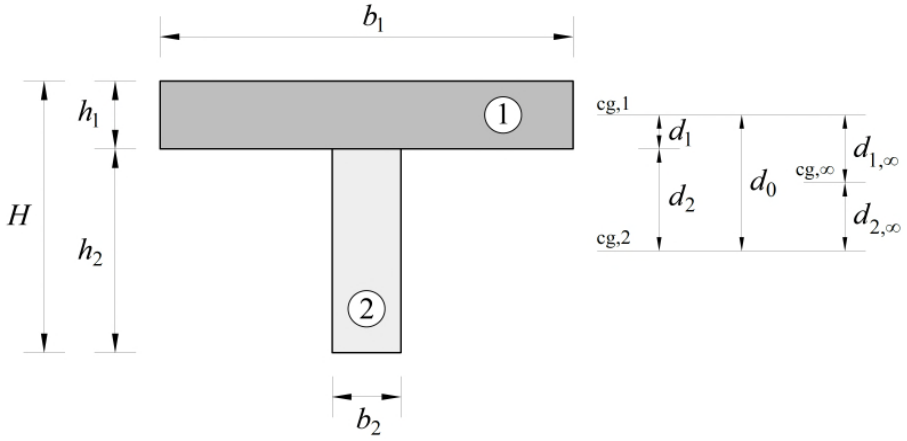


Fig. 2. Geometric parameters of composite beam section: cg,1, cg,2 and cg,∞ are the centroids of layers 1, 2 and of fully composite section, respectively; d1,∞ and d2,∞ are the distances of cg,∞ from cg,1 and cg,2, respectively.

A continuous distribution of linear springs with stiffness k_h (in units of force per unit area) links the two layers at the interface; the corresponding interlayer shear force per unit length is expressed as:

$$q_s(x) = k_h u_s = k_h(u_2 - u_1 + d_0 v') \tag{4}$$

In addition, concentrated translational springs at the beam ends, having stiffness $\hat{k}_h$ (in units of force per unit length), introduce end-slip restraints between the two layers; the corresponding concentrated slip forces is equal to:

$$\hat{Q}_s(\hat{x}) = \hat{k}_h u_s = \hat{k}_h(u_2 - u_1 + d_0 v') \qquad \text{for } \hat{x} = 0, L \tag{5}$$

The arrangement of distributed and end connectors, for both cantilever and simply supported beams, is shown in Fig. 28. Newmark's model [15, 25, 35] covers the whole interval of distributed stiffness spanning between the two limiting cases of non-composite (k_h = 0) and fully composite behaviour (k_h = ∞). The concentrated end springs introduce an extra stiffness parameter governing the local response near the supports and, consequently, the associated end effects.

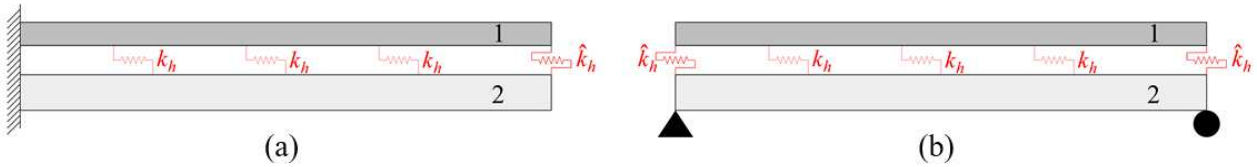


Fig. 3. Shear connection model: distributed springs with stiffness k_h along the interface and end springs with stiffness $\hat{k}_h$. (a) Cantilever beam; (b) Simply supported beam.

Under the assumptions of Euler–Bernoulli beam theory and making use of the Eq. (1), the only non-zero strain component is the axial strain:

$$\varepsilon_x^{(i)} = \frac{\mathrm{d}\,u^{(i)}}{\mathrm{d}\,x} = u_i' - (y - y_i)\,v'' \qquad \text{for } i = 1, 2 \tag{6}$$

Both layers are assumed to be made of linearly elastic, isotropic materials. The axial stress can be expressed as:

$$\sigma_x^{(i)}(x, y) = E_i\ \varepsilon_x^{(i)} = E_i\ \left[u_i' - (y - y_i)\,v''\right] \qquad \text{for } i = 1, 2 \tag{7}$$

The corresponding normal stress resultants in terms of axial force and bending moment in each layer (Fig. 29) can be written as:

$$N_i = \int_{A_i} \sigma_x^{(i)}\,\mathrm{d}\,A_i = E_i A_i\,u_i' - E_i S_i\,v'' \qquad \text{for } i = 1, 2 \tag{8}$$

$$M_i = \int_{A_i} \sigma_x^{(i)}(y - y_i)\,\mathrm{d}\,A_i = E_i S_i\,u_i' - E_i J_i\,v'' \qquad \text{for } i = 1, 2 \tag{9}$$

where E_iA_i indicates the axial rigidity of the i-th layer of the cross-section, whereas first- and second-order moments of the i-th cross-section layer are given by:

$$S_i = \int_{A_i} (y - y_i)\,\mathrm{d}\,A_i, \quad J_i = \int_{A_i} (y - y_i)^2\,\mathrm{d}\,A_i \qquad \text{for } i = 1, 2\,, \tag{10}$$

respectively. The shear resultants are derived by imposing the equilibrium for each layers, including the interfacial slip force per unit length q_s:

$$T_i = M_i' + q_s d_i \qquad \text{for } i = 1, 2 \tag{11}$$

that agrees with Eqs. (8) in [23, 24].

The beam is subjected to general external loadings acting along the longitudinal and transverse directions, including distributed axial loads $q_{x,1}(x)$, $q_{x,2}(x)$ and transverse load $q_y(x)$, as well as concentrated axial end forces $F_{x,1}$, $F_{x,2}$, vertical point load F_y and couple C, with sign convention consistent with the stress resultants reported in Fig. 29.

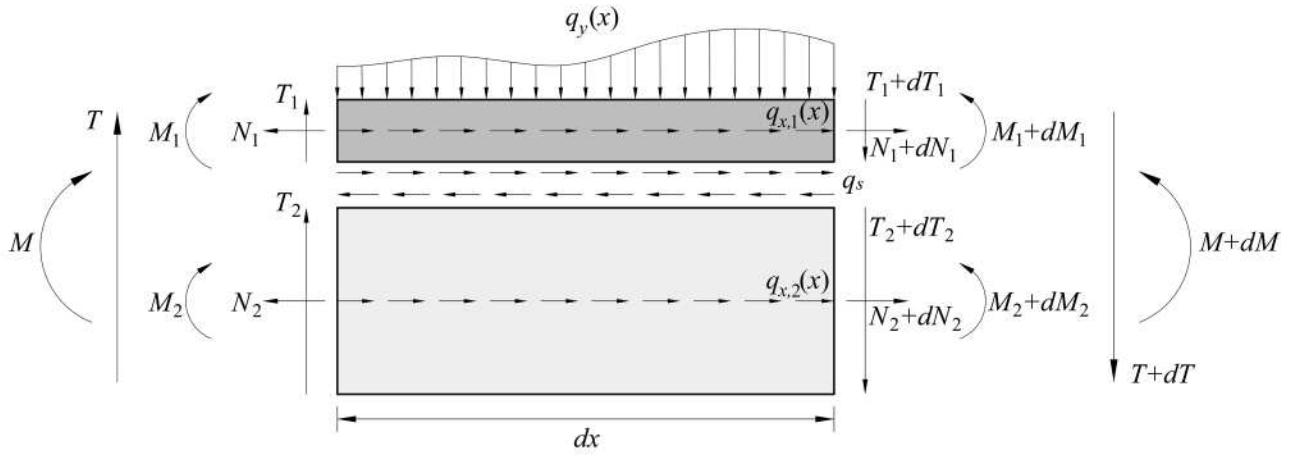


Fig. 4. Free body diagram of an infinitesimal two-layer composite beam segment with compliant interface, illustrating the adopted sign convention.

3. VARIATIONAL FORMULATION

Total potential energy Π of the two-layer beam is comprised of four terms:

$$\Pi = U_1 + U_2 + U_s - V \tag{12}$$

i.e., the elastic deformation energies for the two layers (U_1 and U_2), the strain energy associated with the elastic connections (U_s), and, finally, the work of the external loads (V). Energy term U_s includes, in turn, the contributions due to both distributed shear connections with stiffness k_h and two equal end restraints with stiffness $\hat{k}_h$. By using the strain components (6), the constitutive relations in Eq. (7), and Eqs. (8)–(11), the four energy terms can be written as follows:

$$U_i = \frac{1}{2}\int_{V_i} \sigma_x^{(i)} \varepsilon_x^{(i)} \,\mathrm{d}V_i = \frac{1}{2}\int_0^L [E_i A_i (u_i')^2 + E_i J_i (v'')^2 - 2E_i S_i u_i' v'']\,\mathrm{d}x \qquad \text{for } i = 1, 2 \tag{13}$$

$$U_s = \frac{1}{2}\int_0^L k_h u_s^2 \,\mathrm{d}x + \frac{1}{2}\sum_{\hat{x}=0,L} \hat{k}_h u_s^2 \tag{14}$$

$$V = \int_0^L (q_{x,1}\, u_1 + q_{x,2}\, u_2 + q_y v)\,\mathrm{d}x + [F_y v - C v' + F_{x,1}\, u_1 + F_{x,2}\, u_2]_0^L \tag{15}$$

For prismatic two-layer beams, the stationarity of potential energy Π yields the following system of coupled linear differential equations:

$$E_1 A_1 u_1'' - E_1 S_1 v_1''' + k_h u_s + q_{x,1} = 0 \tag{16a}$$

$$E_2 A_2 u_2'' - E_2 S_2 v_2''' - k_h u_s + q_{x,2} = 0 \tag{16b}$$

$$EJ_0\, v'''' - E_1S_1\, u_1''' - E_2S_2\, u_2''' - k_h\, d_0\, u_s' - q_y = 0 \tag{16c}$$

and the corresponding natural and essential boundary conditions for $\hat{x} = 0, L$:

$$u_1(\hat{x}) = \hat{u}_1 \quad \text{or} \quad E_1A_1\, u_1' - E_1S_1\, v'' + (-1)^{\hat{x}/L}\, \hat{k}_h\, u_s - F_{x,1}\Big|_{\hat{x}} = 0 \tag{17a,b}$$

$$u_2(\hat{x}) = \hat{u}_2 \quad \text{or} \quad E_2A_2\, u_2' - E_2S_2\, v'' - (-1)^{\hat{x}/L}\, \hat{k}_h\, u_s - F_{x,2}\Big|_{\hat{x}} = 0 \tag{17c,d}$$

$$v(\hat{x}) = \hat{v} \quad \text{or} \quad EJ_0\, v''' - E_1S_1\, u_1'' - E_2S_2\, u_2'' - k_h\, d_0\, u_s + F_y\Big|_{\hat{x}} = 0 \tag{17e,f}$$

$$v'(\hat{x}) = \hat{v}' \quad \text{or} \quad EJ_0\, v'' - E_1S_1\, u_1' - E_2S_2\, u_2' - (-1)^{\hat{x}/L}\, \hat{k}_h\, d_0\, u_s + C\Big|_{\hat{x}} = 0 \tag{17g,h}$$

where the hat placed over u_1, u_2, v and v' indicates prescribed displacements or rotation at $\hat{x}$.

First-order moment S_i reported in Eq. (10a) vanishes when computed with reference to a vertical co-ordinate having the origin coinciding with the centroid of the corresponding layer. In this case, field equations (16) become only partially consistent with those reported in [27], where second-order effects are included while disregarding distributed axial loads. Essential boundary conditions similar to Eqs. (17b, d) are also proposed in [46], where, however, that in Eq. (17h) is not included.

3.1. Derivation of governing equations

Two limiting flexural rigidities for the two-layer beam are usually introduced [23, 24]:

$$EJ_0 = E_1J_1 + E_2J_2 \tag{18}$$

$$EJ_\infty = EJ_0 + \frac{d_0^2}{\dfrac{1}{E_1A_1} + \dfrac{1}{E_2A_2}} \tag{19}$$

where subscripts 0 and ∞ refer to the properties of the non-composite and fully composite beam, respectively. Moreover, the following parameters, defined in terms of slip stiffnesses k_h and $\hat{k}_h$, characterise degree of composite action for distributed connections, that for concentrated end connections, and ratio of the latter to the former, respectively:

$$\alpha^2 = k_h \left(\frac{1}{E_1A_1} + \frac{1}{E_2A_2} + \frac{d_0^2}{EJ_0} \right) \tag{20a}$$

$$\hat{\alpha} = \hat{k}_h \left(\frac{1}{E_1 A_1} + \frac{1}{E_2 A_2} + \frac{d_0^2}{E J_0} \right) \tag{20b}$$

$$\hat{\kappa} = \frac{\hat{k}_h}{k_h L} = \frac{\hat{\alpha} L}{(\alpha L)^2} \tag{20c}$$

Low values of dimensionless parameter αL correspond to two-layer beams approaching non-composite behaviour, whereas higher values indicate a response close to full composite action. Dimensionless parameter $\hat{\alpha} L$ describes the degree of interaction when the connection is provided by end-slip restraints only. Finally, parameter $\hat{\kappa}$ denotes the relative influence of concentrated end restraints compared to distributed shear connection. An equivalence between a beam with distributed bonding and an alternative configuration featuring fastenings only at the ends can be established from Eq. (20c) according to $\alpha^2 / k_h = \hat{\alpha} / \hat{k}_h$.

As suggested in [51] and reported in Appendix A, Cramer's rule can be applied to the system of Eqs. (16), giving rise to the following three uncoupled field equations:

$$\frac{\mathrm{d}^3}{\mathrm{d}x^3}\left[\frac{\mathrm{d}^2}{\mathrm{d}x^2} - \alpha^2\right] u_1 = -\frac{\alpha^2 d_{1,\infty}}{E J_\infty}[q_y - (q'_{x,1} d_{1,\infty} - q'_{x,2}\, d_{2,\infty})] + \alpha^2 \frac{(q'_{x,1} + q'_{x,2})}{E_1 A_1 + E_2 A_2} - \frac{q'''_{x,1}}{E_1 A_1} \tag{21a}$$

$$\frac{\mathrm{d}^3}{\mathrm{d}x^3}\left[\frac{\mathrm{d}^2}{\mathrm{d}x^2} - \alpha^2\right] u_2 = \frac{\alpha^2 d_{2,\infty}}{E J_\infty}[q_y - (q'_{x,1} d_{1,\infty} - q'_{x,2}\, d_{2,\infty})] + \alpha^2 \frac{(q'_{x,1} + q'_{x,2})}{E_1 A_1 + E_2 A_2} - \frac{q'''_{x,2}}{E_2 A_2} \tag{21b}$$

$$\frac{\mathrm{d}^4}{\mathrm{d}x^4}\left[\frac{\mathrm{d}^2}{\mathrm{d}x^2} - \alpha^2\right] v = -\frac{\alpha^2}{E J_\infty}[q_y - (q'_{x,1} d_{1,\infty} - q'_{x,2}\, d_{2,\infty})] + \frac{q''_y}{E J_0} \tag{21c}$$

For non-composite beams ($\alpha L = 0$), Eqs. (21a–c) reduce to Eqs. (16a–c) by setting $k_h = 0$ and $S_1 = S_2 = 0$. For fully composite beams ($\alpha L = \infty$), Eqs (21c) reduce to the following classical Euler-Bernoulli beam equation:

$$\frac{\mathrm{d}^4 v}{\mathrm{d}x^4} = \frac{1}{E J_\infty}[q_y - (q'_{x,1} d_{1,\infty} - q'_{x,2}\, d_{2,\infty})] \tag{22}$$

where the beam turns out to be subjected to a distributed vertical load q_y and an equivalent distributed bending couple ($q_{x,1}\, d_{1,\infty} - q_{x,2}\, d_{2,\infty}$).

The present formulation can be extended to composite beams with a non-negligible interlayer thickness (Fig. 30), as in systems characterized by a compliant interlayer (e.g. laminated glass–glass elements or CLT). In this case, the geometric and mechanical parameters of the two-layer beam are redefined to account for the interlayer thickness explicitly. In particular, distance between the centroids of the two layers and interlayer shear stiffness are expressed as:

$$d_0 = d_1 + d_2 + h_a \tag{23a}$$

$$k_h = \frac{G_a b_a}{h_a}, \tag{23b}$$

respectively, where quantity h_a denotes the interlayer thickness, G_a its shear modulus, and b_a the effective interlayer width. The proposed definitions are consistent with analytical models previously developed for laminated systems with compliant interlayers [40, 41]. In particular, non-dimensional interaction parameter λ introduced in [40] reduces to parameter α adopted herein provided that quantities d_0 and k_h are defined as in Eqs. (23).

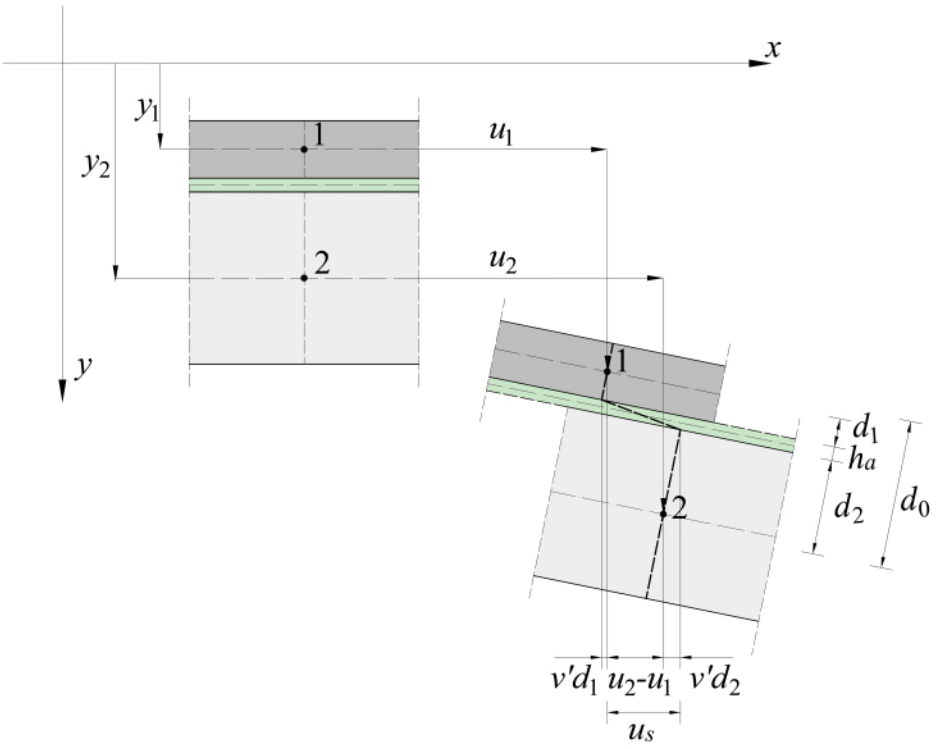


Fig. 5. Kinematic representation of a two-layer composite beam segment with an interlayer of thickness h_a.

3.2. General solution for two-layer beams

The general solutions to system of Eqs. (21a–c) are:

$$u_1(x) = c_1 + c_2 x + c_3 x^2 + c_4 \cosh(\alpha x) + c_5 \sinh(\alpha x) + u_{px,1}(x) + u_{py,1}(x) \tag{24a}$$

$$u_2(x) = -\frac{E_1 A_1}{E_2 A_2}[c_1 + c_2 x + c_3 x^2 + c_4 \cosh(\alpha x) + c_5 \sinh(\alpha x)] + c_6 + c_7 x + u_{px,2}(x) + u_{py,2}(x) \tag{24b}$$

$$v(x) = c_8 + c_9 x + c_{10} x^2 + c_{11} x^3 + c_{12} \cosh(\alpha x) + c_{13} \sinh(\alpha x) + v_{px}(x) + v_{py}(x) \tag{24c}$$

which include eight primary integration constants c_1 to c_8 to be determined by imposing boundary conditions (17). The remaining (secondary) constants are obtained by substituting the general solutions (Eqs. 24a–c) into the field equations (Eqs. 21a–c). Moreover, functions $u_{px,1}(x)$, $u_{px,2}(x)$ and $v_{px}(x)$ represent the particular solutions associated with distributed axial loads, whereas $u_{py,1}(x)$, $u_{py,2}(x)$ and $v_{py}(x)$ are those for distributed transverse load.

The secondary constants may be written as:

$$c_9 = \frac{c_1}{d_{1,\infty}} - \frac{2 E_1 A_1 c_3 + k_h c_6}{k_h d_0} \tag{25a}$$

$$c_{10} = \frac{c_2}{2 d_{1,\infty}} - \frac{c_7}{2 d_0} \tag{25b}$$

$$c_{11} = \frac{c_3}{3 d_{1,\infty}} \tag{25c}$$

$$c_{12} = -\frac{E_1 A_1 d_0}{\alpha E J_0} c_5 \tag{25d}$$

$$c_{13} = -\frac{E_1 A_1 d_0}{\alpha E J_0} c_4 \tag{25e}$$

whereas the particular solutions take the following forms:

$$u_{px,1}(x) = \left[-\frac{d_{1,\infty}}{E J_\infty}(q_{x,1} d_{1,\infty} - q_{x,2} d_{2,\infty}) - \frac{(q_{x,1} + q_{x,2})}{E_1 A_1 + E_2 A_2} \right] \frac{x^2}{2} \tag{26a}$$

$$u_{px,2}(x) = \left[\frac{d_{2,\infty}}{E J_\infty}(q_{x,1} d_{1,\infty} - q_{x,2} d_{2,\infty}) - \frac{(q_{x,1} + q_{x,2})}{E_1 A_1 + E_2 A_2} \right] \frac{x^2}{2} \tag{26b}$$

$$v_{px}(x) = -\frac{x}{\alpha^2 d_0}\left(\frac{q_{x,1}}{E_1 A_1} - \frac{q_{x,2}}{E_2 A_2}\right) - \frac{1}{EJ_\infty}(q_{x,1} d_{1,\infty} - q_{x,2}\, d_{2,\infty})\frac{x^3}{6} \tag{26c}$$

$$u_{py,1}(x) = d_{1,\infty} q_y x\left(\frac{1}{\alpha^2 EJ_0} + \frac{x^2}{6\, EJ_\infty}\right) \tag{26d}$$

$$u_{py,2}(x) = -d_{2,\infty} q_y x\left(\frac{1}{\alpha^2 EJ_0} + \frac{x^2}{6\, EJ_\infty}\right) \tag{26e}$$

$$v_{py}(x) = \frac{q_y L^4}{24\, EJ_\infty}\left(\frac{x}{L}\right)^4 \tag{26f}$$

4. INTRODUCTION TO CASE STUDIES

Extended closed-form solutions for 18 case studies including cantilever and simply supported two-layer composite beams subjected to point forces and couples, as well as to uniformly distributed loads, are reported as supplementary material to this paper.

For each case study, loading scheme and support conditions are summarised in Table 2. Also reported in the same table are the smallest values of parameter αL resulting in a difference smaller than 1% between maximum deflection v_{max} and maximum deflection for fully composite beam, $v_{max,\infty}$ (i.e., $|1 - v_{max} / v_{max,\infty}| < 1\%$). This condition is evaluated for $\hat{\kappa} = 0$ and $\hat{\kappa} = 1$ (see Eq. (20c)), and for the two stiffness ratios $EJ_\infty/EJ_0 = 2.5$ and 4. A value of 2.5 is representative of steel–concrete composite beams [1, 2, 3, 30–32]. Conversely, ratio $EJ_\infty/EJ_0 = 4$ characterises two equal layers, but is adopted here to represent those cases where the fully composite limit provides a significantly higher flexural rigidity than the non-composite limit [6–11], regardless of whether the layers are different or nominally identical to one another (e.g., timber–concrete, timber–timber, and glass–glass systems).

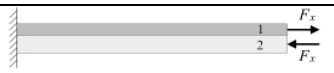
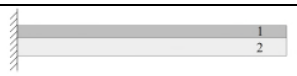
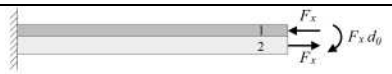
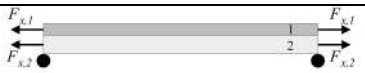
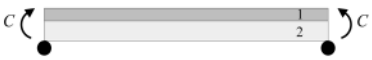
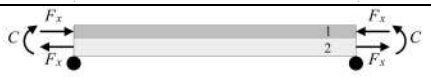
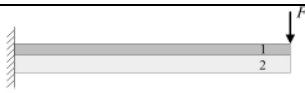
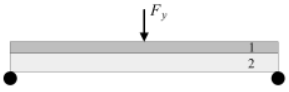
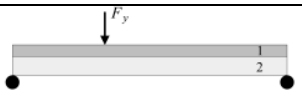
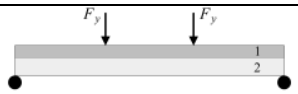
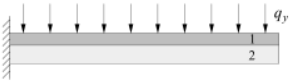
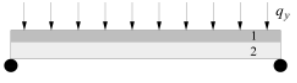
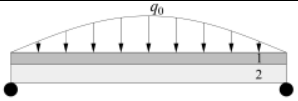
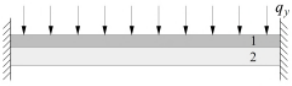
Condition $|1 - v_{max} / v_{max,\infty}| < 1\%$ defines a practical criterion to classify the response as near-fully composite, based on the maximum deflection relative to the fully composite limiting case. For example, a simply supported two-layer beam under uniformly distributed transverse load (case S.15 in Table 2) featuring $EJ_\infty/EJ_0 = 4$ and no end restraint ($\hat{\kappa} = 0$) may be considered as fully composite

for $\alpha L \geq 53.4$. In the presence of end connections such that $\hat{\kappa} = 1$, the same beam attains the fully composite condition on v_{max} for $\alpha L \geq 51.6$. Thus, the inclusion of end slip restraints has only a minor influence on v_{max}. This circumstance also occurs for cantilever and simply supported beams subjected to vertical point loads or uniformly distributed transverse loads (cases S.9–S.12 and S.14, S.16 in Table 2), as well as in the case of distributed axial loading (case S.13). In these cases, the low slip occurring at high αL values restricts the overall impact of end slip restraints. Conversely, end restraints become most effective when the loading configuration induces a significant slip demand at the boundaries (cases S.1–S.8 in Table 2).

The last two case studies presented in Table 2 (S.17 and S.18) differ from all previous configurations, as they correspond to built-in two-layer beam and do not include end-slip restraints. In solution S.17, which involves uniformly distributed transverse loading, very high values of αL are required to satisfy criterion $|1 - v_{max} / v_{max,\infty}| < 1\%$. This outcome follows from the combined effect of distributed loading and boundary conditions, which impose zero displacements and rotation at both ends. As a consequence, the slip between layers is primarily concentrated in the midspan region, and convergence to the fully composite limit is achieved only for large interlayer stiffness values. In contrast, solution S.18 addresses a built-in two-layer beam under a uniformly distributed axial load. In this case, the response is dominated by axial deformation, and vertical displacements tend to vanish as αL increases. According to Table 2, the fully composite condition is practically recovered already for $\alpha L \approx 7.1$ regardless of ratio EJ_∞/EJ_0.

In the following sections, the discussion of the results and figures makes use of dimensionless parameters αL and $\hat{\alpha} L$ (see Eqs. (20a, b)), which provide a unified framework to analyse different connection layouts and to establish an equivalence between a uniformly bonded beam and an end-fastened configuration. In the plots, red circles denote reference situations incorporating end-slip restraints only ($\alpha L = 0$), and are positioned at those αL values that would provide an equivalent degree of interaction for a beam with distributed connection.

Table 1. Case studies S.1–S.18: αL values satisfying condition $|1 - v_{max} / v_{max,\infty}| < 1\%$ for two EJ_∞/EJ_0 ratios and two values of end spring parameter $\hat{\kappa}$.

Solution	Load and boundary condition	Values of αL for $\lvert 1 - v_{max} / v_{max,\infty} \rvert < 1\%$			
		$\hat{\kappa} = 0$		$\hat{\kappa} = 1$	
		$\frac{EJ_\infty}{EJ_0} = 4$	$\frac{EJ_\infty}{EJ_0} = 2.5$	$\frac{EJ_\infty}{EJ_0} = 4$	$\frac{EJ_\infty}{EJ_0} = 2.5$
(S.1)		14.4		5.5	
(S.2)		14.4		5.5	
(S.3)		24.5	17.3	8.1	6.4
(S.4)		(a) 16.0	10.6	6.0	4.5
		(b) 24.4	34.6	8.1	10.3
(S.5)		2.6	1.9	1.4	1.0
(S.6)		28.3		8.9	
(S.7)		49.0	34.6	13.1	10.3
(S.8)		(a) 32.1	21.2	9.7	7.2
		(b) 49.0	69.3	13.1	16.5
(S.9)		29.5	20.7	28.9	20.2
(S.10)		59.0	41.4	57.9	40.3
(S.11)		(c) 54.8	40.2	46.1	38.9
(S.12)		(c) 51.2	36.2	49.1	34.1
(S.13)		16.8		16.3	
(S.14)		33.6	23.5	33.6	23.4
(S.15)		53.4	37.8	51.6	35.8
(S.16)		54.3	38.3	52.7	36.7
(S.17)		118.0	82.8	–	–
(S.18)		(d) 7.10		–	

(a) Loading configuration $(C_L - F_x d_0)/EJ_0 - C_L/EJ_\infty$, (b) Loading configuration $(C_L - F_x d_0)/EJ_\infty - C_L/EJ_0$, (c) Values obtained for L_L = 1/4 L, (d) $|v_{max}| < 0.01$ ($C_\infty L^3/EJ_0$)

For the asymptotic connection configuration with $\alpha L = 0$, $\hat{\alpha} L = \infty$, the axial stress in the lower layer obtained for cases S.2, S.3, S.7, S.9, S.10, S.14 and S.15 coincides with the expression given by Eq. (4) in [45] for unbonded tendons anchored at the ends. This confirms the consistency of the present formulation with established analytical solutions for end-fastened systems. Analytical solutions for configurations with only end-slip restraints, described by parameter $\hat{\alpha} L$, are also included into the supplementary material for all relevant case studies. Exceptions are solutions S.5 and S.8, which follow directly by superposition of previously reported solutions, and solutions S.17 and S.18, for which end springs are not defined due to the built-in static scheme.

5. TWO-LAYER BEAM SUBJECTED TO POINT LOADS

This section examines the closed-form solutions reported in the supplementary material for cases S.1 to S.12 in Table 2, which cover several static configurations of two-layer beams subjected to concentrated loads. The analysed configurations include cantilever and simply supported beams, with point loads applied either vertically or horizontally at different locations along the span.

5.1. Cantilever two-layer beam subjected to end axial forces $F_{x,1}$ and $F_{x,2}$

The first example concerns a cantilever two-layer beam subjected to end axial forces $F_{x,1}$ and $F_{x,2}$, applied at the free end. The corresponding closed-form solution, reported in supplementary material S.1, is evaluated for flexural stiffness ratio $EJ_\infty/EJ_0 = 2.5$ and 4, and for end restraint-to-distributed connection stiffness ratio $\hat{\kappa} = 0$, 10 and 100. For general cross-sectional configurations, dimensionless axial displacement of layer 1 and interlayer slip are plotted in Fig. 31 versus αL. The dimensionless quantities represented on the plot vertical axes of Figs. 31a and 31b are defined as follows:

$$\upsilon_1(L) = \frac{u_1(L) - u_\infty(L)}{\varphi_\infty(L)\, d_{1,\infty}} = 1 + \left(\frac{EJ_\infty}{EJ_0} - 1 \right)^{-1} \frac{\tanh(\alpha L)}{\alpha L\, \hat{c}_1} \tag{27a}$$

$$\upsilon_s(L) = \frac{u_s(L)}{u_{1,0}(L) - u_{2,0}(L)} = \frac{\tanh(\alpha L)}{\alpha L\, \hat{c}_1}, \tag{27b}$$

respectively, where

$$\hat{c}_1 = 1 + \alpha L\, \hat{\kappa}\, \tanh(\alpha L) \tag{28a}$$

$$u_\infty(L) = \frac{(F_{x,1} + F_{x,2})L}{E_1 A_1 + E_2 A_2} \tag{28b}$$

$$\varphi_\infty(L) = \frac{(F_{x,1} d_{1,\infty} - F_{x,2} d_{2,\infty})\, L}{EJ_\infty} \tag{28c}$$

$$u_{i,0}(L) = \frac{F_{x,i}\, L}{E_i A_i} \qquad \text{for } i = 1, 2 \tag{28d}$$

In Eq. (27a) the axial displacement of layer 1 is normalized by the product of quantities related with the fully composite beam, namely end section rotation $\varphi_\infty(L)$ and distance $d_{1,\infty}$ between centroid of layer 1 and overall centroid. Accordingly, a dimensionless value $\upsilon_1(L) = 1$ indicates rigid-body kinematics of layer 1 in the fully composite limiting case ($\alpha L = \infty$), with no relative slip. This interpretation is consistent with Fig. 31b, where the interlayer slip is normalized with respect to the corresponding value in the non-composite configuration. In fact, as αL increases, the slip progressively reduces, and the response converges to the fully composite case. Conversely, for $\alpha L = 0$ the dimensionless slip equals 1, i.e., $u_s(L) = u_{1,0}(L) - u_{2,0}(L)$, indicating independent behaviour of the two layers.

The axial displacement of layer 1 strongly depends on flexural stiffness ratio (Fig. 31a), with $EJ_\infty/EJ_0 = 2.5$ leading to the greatest deformability. This is particularly evident for small αL values. In contrast, the slip response is independent of EJ_∞/EJ_0 (Fig. 31b).

In the presence of end-slip restraints only ($\alpha L = 0$), Eqs. (27a–b) take the following forms:

$$\upsilon_1(L) = \frac{\hat{u}_1(L) - u_\infty(L)}{\varphi_\infty(L)\, d_{1,\infty}} = 1 + \left(\frac{EJ_\infty}{EJ_0} - 1\right)^{-1} \frac{1}{1 + \hat{\alpha} L} \tag{29a}$$

$$\upsilon_s(L) = \frac{\hat{u}_s(L)}{u_{1,0}(L) - u_{2,0}(L)} = \frac{1}{1 + \hat{\alpha} L}. \tag{29b}$$

For comparison, the corresponding results (for $EJ_\infty/EJ_0 = 4$ only) are shown in Fig. 31 as red marks for $\hat{\kappa} = 10$ and 100 at prescribed values of αL. For the only-end fastening case, the imposed free-end stiffness has been calculated according to Eq. (20c) such that $\hat{\alpha} L = \hat{\kappa}(\alpha L)^2$. In other words, by virtue of this equivalence, two-layer cantilevers featuring prescribed global stiffness of distributed connections, but exclusively concentrated at the end, were analyzed. The substantial agreement between these results and those derived from a combination of distributed and concentrated connections indicates that, for the explored values of $\hat{\kappa}$, deformability is essentially governed by the end connection.

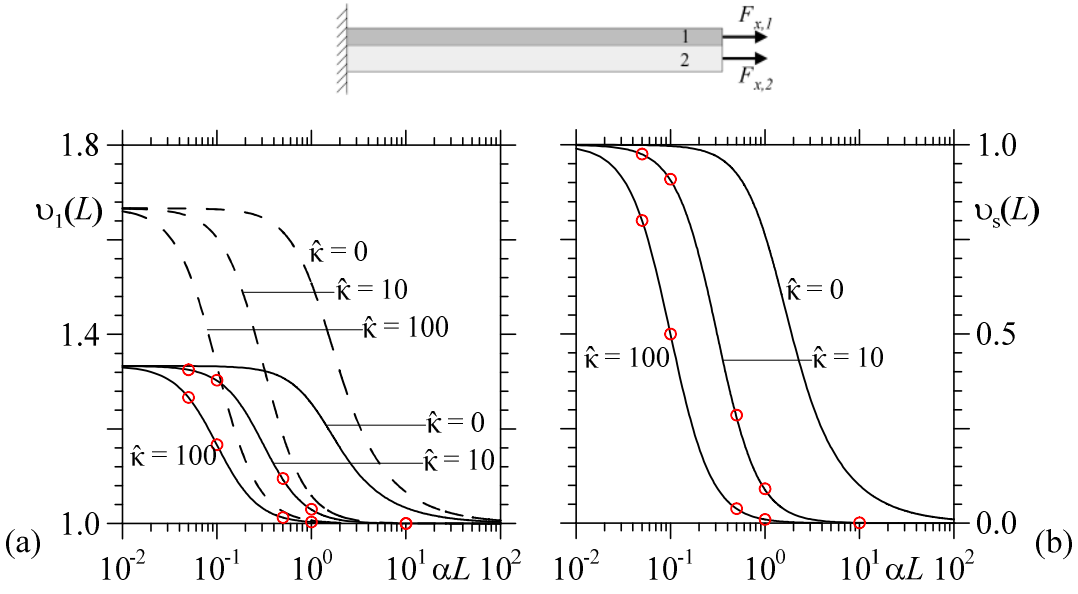


Fig. 6. Cantilever two-layer beam subjected to end axial forces $F_{x,1}$ and $F_{x,2}$: dimensionless (a) axial displacement of layer 1 at $x = L$, and (b) interlayer slip at $x = L$. Dashed and solid curves refer to $EJ_\infty/EJ_0 = 2.5$ and 4, respectively. Red marks denote end-slip restraints only configurations, reported at the equivalent αL according to Eq. (20c).

5.2. Cantilever two-layer beam subjected to a clockwise end couple $F_x\, d_0$

A cantilever two-layer beam subjected to a clockwise end couple $F_x\, d_0$ is analysed in supplementary material S.2. Fig. 32 shows, in dimensionless forms, the axial displacement of layer 1 (Fig. 32a) and vertical displacement at the free end (Fig. 32c) versus αL. Nondimensional axial stress resultant in layer 1 and total bending moment, both evaluated at the fixed end, are shown in Figs. 32b and 32d, respectively. Total bending moment is defined as the sum of bending moments arising in the two layers. The plotted quantities are defined as follows:

$$\frac{u_1(L)}{u_{1,0}(L)} = 1 - \frac{EJ_0}{EJ_\infty}\left(1 - \frac{\tanh(\alpha L)}{\alpha L\,\hat{c}_1}\right) \tag{30a}$$

$$\frac{v(L)}{v_\infty(L)} = 1 - 4\,\frac{\sinh^2(\alpha L/2)}{(\alpha L)^2\hat{c}_1\cosh(\alpha L)} \tag{30b}$$

$$\frac{N_1(0)}{F_x} = 1 - \frac{EJ_0}{EJ_\infty}\left[1 - \frac{1}{\hat{c}_1\cosh(\alpha L)}\right] \tag{30c}$$

$$\frac{M_1(0) + M_2(0)}{(-F_x d_0)} = \frac{EJ_0}{EJ_\infty}\left[1 - \frac{1}{\hat{c}_1\cosh(\alpha L)}\right] \tag{30d}$$

where $\hat{c}_1$ is reported in Eq. (28a), $u_{1,0}(L)$ is obtained from Eq. (28d), whereas $v_\infty(L)$ is given by

$$v_\infty(L) = \frac{F_x d_0 L^2}{2EJ_\infty} \tag{31}$$

Dimensionless axial displacement (Fig. 32a) and stress resultant (Fig. 32b) tend to 1 as αL tends to 0, and decrease as αL increases, indicating a progressive redistribution of axial load between the two layers. Moreover, tip deflection (Fig. 32c) and bending moment at the fixed end (Fig. 32d) vanish at $\alpha L = 0$, since no global bending develops in the absence of interlayer stiffness. As αL increases, composite action is progressively mobilised and the flexural response develops, involving increases in both vertical displacement and bending moment up to their fully composite reference values. For $\hat{\kappa} = 10$ and 100, this limiting situation is essentially recovered for $\alpha L = 3$ and 1, respectively.

For the alternative configuration with $\alpha L = 0$, in which the connection relies solely on end-slip restraints characterised by $\hat{\alpha} L$, Eqs. (30a–d) become:

$$\frac{\hat{u}_1(L)}{u_{1,0}(L)} = \left[1 + \hat{\alpha} L\left(1 - \frac{EJ_0}{EJ_\infty}\right)\right]\frac{1}{1 + \hat{\alpha} L} \tag{32a}$$

$$\frac{\hat{v}(L)}{v_\infty(L)} = \frac{\hat{\alpha} L}{1 + \hat{\alpha} L} \tag{32b}$$

$$\frac{\hat{N}_1(0)}{F_x} = 1 - \frac{EJ_0}{EJ_\infty}\frac{\hat{\alpha} L}{1 + \hat{\alpha} L} \tag{32c}$$

$$\frac{\hat{M}_1(0)+\hat{M}_2(0)}{(-F_x d_0)}=\frac{EJ_0}{EJ_\infty}\frac{\hat{\alpha}L}{1+\hat{\alpha}L} \tag{32d}$$

The corresponding results are reported with red marks in Fig. 32 by making use of the same equivalence in terms of αL as described for the previous case study. Even in this case, the end restraint-only solutions closely follow the response obtained with a combination of distributed and concentrated end connections, confirming that in the presence of non-negligible axial load in each of the layers the end restraints alone can provide an accurate approximation of the global response.

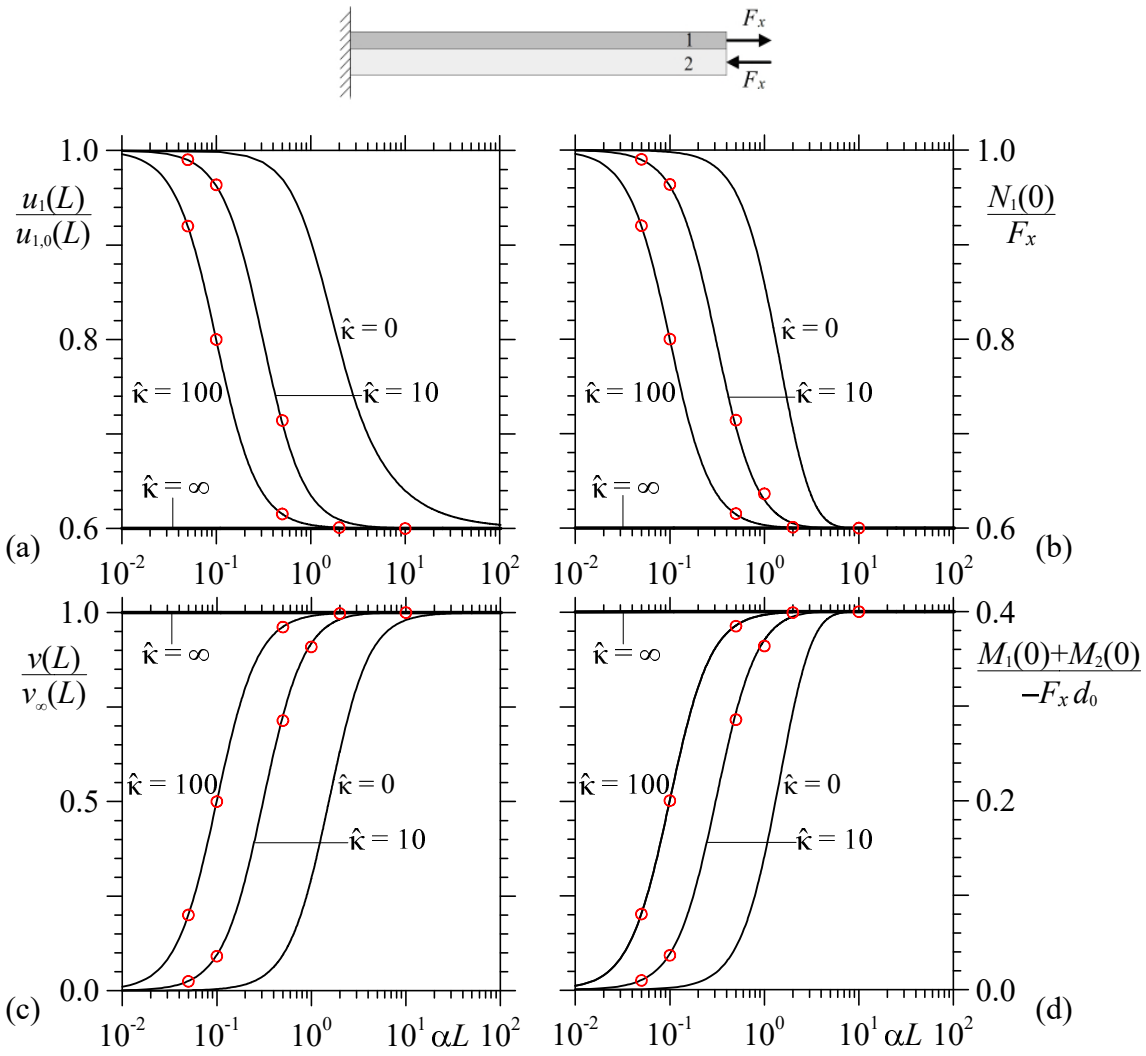


Fig. 7. Cantilever two-layer beam subjected to a clockwise end couple $F_x d_0$: dimensionless (a) axial displacement of layer 1 at $x = L$; (b) axial stress resultant of layer 1 at $x = 0$; (c) vertical displacement at $x = L$, and (d) sum of bending moment of the two layers at $x = 0$. Results refer to $EJ_\infty/EJ_0 = 2.5$. Red marks denote end-slip restraints only configurations.

5.3. Cantilever two-layer beam subjected to a clockwise end couple C_L

A cantilever two-layer beam subjected to a clockwise end couple C_L is analysed in supplementary material S.3. Fig. 33 shows some displacement and stress resultant quantities, reported in nondimensional form versus αL. In particular, the following functions are plotted in the figure:

$$\frac{u_1(L)}{u_{1,\infty}(L)} = 1 - \frac{\tanh(\alpha L)}{\alpha L\, \hat{c}_1} \tag{33a}$$

$$\frac{v(L)}{v_\infty(L)} = 1 + 4\left(\frac{EJ_\infty}{EJ_0} - 1\right)\frac{\sinh^2(\alpha L/2)}{(\alpha L)^2\, \hat{c}_1\, \cosh(\alpha L)} \tag{33b}$$

$$\frac{N_1(0)}{C_L / d_0} = \left(1 - \frac{EJ_0}{EJ_\infty}\right)\left[1 - \frac{1}{\hat{c}_1\, \cosh(\alpha L)}\right] \tag{33c}$$

$$\frac{M_1(0) + M_2(0)}{(-C_L)} = \frac{EJ_0}{EJ_\infty}\left[1 + \left(\frac{EJ_\infty}{EJ_0} - 1\right)\frac{1}{\hat{c}_1 \cosh(\alpha L)}\right] \tag{33d}$$

where $\hat{c}_1$ still coincides with parameter provided by Eq. (28a) and

$$u_{1,\infty}(L) = \varphi_\infty(L)\, d_{1,\infty} = \frac{C_L L}{EJ_\infty} d_{1,\infty} \tag{34a}$$

$$v_\infty(L) = \frac{C_L L^2}{2EJ_\infty} \tag{34b}$$

For $\alpha L = 0$, with interaction provided only by end-slip restraint stiffness, the corresponding dimensionless quantities are given below and plotted in Fig. 33 as red marks positioned at equivalent αL values in analogy to the approach adopted in the previous two case studies:

$$\frac{\hat{u}_1(L)}{u_{1,\infty}(L)} = \frac{\hat{\alpha} L}{1 + \hat{\alpha} L} \tag{35a}$$

$$\frac{\hat{v}(L)}{v_\infty(L)} = 1 + \left(\frac{EJ_\infty}{EJ_0} - 1\right)\frac{1}{1 + \hat{\alpha} L} \tag{35b}$$

$$\frac{\hat{N}_1(0)}{C_L / d_0} = \left(1 - \frac{EJ_0}{EJ_\infty}\right)\frac{\hat{\alpha} L}{1 + \hat{\alpha} L} \tag{35c}$$

$$\frac{\hat{M}_1(0) + \hat{M}_2(0)}{(-C_L)} = \left(1 + \frac{EJ_0}{EJ_\infty}\hat{\alpha} L\right)\frac{1}{1 + \hat{\alpha} L} \tag{35d}$$

At $\alpha L = 0$, the axial displacement of layer 1 is zero (Fig. 33a), since in the absence of interaction the applied couple induces pure flexural rotations in the two layers without mean axial deformation. As αL increases, the interlayer connection progressively reduces the global rotation while increasing the contribution of axial deformation, resulting in a greater axial displacement accompanied by a reduction in vertical displacement. This parameter (Fig. 33c) is maximum in the non-composite configuration and decreases as a growing portion of the applied moment is carried through axial force components within the layers. This behaviour is consistent with the responses in Fig. 33b and 33d: the axial stress resultants in layer 1 increases with αL, whereas the total bending moment decreases, reflecting the progressive redistribution of internal equilibrium of each layer from pure bending to combined axial–bending response.

As in the previous cases, the influence of the end restraints is mainly observed in the intermediate range of αL, wherein the transition to fully composite behaviour is expedited without altering the asymptotic response. The red marks in Fig. 33 highlight the same perfect agreement already noted in Figs. 31 and 32, showing that end-slip restraints yield a response that is nearly indistinguishable from that obtained for a combination of distributed and concentrated end connections.

As an additional validation, consider two identical rectangular layers with width b, height $H/2$, Young's modulus E and $\hat{k}_h = 0$. In this case, $\alpha^2 = 16k_h/(EbH)$, $J_0 = bH^3/48$ and $J_\infty = bH^3/12$. Consequently, $J_\infty/J_0 = 4$ and the vertical displacement reduces to

$$v(x) = v_\infty(L)\left[\left(\frac{x}{L}\right)^2 + 6\,\frac{\cosh(\alpha x) - 1}{(\alpha L)^2\cosh(\alpha L)}\right] \tag{36}$$

in agreement with Eq. (14) proposed in [36].

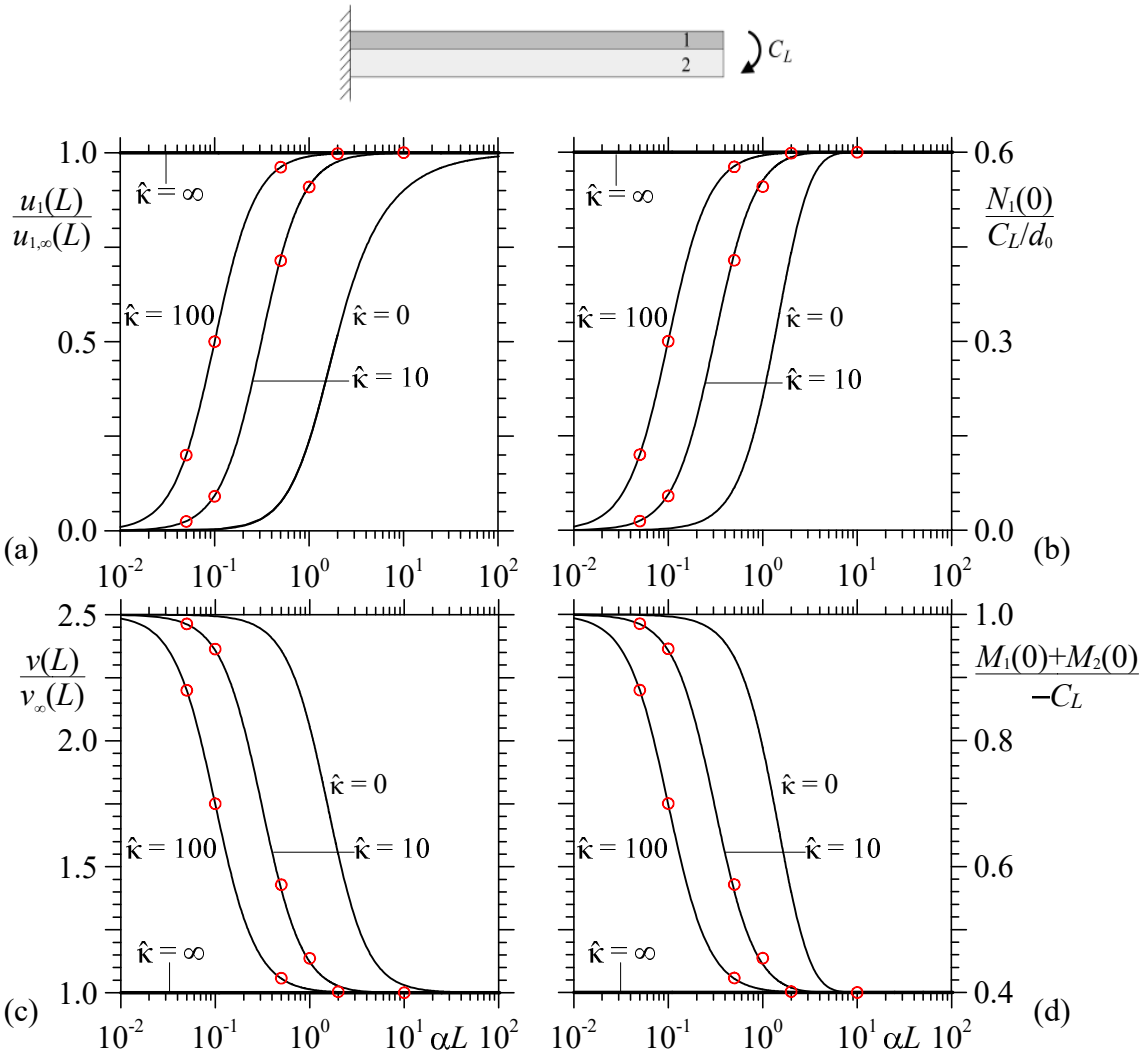


Fig. 8. Cantilever two-layer beam subjected to a clockwise end couple C_L: dimensionless (a) axial displacement of layer 1 at $x = L$; (b) axial stress resultant of layer 1 at $x = 0$; (c) vertical displacement at $x = L$, and (d) sum of bending moment of the two layers $x = 0$. Results refer to $EJ_\infty/EJ_0 = 2.5$. Red marks denote end-slip restraints only configurations.

5.4. Cantilever two-layer beam subjected to a clockwise end couple $C_L + F_x\, d_0$

The closed-form solution for a cantilever two-layer beam subjected to a clockwise end couple $C_L + F_x\, d_0$ is reported in supplementary material S.4. This solution is the sum of the findings reported in S.2 and S.3, but several noteworthy implications can be made. Firstly, no interlayer slip occurs, i.e., $u_s = 0$, if the following condition is fulfilled

$$\frac{F_x d_0 + C_L}{EJ_\infty} - \frac{C_L}{EJ_0} = 0 \tag{37}$$

from which it follows that

$$N_1 = -N_2 = F_x \tag{38a}$$

$$M_i = -\frac{E_i J_i}{E J_\infty}(F_x d_0 + C_L) \qquad \text{for } i = 1, 2 \tag{38b}$$

Thus, the layers behave independently of one another and end couple $F_x\, d_0 + C_L$ is distributed across the section based on the ratio $E_i J_i / E J_\infty$.

Secondly, in the limiting case of full interaction ($\alpha L = \infty$), stress resultants are given by:

$$N_{1,\infty} = -N_{2,\infty} = \left(1 - \frac{E J_0}{E J_\infty}\right)\left(F_x + \frac{C_L}{d_0}\right) \tag{39a}$$

$$M_{i,\infty} = -\frac{E_i J_i}{E J_\infty}(F_x d_0 + C_L) \qquad \text{for } i = 1, 2 \tag{39b}$$

that agree with findings reported in [25, 26] and Eq. (39b) coincides with Eq. (38b).

For $\alpha L = \hat{\alpha} L = 0$, interlayer slip $u_s \neq 0$ and stress resultants reduce to

$$N_1 = -N_2 = F_x \tag{40a}$$

$$M_i = -\frac{E_i J_i}{E J_0} C_L \qquad \text{for } i = 1, 2 \tag{40b}$$

where Eq. (40a) coincides with Eq. (38a), but only end couple C_L is now distributed across the section based on the ratio $E_i J_i / E J_0$.

For high value of αL, boundary-layer effects arise [26], i.e., near the beam ends the stress resultants vary rapidly due to the transition from a layer-wise response to a global behaviour. For a cantilever two-layer beam subjected to clockwise end couples $F_x\, d_0$ and C_L, the dimensionless axial forces and bending moments along are reported versus x/L in Fig. 34 for some values of interaction parameter αL. In particular, Figs. 34a and c illustrate the responses in terms of axial load and bending moment, respectively, for the case of end couple $F_x\, d_0$. Analogous functions are plotted in Figs. 34b, d for end couple C_L. Connection stiffness ratio $\hat{\kappa}$ is assumed to be null (i.e., distributed connection with no end-slip restraint) in Figs. 34a, b, d and unity in Fig. 34c. The dimensionless ratios shown on the vertical axes are defined as:

$$\frac{N_i^{F_x}(x)}{F_x} = 1 - \frac{E J_0}{E J_\infty}\left(1 - \frac{\cosh(\alpha x)}{\hat{c}_1 \cosh(\alpha L)}\right) \tag{41a}$$

$$\frac{M_i^{F_x}(x)}{M_{i,\infty}^{F_x}} = \frac{N_i^{C_L}(x)}{N_{i,\infty}^{C_L}} = 1 - \frac{\cosh(\alpha x)}{\hat{c}_1 \cosh(\alpha L)} \tag{41b}$$

$$\frac{M_i^{C_L}(x)}{M_{i,\infty}^{C_L}} = 1 + \left(\frac{EJ_\infty}{EJ_0} - 1 \right) \frac{\cosh(\alpha x)}{\hat{c}_1 \cosh(\alpha L)} \tag{41c}$$

where $\hat{c}_1$ is the same as reported in Eq. (28a) and

$$M_{i,\infty}^{F_x} = -F_x d_0 \frac{E_i J_i}{EJ_\infty} \tag{42a}$$

$$N_{i,\infty}^{C_L} = \left(1 - \frac{EJ_0}{EJ_\infty} \right) \frac{C_L}{d_0} \tag{42b}$$

$$M_{i,\infty}^{C_L} = -\frac{E_i J_i}{EJ_\infty} C_L \tag{42c}$$

The expressions for axial force and bending moment in the fully composite beam reported in Eqs. (42b) and (42c) for the case of couple C_L are in agreement with Eqs. (4) and (26) proposed in [26], respectively.

As αL increases, the variations in the stress resultants reduce and the curves converge toward the constant values associated with the fully composite limit. Nevertheless, even for large αL, a localized region near the free end still exhibits steep gradients in axial force and bending moment, indicating that the boundary-layer effect does not vanish completely but becomes progressively confined to a shorter region near the free end. This is not only true for two-layer beam with solely distributed connections (as observed in [26]), but also featuring end-slip restraint of same total stiffness (Fig. 34c).

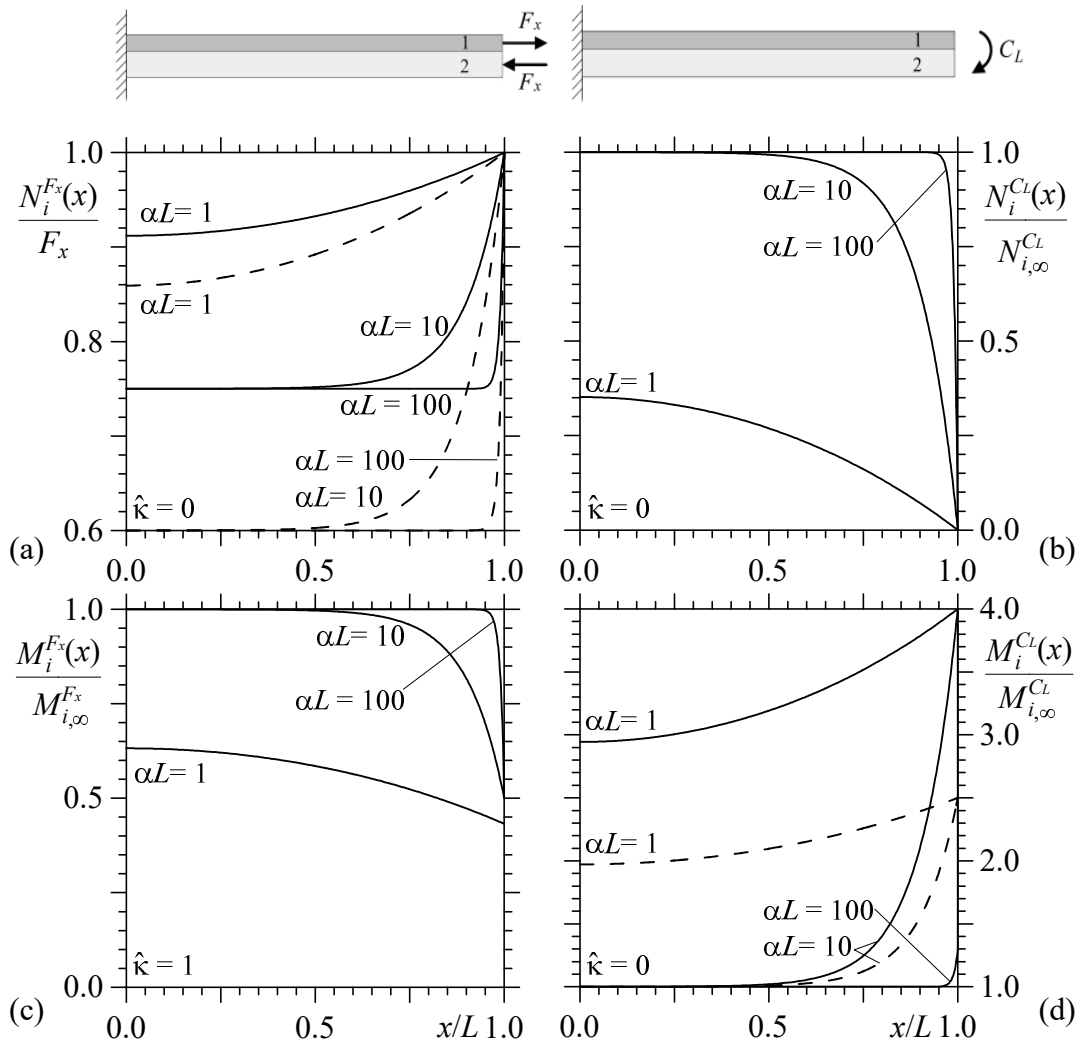


Fig. 9. Cantilever two-layer beam subjected to clockwise end couples (a, c) $F_x\, d_0$ and (b, d) C_L. Effect of parameter αL on the dimensionless (a, b) axial force and (c, d) bending moment along the beam. Dashed and solid curves refer to $EJ_\infty/EJ_0 = 2.5$ and 4, respectively.

5.5. Cantilever two-layer beam subjected to a self-equilibrated end couple $C_L - F_x\, d_0$, with $C_L = F_x\, d_0$

To provide deeper insight into boundary-layer effects, a cantilever two layer beam subjected to a self-equilibrated end couple $C_L - F_x\, d_0$, with $C_L = F_x\, d_0$, is considered, and the corresponding closed-form solution is reported in supplementary material S.5.

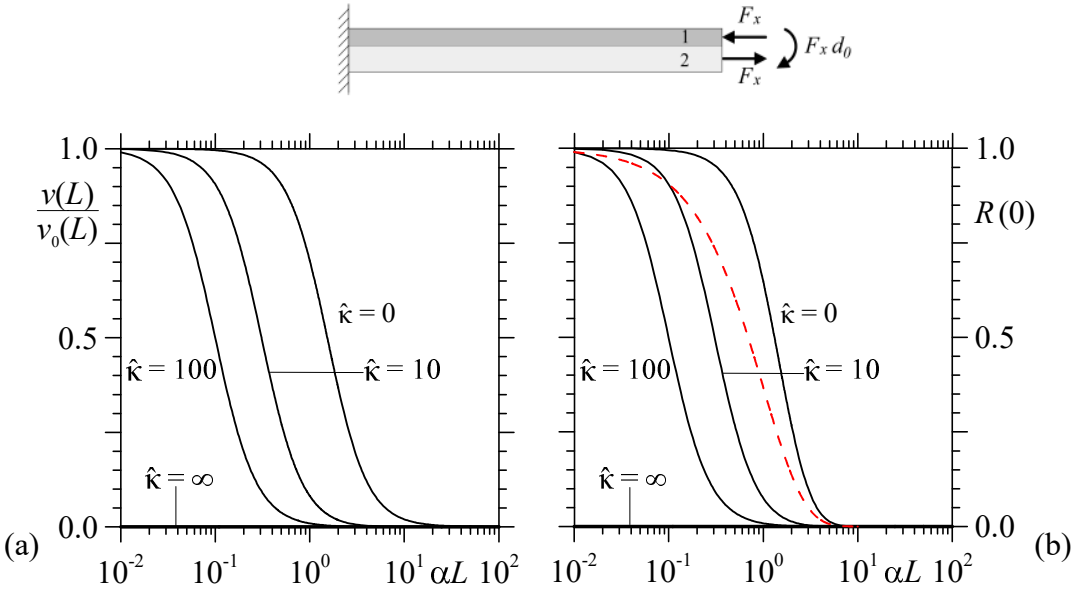


Fig. 10. Cantilever two-layer beam subjected to a self-equilibrated end couple $C_L - F_x\, d_0$, with $C_L = F_x\, d_0$: dimensionless (a) vertical displacement at $x = L$, and (b) stress resultants $R(0)$ in layer 1 at $x = 0$. Red dashed line in (b) corresponds to the asymptotic exponential decay solution proposed in [47, 48].

Fig. 35a shows dimensionless vertical displacement $v(L)$, whereas dimensionless stress resultants at the fixed end are provided in Fig. 35b; both quantities are plotted versus αL. The dimensionless ratios shown on the vertical axes are defined as follows:

$$\frac{v(L)}{v_0(L)} = 4\,\frac{\sinh^2(\alpha L/2)}{(\alpha L)^2\,\hat{c}_1\cosh(\alpha L)} \tag{43a}$$

$$R(0) = \frac{N_1(0)}{(-F_x)} = \frac{M_1(0)}{(-F_x d_0\, E_1 J_1 / E J_0)} = \frac{1}{\hat{c}_1\cosh(\alpha L)} = \frac{2\,\mathrm{e}^{-\alpha L}}{\hat{c}_1(1+\mathrm{e}^{-2\alpha L})} \tag{43b}$$

where $\hat{c}_1$ is reported in Eq. (28a) and

$$v_0(L) = \frac{F_x d_0\, L^2}{2\,E J_0} \tag{44}$$

Dimensionless vertical displacement at the free end (Fig. 35a) is equal to 1 for $\alpha L = 0$ and tends to zero as the $\alpha L \to \infty$, indicating that in the fully composite limiting case the effects of the two applied couples vanish and no vertical deformation develops. In the presence of end-slip restraint such that $\hat{\kappa} = 10$ and 100, the fully composite condition is recovered for $\alpha L = 3$ and 1, respectively.

Parameter $R(0)$ in Fig. 35b provides a synthetic measure of the decay rate of end effects due to a self-equilibrated load distribution. Consistently with Fig. 35a, $R(0) \to 0$ as $\alpha L \to \infty$.

In [47, 48] the axial decay of Saint-Venant end effects was investigated for plane strain deformations of semi-infinite bimaterial strip having imperfect bonding conditions at the interfaces. The decay rate of the end effects due to a self-equilibrated load distribution was studied by seeking a decaying solution in the exponential form $\exp(-2\lambda x_1/H)$, where $x_1 = L - x$ and λ is an eigenvalue given by a transcendental equation. It is worth noting that no clamped section is introduced in the semi-infinite strip and length L is used as a reference distance at which evaluate the stress field. For two equal layers in plane stress state having width b, height $H/2$, Young modulus E, $\hat{k}_h = 0$ and so $\alpha^2 = 16k_h/(EbH)$, the following transcendental equation for eigenvalue λ can be obtained:

$$[\sin(2\lambda) + 2\lambda][\sin(2\lambda) - 2\lambda - \chi\lambda(\sin^2\lambda - \lambda^2)] = 0 \tag{45}$$

where

$$\chi = \frac{Eb}{k_h H} = \frac{16}{(\alpha L)^2}\left(\frac{L}{H}\right)^2 \tag{46}$$

The eigenvalues λ can be real or complex and the stress decay rate is characterized by eigenvalue λ_1 with smallest real part. Small values of λ_1 correspond to large decay lengths for end effects. For perfect bonding ($\chi = 0$ or $\alpha L \to \infty$), Eq. (45) reduces to $\sin 2\lambda \pm 2\lambda = 0$ that is the classical transcendental equation proposed by Fadle-Papkovich [49, 50]. For frictionless contact between the layers ($\chi \to \infty$ or $\alpha L = 0$), Eq. (45) reduces to $\sin\lambda \pm \lambda = 0$, i.e., the Fadle-Papkovich transcendental equation referred to the single layer. Edge delamination has to be prevented in plane stress state, whereas, for plane strain deformations, Young modulus E has to be replaced by $E/(1-\nu^2)$, being ν the Poisson ratio. For the problem at hand, the stress resultants arising by the beam solution coincide with those of a two-dimensional elastic solution by assuming $\nu = 0$.

Making use of transcendental equation (45), which contains parameter χ in the square brackets, function $\exp(-2\lambda_1 L/H)$ is shown in Fig. 35b with a red dashed line, which holds for any given slenderness ratio $L/H \geq 10$. This solution disagrees with the two-layer beam solution for $\hat{\kappa} = 0$ and strongly underestimates the effective decay length of the end effects. For $\alpha L = 1$, Eq. (43b) provides $R(0) = 0.647$, whereas the analysis arising from Eq. (45) leads to $R(0) = 0.368$, with a decrease of

43%. For $\alpha L \geq 5.3$ both analyses provide $R(0) \leq 1\%$, which is the commonly used criterion to estimate the decay length of end effects [50]. Thus, for $\alpha L < 5.3$ the first term of the eigenfunction expansion related to Eq. (45) is unable to describe the end effects decay accurately, and a complete two-dimensional elasticity solution is required to obtain a response comparable with the beam solution.

5.6. Comparative response of a cantilever two-layer beam under different end loading conditions

Fig. 36 provides a qualitative comparison of the deformed shapes and stress distributions in the two layers at the free end of a cantilever two-layer beam for $\alpha L = 0$, for three loading configurations: (a) a pair of axial forces F_x, (b) a concentrated couple C_L, and (c) the combination $C_L - F_x\, d_0$, with $C_L = F_x\, d_0$.

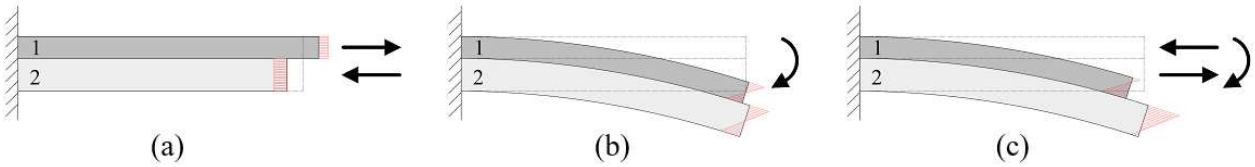


Fig. 11. Cantilever two-layer beam with $\alpha L = 0$ subjected to: (a) clockwise end couple $F_x\, d_0$; (b) clockwise end couple C_L; (c) self-equilibrated end couple $C_L - F_x\, d_0$, with $C_L = F_x\, d_0$.

In case (a), uniform tensile and compressive stress distributions develop in the two layers, resulting in purely axial deformation with interlayer slip and no rotation of the cross-section. In case (b), the response is purely rotational, and stress distribution within each layer is triangular and vanishing at the centroid. In case (c), the combined loading produces rotation, axial displacement, and interlayer slip. The stress distribution remains triangular but becomes asymmetric: for each layer, the neutral axis is no longer coinciding with the centroid. This configuration represents the general kinematics of a partially interacting section.

Cases (a) and (b) represent limiting responses dominated by axial and rotational kinematics, respectively. In the self-equilibrated case (c), both mechanisms are present: the interlayer slip reflects the difference between the two limiting responses, whereas the vertical displacement

follows from their superposition. Moreover, the stress distribution at the free end is essentially unaffected by αL. The comparison highlights how the loading type governs stress distribution, development of slip, and kinematic compatibility between the two layers.

5.7. Simply supported two-layer beam subjected to symmetric end axial forces and couples

Closed-form solutions for a simply supported two-layer beam subjected to symmetric end couples $F_x\ d_0$ and C are reported in the supplementary material S.6 and S.7, respectively. For $\hat{\kappa} = 0$, the simply supported two-layer beam subjected to symmetric end couples C was extensively studied in [26]. In particular, the axial force N_1 and bending moment M_1 reported in the supplementary material (S.7) reduce to Eqs. (3) and (25) proposed in [26], respectively. By symmetry, the simply supported configuration is equivalent to a cantilever of length $L/2$; therefore, the comments in Sections 5.2 and 5.3 also apply to the present cases.

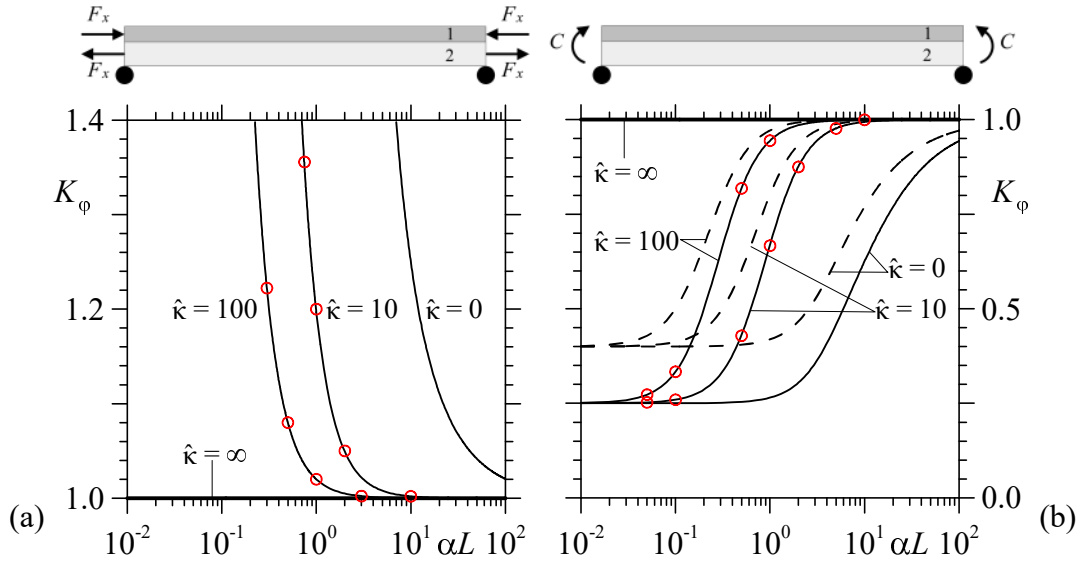


Fig. 12. Simply supported two-layer beam subjected to symmetric end axial forces and couples. Dimensionless rotational stiffness K_φ for symmetric end couples: (a) $F_x\ d_0$; (b) C. Dashed and solid curves refer to $EJ_\infty/EJ_0 = 2.5$ and 4, respectively. Red marks denote end-slip restraints only configurations.

Fig. 37 show the dimensionless end rotational stiffness versus αL for the two loading cases. The plotted ratios $K_{\varphi,Fx}/K_{\varphi,\infty}$ and $K_{\varphi,C}/K_{\varphi,\infty}$ are defined from the corresponding end rotational stiffnesses as:

$$K_{\varphi,F_x} = \frac{F_x\, d_0}{v'_{F_x}(0)} = K_{\varphi,\infty}\left(1 - 2\frac{\tanh(\alpha L/2)}{\alpha L\,\hat{c}_1}\right)^{-1} \tag{47a}$$

$$K_{\varphi,C} = \frac{C}{v'_C(0)} = K_{\varphi,\infty}\left(1 + 2\left(\frac{EJ_\infty}{EJ_0} - 1\right)\frac{\sinh(\alpha L/2)}{\alpha L\,\hat{c}_1\cosh(\alpha L/2)}\right)^{-1} \tag{47b}$$

where

$$K_{\varphi,\infty} = \frac{2\,EJ_\infty}{L} \tag{48}$$

For F_x d_0 and αL = 0, the two layers deform independently (Fig. 36a); consequently, the rotational stiffness $K_{\varphi,Fx}$ in Fig. 37a tends to infinity as the end rotation vanishes. By contrast, under the applied couple C (Fig. 36b), a non-zero end rotation occurs even without interlayer connection (αL = 0); accordingly, $K_{\varphi,C}$ in Fig. 37b starts from a finite value and increases with αL, approaching the fully composite limiting case. Moreover, Fig. 37 includes, as red marks, the end-slip restraints only configurations (αL = 0) that is evaluated as a function of αL according to Eq. (20c). These marks represent equivalent configurations exhibiting the same transition trend as the distributed-connection solutions. The corresponding rotational stiffness parameters are expressed as follows:

$$K_{\varphi,F_x} = \frac{F_x\, d_0}{\hat{v}'_{F_x}(0)} = K_{\varphi,\infty}\left(\frac{2+\hat{\alpha}L}{\hat{\alpha}L}\right) \tag{49a}$$

$$K_{\varphi,C} = \frac{C}{v'_C(0)} = K_{\varphi,\infty}\left[\left(2\frac{EJ_\infty}{EJ_0} + \hat{\alpha}L\right)\frac{1}{2+\hat{\alpha}L}\right]^{-1} \tag{49b}$$

5.8. Cantilever two-layer beam subjected to a vertical end point load F_y

In supplementary material S.9, a cantilever two-layer beam subjected to a vertical end point load F_y is analysed. Its response is shown in Figs. 38 and 39 in dimensionless form versus the composite interaction parameter αL. At the free end, the axial displacement of layer 1, the vertical displacement, the interlayer slip and the cross-sectional rotation are considered; at the fixed end, the axial stress in layer 1 and the total bending moment (sum of the layer bending moments) are reported. The dimensionless ratios shown on the ordinate are defined as:

$$\frac{u_1(L)}{u_{1,\infty}(L)} = 1 - \frac{4\sinh^2(\alpha L/2)}{(\alpha L)^2 \hat{c}_1 \cosh(\alpha L)} \tag{50a}$$

$$\frac{v(L)}{v_\infty(L)} = 1 + \frac{3}{(\alpha L)^3}\left(\frac{EJ_\infty}{EJ_0} - 1\right)\left[\alpha L - \tanh(\alpha L)\,\frac{1 + 2\,\alpha L\,\hat{\kappa}\,\tanh(\alpha L/2)}{\hat{c}_1}\right] \tag{50b}$$

$$\frac{u_s(L)}{\varphi_0(L)\,d_0} = \frac{4\sinh^2(\alpha L/2)}{(\alpha L)^2 \hat{c}_1 \cosh(\alpha L)} \tag{50c}$$

$$\frac{v'(L)}{\varphi_\infty(L)} = 1 + \frac{2}{(\alpha L)^2}\left(\frac{EJ_\infty}{EJ_0} - 1\right)\frac{1 - 1/\cosh(\alpha L)}{\hat{c}_1} \tag{50d}$$

$$\frac{N_1(0)}{F_y L/d_0} = \left(1 - \frac{EJ_0}{EJ_\infty}\right)\left(1 - \frac{\hat{c}_1^{(S.9)}}{\alpha L}\right) \tag{50e}$$

$$\frac{M_1(0) + M_2(0)}{-F_y L} = \frac{EJ_0}{EJ_\infty}\left[1 - \frac{\hat{c}_1^{(S.9)}}{\alpha L}\left(1 - \frac{EJ_\infty}{EJ_0}\right)\right] \tag{50f}$$

where $\hat{c}_1$ is the same as reported in Eq. (28a) and

$$\hat{c}_1^{(S.9)} = \tanh(\alpha L)\,[1 + \alpha L\,\hat{\kappa}\,\tanh(\alpha L/2)]/\hat{c}_1 \tag{51a}$$

$$u_{1,\infty}(L) = \varphi_\infty(L)\,d_{1,\infty} = \frac{F_y L^2}{2EJ_\infty}\,d_{1,\infty} \tag{51b}$$

$$v_\infty(L) = \frac{F_y L^3}{3EJ_\infty} \tag{51c}$$

$$\varphi_\infty(L) = \frac{F_y L^2}{2EJ_\infty} \tag{51d}$$

$$\varphi_0(L) = \frac{F_y L^2}{2EJ_0} \tag{51e}$$

Figs. 38 and 39 also include, as red marks, the response of configurations with end-slip restraints only and no distributed bonding. The corresponding dimensionless formulations are reported below.

$$\frac{\hat{u}_1(L)}{u_{1,\infty}(L)} = \frac{\hat{\alpha} L}{1 + \hat{\alpha} L} \tag{52a}$$

$$\frac{\hat{v}(L)}{v_\infty(L)} = 1 + \frac{1}{2}\left(\frac{EJ_\infty}{EJ_0} - 1\right)\left[\frac{6 + 3\,\hat{\alpha} L}{2\,(1 + \hat{\alpha} L)} - 1\right] \tag{52b}$$

$$\frac{\hat{u}_s(L)}{\varphi_0(L)\,d_0} = \frac{2+\hat{\alpha}L}{1+\hat{\alpha}L} - 1 \tag{52c}$$

$$\frac{\hat{v}'(L)}{\varphi_\infty(L)} = \left(\frac{EJ_\infty}{EJ_0} + \hat{\alpha}L\right)\frac{1}{1+\hat{\alpha}L} \tag{52d}$$

$$\frac{\hat{N}_1(0)}{F_y L/d_0} = \left(1 - \frac{EJ_0}{EJ_\infty}\right)\frac{\hat{\alpha}L}{2(1+\hat{\alpha}L)} \tag{52e}$$

$$\frac{\hat{M}_1(0)+\hat{M}_2(0)}{-F_y L} = \left[2+\hat{\alpha}L\left(1+\frac{EJ_0}{EJ_\infty}\right)\right]\frac{1}{2(1+\hat{\alpha}L)} \tag{52f}$$

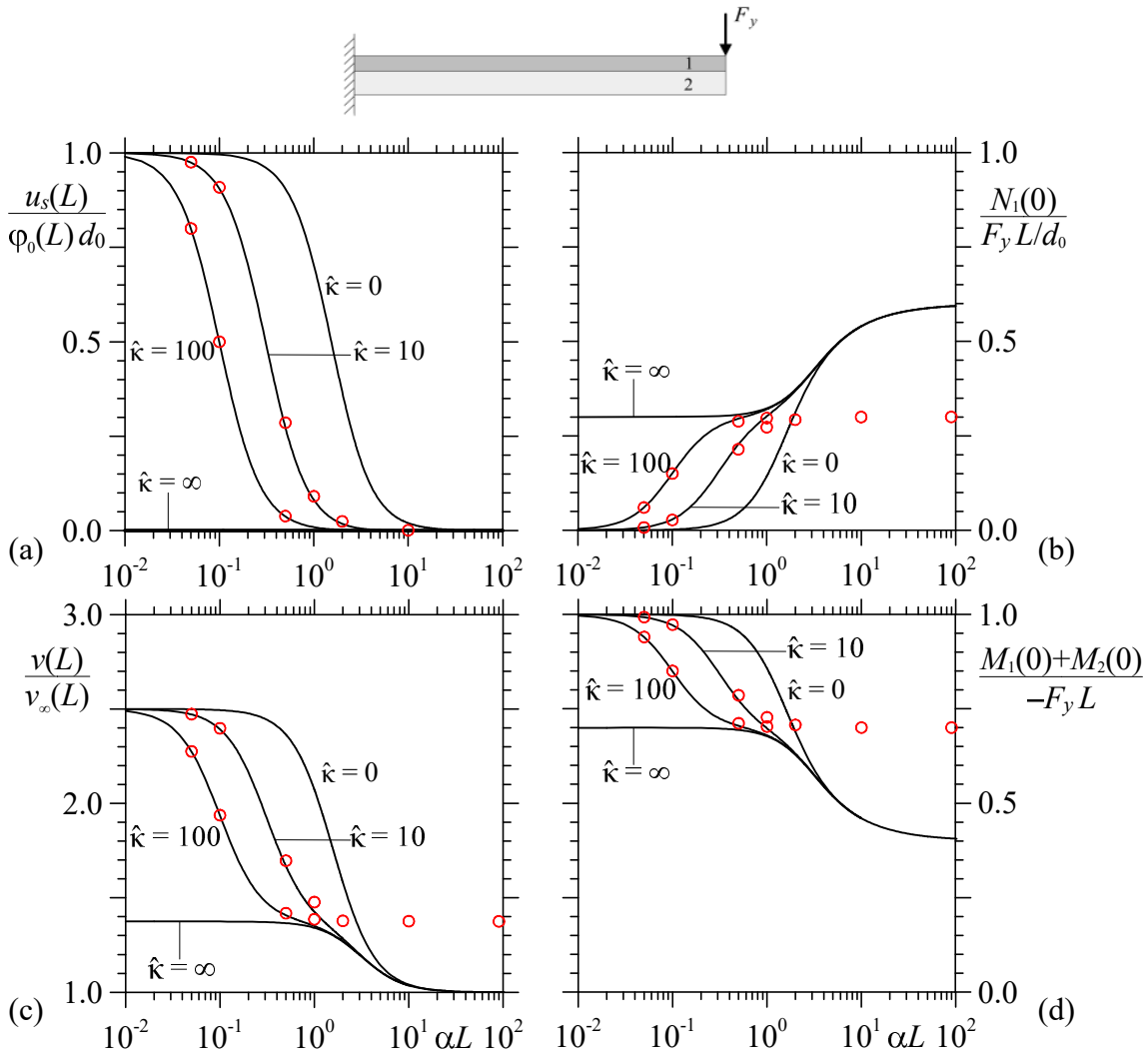


Fig. 13. Cantilever two-layer beam subjected to a vertical end point load F_y: dimensionless (a) interlayer slip at $x = L$; (b) axial stress resultant in layer 1 at $x = 0$; (c) vertical displacement at $x = L$, and (d) sum of bending moment of the two layers at $x = 0$. Results refer to $EJ_\infty/EJ_0 = 2.5$. Red marks denote end-slip restraints only configurations.

Fig. 38c shows that end-slip restraints significantly reduce the free-end vertical displacement in the low-interaction range. In particular, $v(L)/v_\infty(L)$ is nearly constant for $\hat{\kappa} = \infty$ and $\alpha L \le 1$; in fact,

the end springs limit the slip near the free end while the distributed connections are too weak to enforce full curvature compatibility along the span. As αL increases, interaction progressively extends along the beam and the response converges toward the fully composite limiting case. Similar trends are observed for the stress resultants (Figs. 38b, d): the axial force and the total bending moment are nearly stable at very small αL and then gradually approach the fully composite values as the interaction increases, while remaining sensitive to the end-restraint stiffness. The end-slip restraints only configurations (red marks) does not coincide with the distributed-connection curves at large equivalent αL, confirming that fully composite behaviour under transverse loading cannot be reproduced by end restraints alone. At very small αL, however, the two responses nearly coincide, since the layers deform almost independently and the contribution of either distributed or concentrated connection is negligible. The interlayer slip (Fig. 38a) decreases monotonically with the stiffness of the end restraints, consistently with the progressive enforcement of displacement compatibility near the free end. The red marks follow the same qualitative trend as the distributed-connection curves, indicating that the local slip response is captured also for end-only restraint conditions.

Figs. 39a and 39b show that increasing αL leads to larger axial displacement and smaller rotation. This correlation is also reflected in the distributions along the beam length (Figs. 39c, d), reported for $\alpha L = 0.5$ and 1.0. End-slip restraints modify the rotation profile (Fig. 39d), shifting the peak rotation from the free end toward the interior of the span.

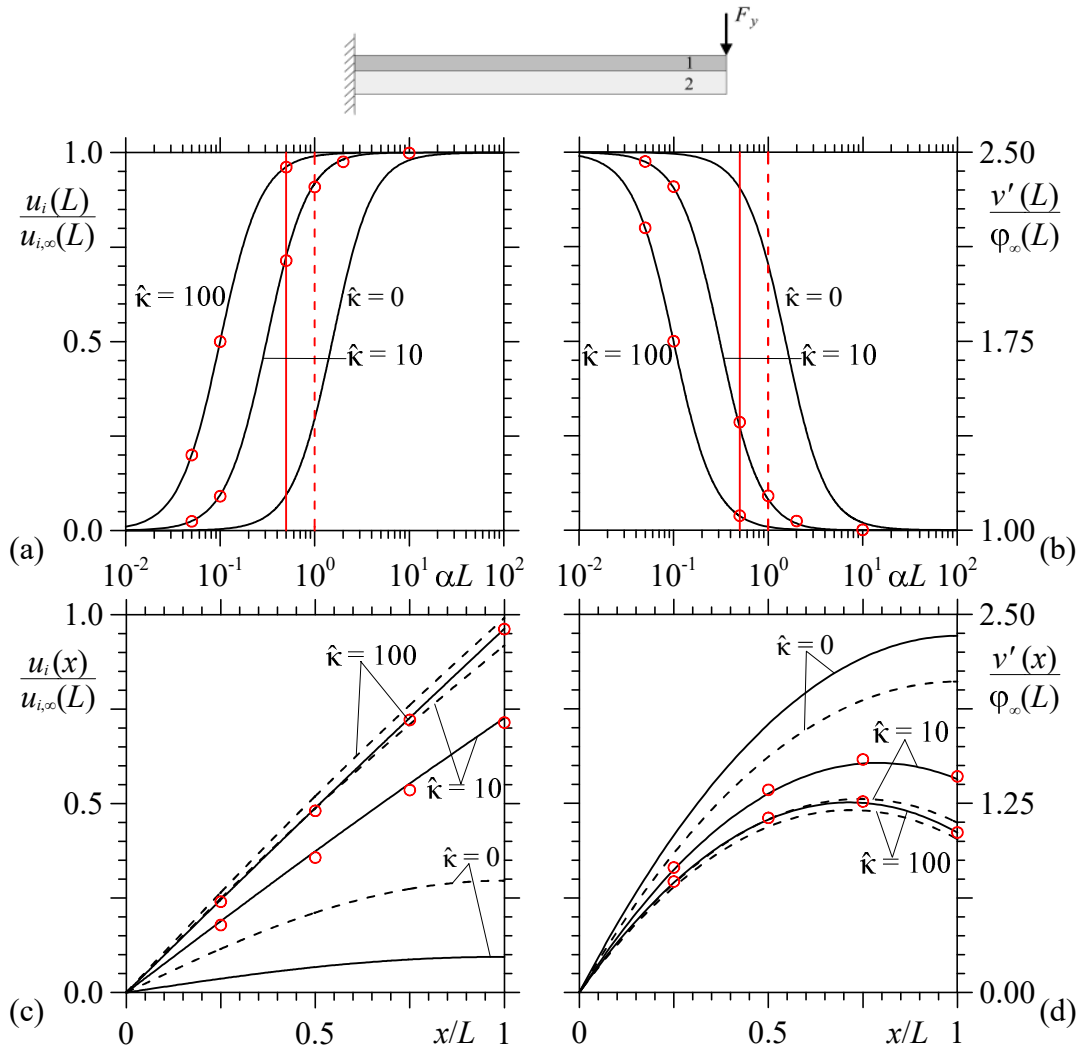


Fig. 14. Cantilever two-layer beam subjected to a vertical end point load F_y: dimensionless (a) axial displacement of layer i at $x = L$, and (b) rotation at $x = L$; dimensionless (c) axial displacement and (d) rotation along the span for $\alpha L = 0.5$ (solid) and $\alpha L = 1.0$ (dashed) and $\hat{\kappa} = 0$, 10, 100. Vertical red lines at $\alpha L = 0.5$ (solid) and $\alpha L = 1.0$ (dashed) are used as reference for plot in (c, d). Results refer to $EJ_\infty/EJ_0 = 2.5$. Red marks denote end-slip restraints only configurations.

5.9. Simply supported two-layer beam subjected to a point load F_y

The supplementary material S.11 studies the case of a simply supported two-layer beam subjected to a concentrated transverse load F_y applied at a generic position $x = L_L$. In the absence of end-slip springs, the same problem was already examined in early contributions, notably by Newmark et al. [15,16], who derived closed-form expressions for axial actions, interlayer slip and vertical deflection, which coincide with those reported in the supplementary material for $\hat{\kappa} = 0$.

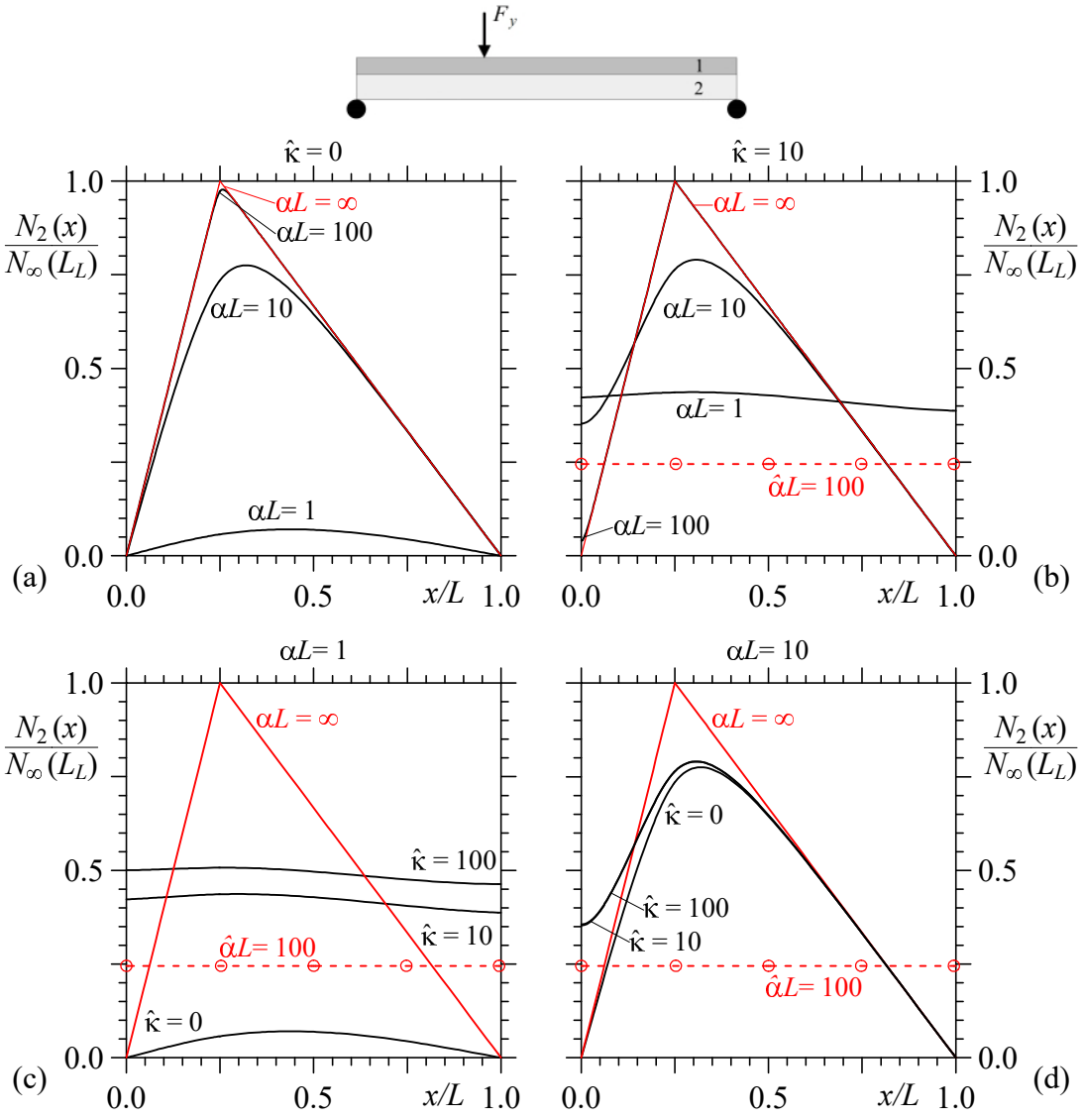


Fig. 15. Simply supported two-layer beam subjected to a point load F_y applied at $x = L/4$ with $EJ_\infty/EJ_0 = 2.5$. Dimensionless axial force distribution in the lower layer along the beam length for (a) $\hat{\kappa} = 0$, (b) $\hat{\kappa} = 10$, (c) $\alpha L = 1$ and (d) $\alpha L = 10$. Red solid line: fully composite limit. Red marks and dashed line: configurations with end-slip restraints only with $\hat{\alpha} L = 100$.

In Fig. 40 the ordinate represents the dimensionless axial force in the lower layer:

$$\frac{N_{2,L}(x)}{N_\infty(L_L)} = \frac{x}{L_L} - \frac{L}{L_L} f_L(x) \qquad \text{for } x \le L_L \tag{53a}$$

$$\frac{N_{2,R}(x)}{N_\infty(L_L)} = 1 - \frac{x}{L_L} - \frac{L}{L_L} f_R(x) \qquad \text{for } L_L < x \le L_R \tag{53b}$$

where, the functions $f_L(x)$ and $f_R(x)$, as well as the expressions for the axial actions $N_{2,L}(x)$ and $N_{2,R}(x)$, are reported in the supplementary material S.11. The fully composite axial force at the load point $N_\infty(L_L)$, consistently with Eq. (14) in [16], corresponds to:

$$N_{\infty}(L_L)=\left(\frac{1}{E_1A_1}+\frac{1}{E_2A_2}\right)^{-1}\frac{d_0}{EJ_{\infty}}\frac{L_RL_L}{L} \tag{54}$$

Figs. 40a, b show that the differences with respect to the fully composite limiting case (red curve) are governed primarily by αL. For large αL, the response approaches the fully composite solution over most of the span, whereas for small αL the deviation remains significant over a wider region. In the absence of end-slip springs (Fig. 40a with $\hat{\kappa}=0$), this behaviour coincides with that reported by Newmark et al. [16], who discussed the same trend in terms of a non-dimensional parameter inversely related to αL.

The contribution of end restraints is most clearly isolated in the end-slip restraints only configurations (Figs. 40b,c,d with $\hat{\alpha}L=100$), in which the distributed shear connection is absent and the interaction is provided solely by end-slip springs. In this case, the distributed interfacial shear transfer along the span is zero and the axial force in the lower layer remains uniform over the beam span. When distributed interaction is present (Fig. 40d), end restraints primarily introduce a change at the boundary, while the global trend remains governed by αL.

5.10. Simply supported two-layer beam subjected to two point loads F_y

The closed-form solutions of a simply supported two-layer beam under two point loads F_y are reported in the supplementary material S.12. For $\hat{k}_h$ =0, the vertical displacement response has been discussed in [33], whereas the slip response can be deduced by Eq. (3.30) in [29]. The agreement with [33] also extends to the axial force, except in the length between the two point loads, where Table 1 in [33] contains a misprint; conversely, [29] matches the axial-force distribution over the entire beam axis.

Fig. 41 shows the dimensionless interlayer slip and the vertical displacement along the beam length for αL = 0.1 and 1. The dimensionless quantities are defined with respect to the following reference values:

$$\varphi_0(0)=\frac{F_yL}{2EJ_0}L_L\left(1-\frac{L_L}{L}\right) \tag{55a}$$

$$v_\infty(L/2) = \frac{F_y L^2}{6 E J_\infty} L_L \left[\frac{3}{4} - \left(\frac{L_L}{L} \right)^2 \right] \tag{55b}$$

End-slip restraints ($\hat{\kappa} > 0$) mainly influence the response near the supports for the slip distribution and within the span for the vertical displacement, with a more evident effect as αL increases. Finally, the end-slip restraints only configurations (red marks), reported at the αL value corresponding to the equivalence criterion in Eq. (20c), clarifies the conditions under which end-only restraints can reproduce the global response of a distributed connection.

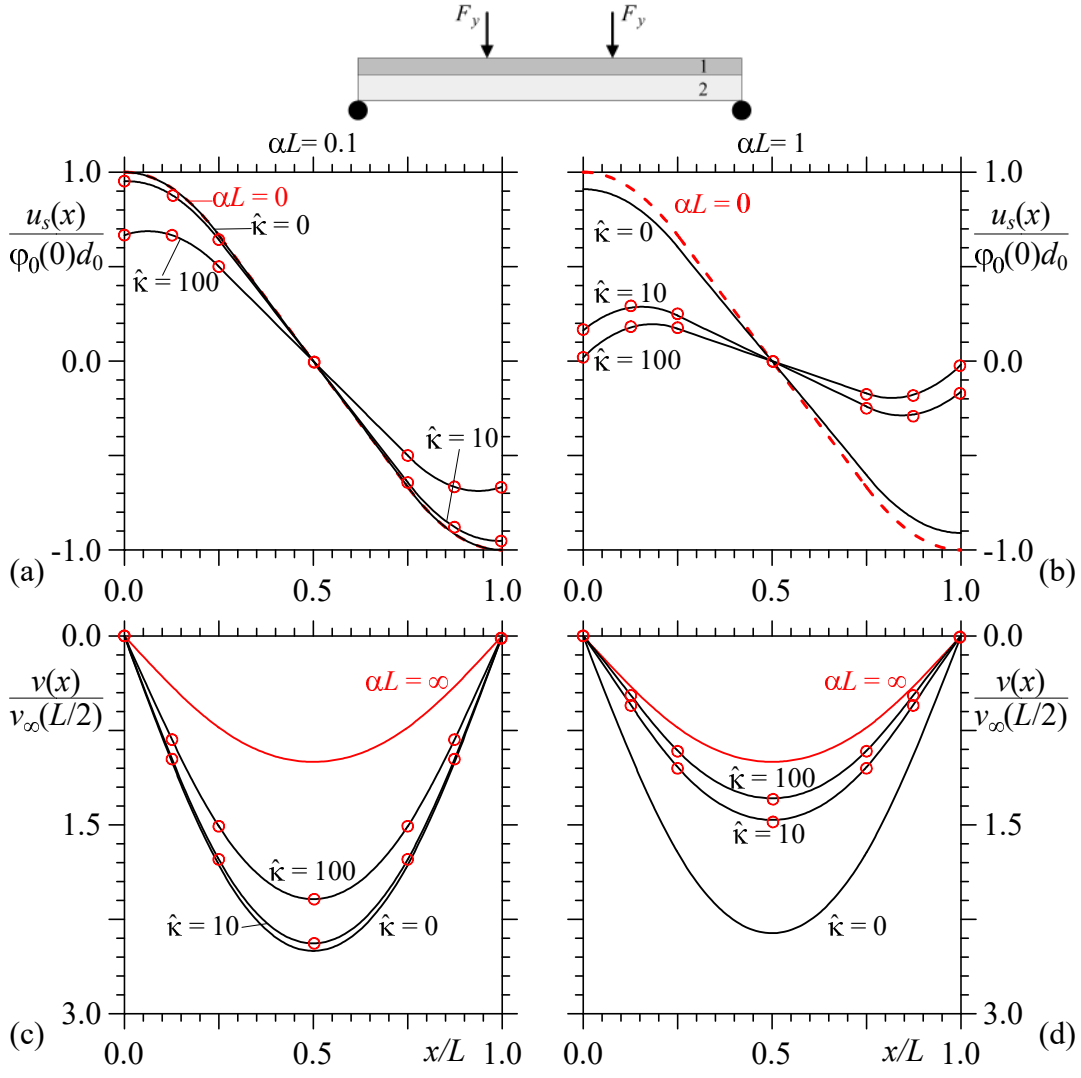


Fig. 16. Simply supported two-layer beam subjected to two point loads F_y applied at $x = L/4$ with $EJ_\infty/EJ_0 = 2.5$: dimensionless (a, b) interlayer slip and (c, d) vertical displacement for (a, c) $\alpha L = 0.1$ and (b, d) $\alpha L = 1$. Red dashed line refer to $\alpha L = 0$ for (a, b) and $\alpha L = \infty$ for (c, d). Red marks denote end-slip restraints only configurations.

The four-point bending test is also relevant to the mechanical characterisation of cross-laminated timber (CLT) elements. In that context, simplified interpretations frequently rely on the γ-method as

given in Annex B of Eurocode 5 [13], where the transverse layers are idealised as a shear-deformable core controlled by rolling shear [39]. A direct comparison between the present closed-form solution and the γ-method-based interpretation is provided in Section 7.4.

6. TWO-LAYER BEAM SUBJECTED TO DISTRIBUTED AXIAL LOADS

This section discusses the response of two-layer beams under distributed axial loading, with emphasis on the role of distributed interaction and end-slip restraints.

6.1. Cantilever two-layer beam subjected to axial distributed loads

Based on the closed-form solution reported in supplementary material S.13, Figs. 42 and 43 describe the cantilever response under distributed axial loads. Fig. 42 shows the dimensionless axial displacement of layer 1 and the dimensionless vertical displacement at $x = L$ versus αL, for different values of the end-restraints parameter $\hat{\kappa}$. The adopted dimensionless ratios are:

$$\upsilon_1(L) = \frac{u_1(L) - u_\infty(L)}{\varphi_\infty(L)\, d_{1,\infty}} = 1 + \left(\frac{EJ_\infty}{EJ_0} - 1 \right)^{-1} \frac{4 \sinh^2(\alpha L/2)}{(\alpha L)^2 \hat{c}_1 \cosh(\alpha L)} \tag{56a}$$

$$\frac{v(L)}{v_\infty(L)} = 1 - \frac{3}{(\alpha L)^3} \left[\alpha L - \tanh(\alpha L) \frac{1 + 2\,\alpha L\,\hat{\kappa} \tanh(\alpha L/2)}{\hat{c}_1} \right] \tag{56b}$$

where $\hat{c}_1$ is reported in Eq. (28a) and

$$v_\infty(L) = \frac{C_\infty L^3}{3EJ_\infty} \tag{57a}$$

$$\varphi_\infty(L) = \frac{C_\infty L^2}{2EJ_\infty} \tag{57b}$$

$$u_\infty(L) = \frac{(q_{x,1} + q_{x,2})L^2}{2(E_1A_1 + E_2A_2)} \tag{57c}$$

$$C_\infty = q_{x,1}\, d_{1,\infty} - q_{x,2}\, d_{2,\infty} \tag{57d}$$

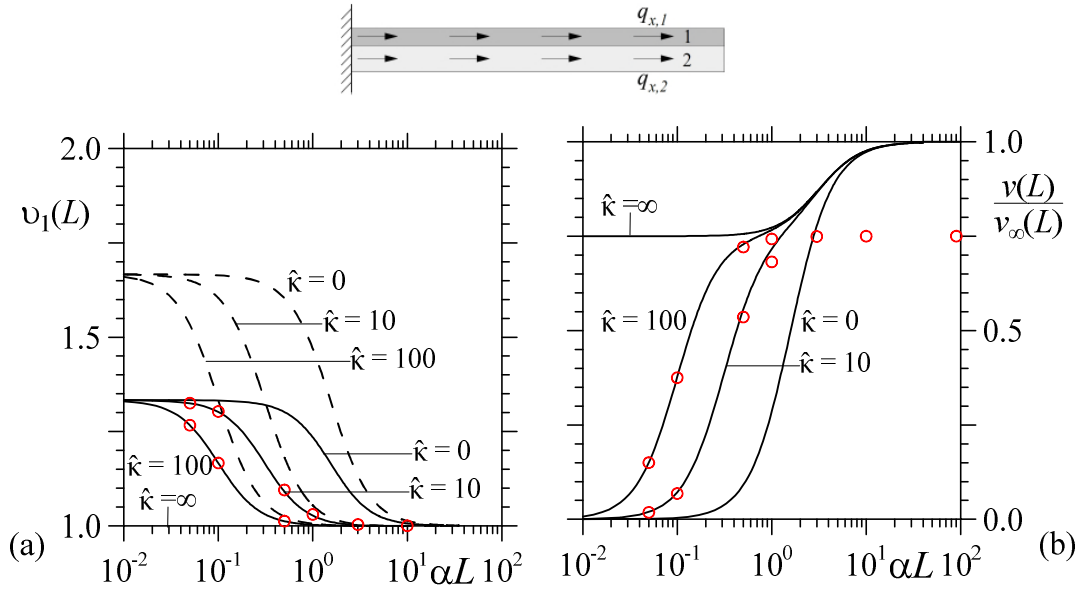


Fig. 17. Cantilever two-layer beam subjected to axial distributed loads $q_{x,1}$ and $q_{x,2}$: (a) dimensionless axial displacement of layer 1 at $x = L$; (b) dimensionless vertical displacement at $x = L$. Dashed and solid curves refer to $EJ_\infty/EJ_0 = 2.5$ and 4, respectively. Red marks denote end-slip restraints only configurations.

In Fig. 42a, the axial displacement of layer 1 decreases monotonically with αL and approaches unity, which corresponds to the rigid-body translation and rotation of the fully composite section. The stiffness ratio $EJ_\infty/EJ_0 = 2.5$ leads to larger axial displacements with respect to $EJ_\infty/EJ_0 = 4$. End-slip restraints promote a more rapid transition toward fully composite limiting case; for sufficiently stiff springs ($\hat{\kappa} \to \infty$), the axial displacement approaches the fully composite value already at small αL. The vertical displacement at the free end (Fig. 42b) exhibits a different trend. For $\alpha L = 0$ and weak end restraints, $v(L)$ is null, consistently with negligible interaction. As αL increases, $v(L)$ rises and asymptotically approaches the fully composite value. For very stiff end springs ($\hat{\kappa} \to \infty$), a non-zero vertical displacement is obtained already at $\alpha L = 0$, reaching approximately 75% of the fully composite reference. Stiff end springs generate a bending moment that induces cross-sectional rotation and a finite vertical displacement even without distributed connection. Full composite behaviour is recovered only when the distributed stiffness is sufficiently high.

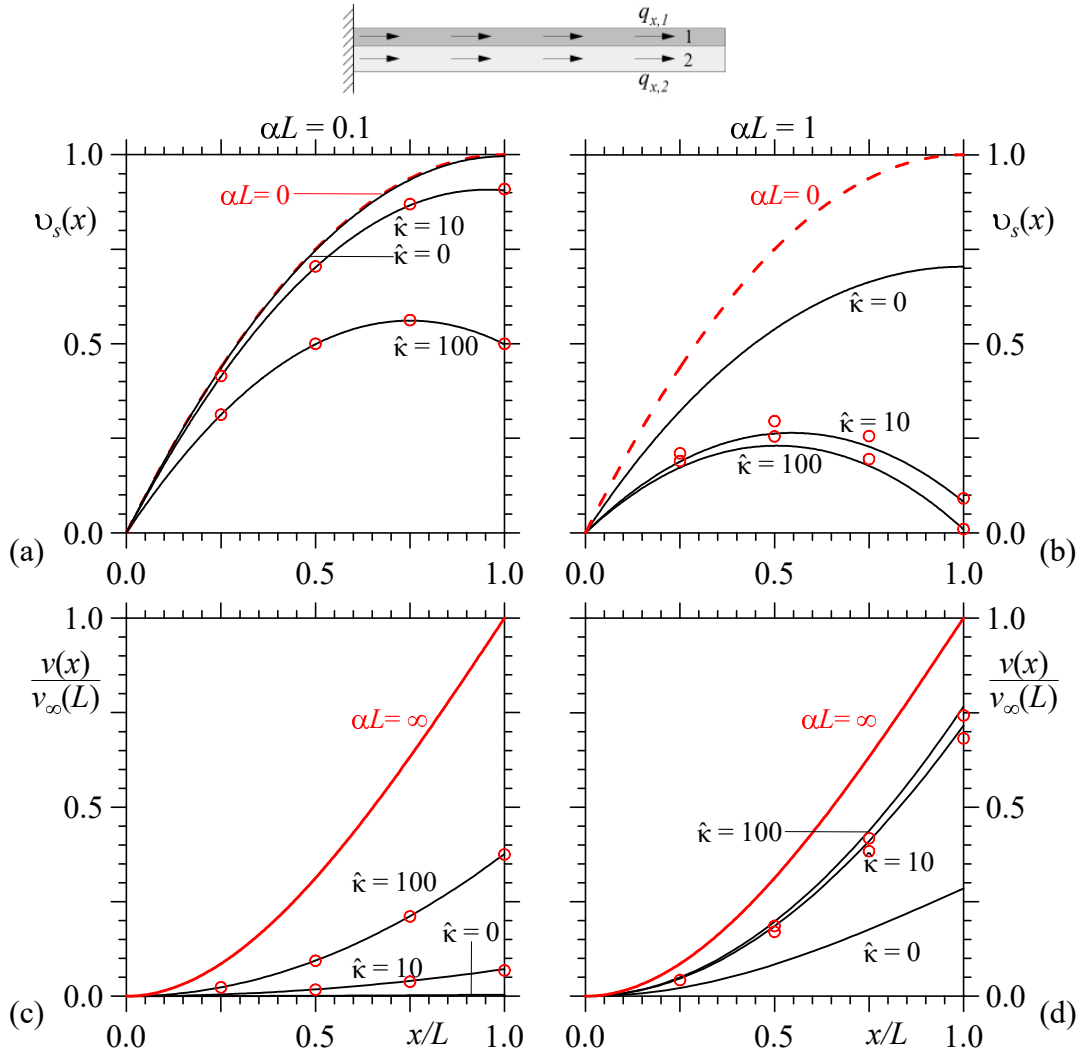


Fig. 18. Cantilever two-layer beam subjected to axial distributed loads $q_{x,1}$ and $q_{x,2}$ for $EJ_\infty/EJ_0 = 2.5$: (a, b) dimensionless slip; (c, d) dimensionless vertical displacement for (a, c) $\alpha L = 0.1$ and (b, d) $\alpha L = 1$. Red dashed line refers to $\alpha L = 0$ for (a, b) and $\alpha L = \infty$ for (c, d). Red marks denote end-slip restraints only configurations.

Fig. 43 shows the dimensionless interlayer slip and vertical displacement for $\alpha L = 0.1$ and $\alpha L = 1$ along the beam axis. The slip corresponding to $\alpha L = 0$ and the vertical displacement with the fully composite limiting case ($\alpha L = \infty$) are also reported. The dimensionless slip is defined as:

$$\upsilon_s(x) = \frac{u_s(x)}{(q_{x,2}/E_2A_2 - q_{x,1}/E_1A_1)\,L^2/2} \tag{58}$$

that reduces to

$$\upsilon_s(x) = \frac{1}{2}\frac{x}{L}\left(2 - \frac{x}{L}\right) \qquad \text{for } \alpha L = 0 \tag{59}$$

and it is shown in Fig. 43a and 43b with a dashed red line.

For $\alpha L = 0.1$ (Fig. 43a, c), the response without end restraints is close to that of two independent layers, with high slip along the span and negligible vertical displacement. The end-slip springs mitigate the slip, thereby inducing a clear vertical response. For $\alpha L = 1$ (Fig. 43b, d), end restraints strongly reshape the slip profile by suppressing it near the ends and shifting its maximum towards the interior, while the vertical displacement becomes closer to the fully composite values. These distributions corroborate the global trends observed in Fig. 42, confirming that end restraints primarily act through boundary control of slip, whereas increasing αL governs the extent of interaction along the span. The end-slip restraints only configurations are also reported in Figs. 42 and 43, where composite action is provided exclusively by the end-slip restraints and is governed by parameter $\hat{\alpha} L$, related to an equivalent αL through Eq. (20c). The corresponding dimensionless expressions are as follows:

$$\upsilon_1(L) = \frac{\hat{u}_1(L) - u_\infty(L)}{\varphi_\infty(L)\, d_{1,\infty}} = 1 + \left(\frac{EJ_\infty}{EJ_0} - 1 \right)^{-1} \frac{1}{1 + \hat{\alpha} L} \tag{60a}$$

$$\frac{\hat{v}(L)}{v_\infty(L)} = \frac{3}{4} \left(\frac{\hat{\alpha} L}{1 + \hat{\alpha} L} \right) \tag{60b}$$

$$\upsilon_s(x) = \frac{\hat{u}_s(x)}{(q_{x,2} / E_2 A_2 - q_{x,1} / E_1 A_1) L^2 / 2} = \frac{x}{L} \frac{\hat{\alpha} L^2 - x + L(2 - \hat{\alpha} x)}{L(1 + \hat{\alpha} L)} \tag{60c}$$

The good agreement between the end-slip restraints only configurations and the distributed-connection configurations at low value of αL, show in Figs. 42 and 43, reflects the limited role of composite interaction in this range: both layouts provide only modest constraint and the slip response is governed by layers that behave independently of each other. As αL increases, the agreement deteriorates, particularly for the slip distribution along the span and for the free-end vertical displacement. End-slip restraints enforce axial compatibility mainly at the boundaries and can reproduce the slip response with good accuracy.

7. TWO-LAYER BEAM SUBJECTED TO DISTRIBUTED VERTICAL LOAD

This section examines the closed-form solutions reported in the supplementary material S.14, S.15 and S.16 for two-layer beams subjected to distributed vertical loads, considering two representative static configurations.

7.1. Cantilever two-layer beam subjected to a vertical distributed load

For the cantilever case S.14, Fig. 44 shows the dimensionless response under a uniformly distributed vertical load as a function of αL, in terms of free-end displacements and fixed-end stress resultants. The dimensionless ratios reported on the ordinates of Figs. 44 and 45 are:

$$\frac{u_1(L)}{u_{1,\infty}(L)} = 1 + 6\frac{\alpha L - \sinh(\alpha L)}{(\alpha L)^3 \hat{c}_1 \cosh(\alpha L)} \tag{61a}$$

$$\frac{v(L)}{v_\infty(L)} = 1 + \frac{4}{(\alpha L)^2}\left(\frac{EJ_\infty}{EJ_0} - 1\right)\left\{1 - 2\tanh(\alpha L)\frac{\alpha L - [1-(\alpha L)^2\hat{\kappa}]\tanh(\alpha L/2)}{(\alpha L)^2 \hat{c}_1}\right\} \tag{61b}$$

$$\frac{u_s(L)}{\varphi_0(L)\, d_0} = -6\frac{\alpha L - \sinh(\alpha L)}{(\alpha L)^3 \hat{c}_1 \cosh(\alpha L)} \tag{61c}$$

$$\frac{N_1(0)}{q_y L^2/(2d_0)} = \left(1 - \frac{EJ_0}{EJ_\infty}\right)\left\{1 - \frac{2\hat{c}_2^{(S.12)}}{(\alpha L)^2 \hat{c}_1 \cosh(\alpha L)}\right\} \tag{61d}$$

$$\frac{M_1(0) + M_2(0)}{(-q_y L^2/2)} = \frac{EJ_0}{EJ_\infty}\left[1 - \left(\frac{EJ_\infty}{EJ_0} - 1\right)\frac{2\hat{c}_2^{(S.12)}}{(\alpha L)^2 \hat{c}_1 \cosh(\alpha L)}\right] \tag{61e}$$

where $\hat{c}_1$ is reported in Eq. (28a) and

$$\hat{c}_2^{(S.12)} = 1 + \alpha L \sinh(\alpha L) - (\hat{c}_1 - (\alpha L)^2 \hat{\kappa})\cosh(\alpha L) \tag{62a}$$

$$u_{1,\infty}(L) = \varphi_\infty(L)\, d_{1,\infty} = \frac{q_y L^3}{6EJ_\infty} d_{1,\infty} \tag{62b}$$

$$v_\infty(L) = \frac{q_y L^4}{8EJ_\infty} \tag{62c}$$

$$\varphi_0(L) = \frac{q_y L^3}{6EJ_0} \tag{62d}$$

In the limiting case $\hat{\kappa} = 0$, the cantilever two-layer beam subjected to a vertical distributed load has been studied in [25]. In particular, the vertical displacement $v(x)$ reported in the supplementary material S.14 reduce to case (1a) in Table (1a) proposed in [25].

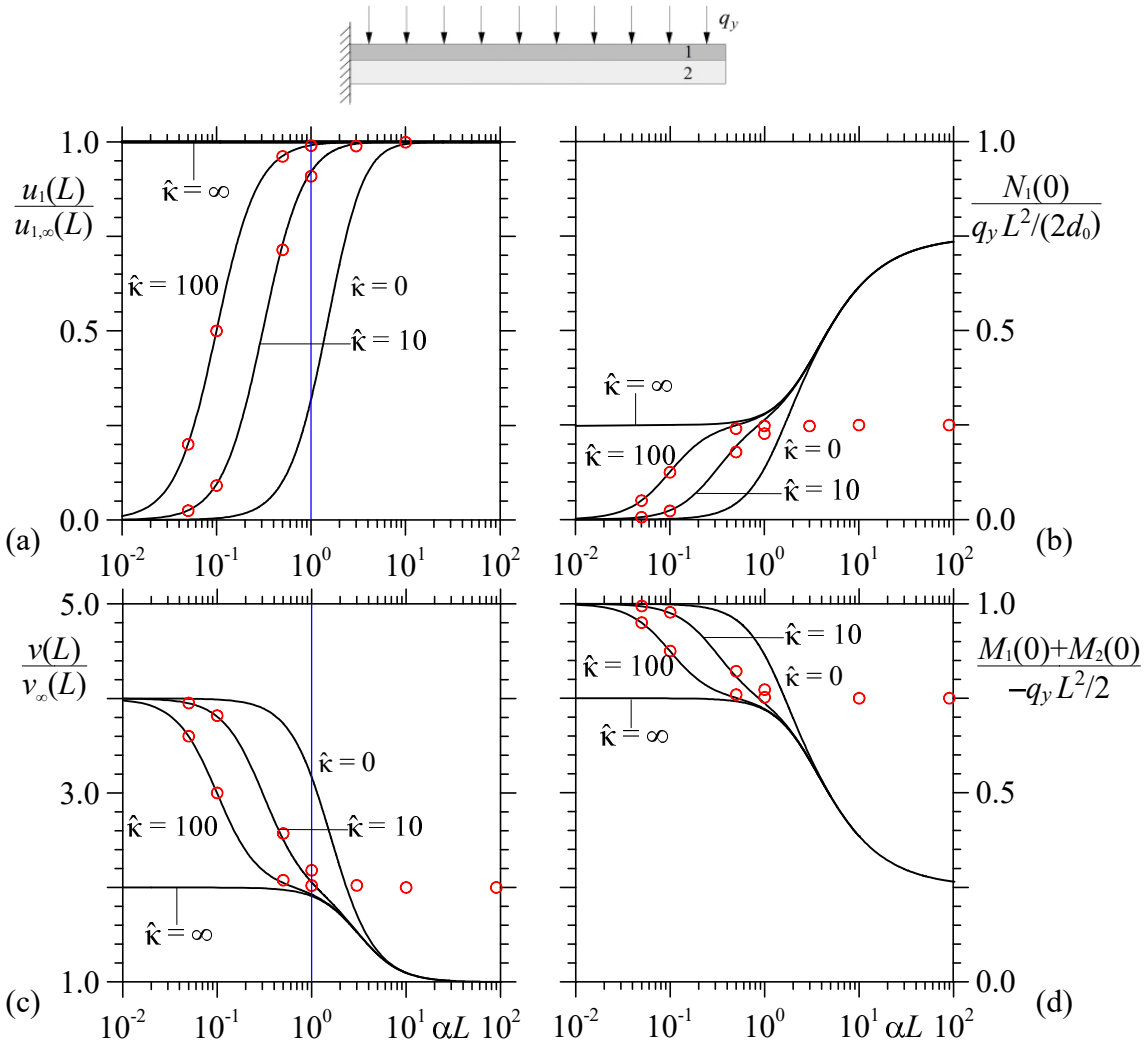


Fig. 19. Cantilever two-layer beam subjected to a vertical distributed load q_y for $EJ_\infty/EJ_0 = 4$: dimensionless (a) axial displacement of layer 1 at $x = L$; (b) axial stress resultant of layer 1 at $x = 0$; (c) vertical displacement at $x = L$, and (d) sum of bending moment of the two layers at $x = 0$. Red marks denote end-slip restraints only configurations. The blue lines correspond to the case $\alpha L = 1$.

In Fig. 44, red marks denote end-slip restraints only configurations (no distributed bonding), in which composite action is provided exclusively by the end-slip restraints; the corresponding dimensionless expressions are:

$$\frac{\hat{u}_1(L)}{u_{1,\infty}(L)} = \frac{\hat{\alpha} L}{1 + \hat{\alpha} L} \tag{63a}$$

$$\frac{\hat{v}(L)}{v_\infty(L)} = 1 + \frac{1}{3}\left(\frac{EJ_\infty}{EJ_0} - 1\right)\left[3 - \frac{2\hat{\alpha}L}{1+\hat{\alpha}L}\right] \tag{63b}$$

$$\frac{\hat{u}_s(L)}{\varphi_0(L)\,d_0} = 1 - \frac{\hat{\alpha}L}{1+\hat{\alpha}L} \tag{63c}$$

$$\frac{\hat{N}_1(0)}{q_y L^2/(2d_0)} = \left(1 - \frac{EJ_0}{EJ_\infty}\right)\frac{\hat{\alpha}L}{3(1+\hat{\alpha}L)} \tag{63d}$$

$$\frac{\hat{M}_1(0) + \hat{M}_2(0)}{(-q_y L^2/2)} = \left[3 + \hat{\alpha}L\left(2 + \frac{EJ_0}{EJ_\infty}\right)\right]\frac{1}{3(1+\hat{\alpha}L)} \tag{63e}$$

For low values of αL, Fig. 44 shows that axial displacements and axial forces vanish, whereas the free-end deflection and the total bending moment attain their maximum values. For high values of αL, interlayer shear transfer activates composite action, asymptotically approaching the fully composite limiting case. End-slip restraints ($\hat{\kappa} > 0$) exert a notable influence at low αL; however, they fail to reproduce the fully composite behaviour in the absence of a distributed connection. The end-slip restraints only configurations is further clarified in Fig. 45, which reports the distributions of dimensionless slip and vertical displacement along the beam length. The blue curves refer to beams with end-slip restraints only (αL = 0) and $\hat{\kappa} = 10$ and 100, and correspond to the vertical reference lines in Fig. 44 according to Eq. (20c). The limiting case αL = 0 is included in Fig. 45a for the slip response (red dashed curve), whereas the fully composite condition $\alpha L = \infty$ is reported in Fig. 45b for the vertical displacement (red solid curve). Consistently with Fig. 44c, Fig. 45b shows that the end-slip restraints only configuration differs markedly from the fully composite deflection profile, confirming that curvature compatibility along the span cannot be achieved in the absence of distributed connection. Conversely, the end restraints significantly affect the slip response near the boundaries, where compatibility is locally enforced; however, far from the ends, significant slip still arises because the interaction between the layers along the beam occurs with distributed shear stiffness. To completely suppress slip across the beam span, a distributed connection is required in addition to end restraints. For αL = 5 in Fig. 45a, a marked slip reduction over the beam length is observed, reflecting the progressive spread of composite interaction between the layers.

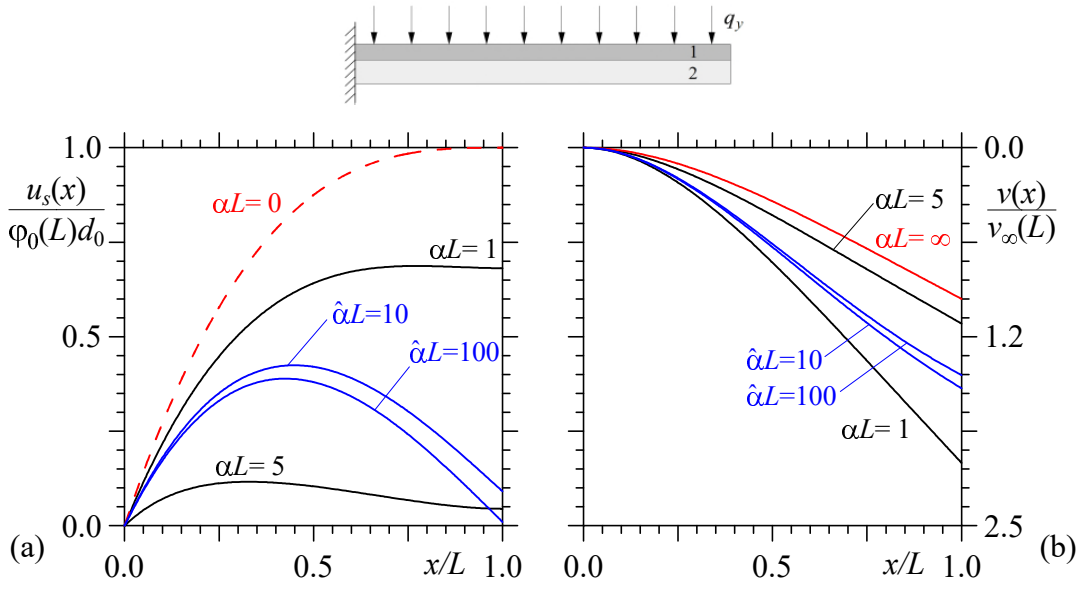


Fig. 20. Cantilever two-layer beam subjected to a vertical distributed load q_y for $EJ_\infty/EJ_0=2.5$: (a) dimensionless slip and (b) vertical displacement along the beam; Red dashed line indicates the slip for $\alpha L=0$, whereas the solid red line refers to the vertical displacement for $\alpha L=\infty$. Blue lines denote end-slip restraints only configurations for $\hat{\alpha} L=10$, 100.

7.2. Simply supported two-layer beam subjected to a vertical load

A preliminarily comparison is presented between simply supported two-layer beams subjected to a vertical point load applied at midspan (S.10) and a uniformly distributed vertical load (S.15). For the midspan point-load case, the maximum dimensionless vertical displacement and the slip along the beam are equal to:

$$\eta_v=\frac{v(L/2)}{v_\infty(L/2)}=1+\frac{12}{(\alpha L)^3}\left(\frac{EJ_\infty}{EJ_0}-1\right)\left[\alpha L-2\tanh(\alpha L/2)\frac{1+2\,\alpha L\,\hat{\kappa}\tanh(\alpha L/4)}{1+\alpha L\,\hat{\kappa}\tanh(\alpha L/2)}\right] \tag{64a}$$

$$\frac{u_s(x)}{\varphi_0(0)\,d_0}=\frac{8}{(\alpha L)^2}\left[1-\frac{\hat{c}_2^{(S.10)}\cosh(\alpha x)-\alpha L\hat{\kappa}(\cosh(\alpha L)-1)\sinh(\alpha x)}{\hat{c}_1^{(S.10)}\cosh(\alpha L/2)}\right] \tag{64b}$$

where the constants and the reference terms are as follow:

$$\hat{c}_1^{(S.10)}=1+\alpha L\,\hat{\kappa}\tanh(\alpha L/2) \tag{65a}$$

$$\hat{c}_2^{(S.10)}=1+\alpha L\,\hat{\kappa}\sinh(\alpha L/2) \tag{65b}$$

$$v_\infty(L/2)=\frac{F_y L^3}{48EJ_\infty} \tag{65c}$$

$$\varphi_0(0) = \frac{F_y L^2}{16 E J_0} \tag{65d}$$

In the limiting case of $\alpha L = 0$, the non dimensional longitudinal slip reduces to:

$$\frac{u_s(x)}{\varphi_0(0)\, d_0} = 1 - 4\left(\frac{x}{L}\right)^2 \qquad \text{for } \alpha L = 0 \tag{66}$$

that is shown in Fig. 47a with a red curve.

In [13] a stiffness criteria for the floor vibration control is prescribed. In particular, the maximum deflection due to a vertical static point load positioned in the midspan of a single span floor has to be considered. Thus, making use of Eq. (64a), $v(L/2) = \eta_v\, v_\infty(L/2)$. In most vibration control cases, the shear deformation can be neglected since slender beams are more prone to small vibration frequencies.

For the vertical distributed load case, the following expressions apply:

$$\frac{v(L/2)}{v_\infty(L/2)} = 1 + \frac{48}{5\,(\alpha L)^2}\left(\frac{EJ_\infty}{EJ_0} - 1\right)\left(1 - 16\frac{\hat{c}_1^{(S.15)}}{(\alpha L)^2}\frac{\sinh^2(\alpha L/4)}{\cosh(\alpha L/2)}\right) \tag{67a}$$

$$\frac{u_s(x)}{\varphi_0(0)\, d_0} = \frac{24}{(\alpha L)^2}\left[\frac{1}{2} - \frac{x}{L} + \frac{\hat{c}_1^{(S.15)}\sinh(\alpha(x - L/2))}{\alpha L \cosh(\alpha L/2)}\right] \tag{67b}$$

where

$$\hat{c}_1^{(S.15)} = [1 + (\alpha L)^2\,\hat{\kappa}/2] \big/ [1 + \alpha L\,\hat{\kappa}\tanh(\alpha L/2)] \tag{68a}$$

$$v_\infty(L/2) = \frac{5 q_y L^4}{384 E J_\infty} \tag{68b}$$

$$\varphi_0(0) = \frac{q_y L^3}{24 E J_0} \tag{68c}$$

For $\alpha L = 0$, the non dimensional longitudinal slip reduces to

$$\frac{u_s(x)}{\varphi_0(0)\, d_0} = 1 - 6\left(\frac{x}{L}\right)^2 + 4\left(\frac{x}{L}\right)^3 \qquad \text{for } \alpha L = 0 \tag{69}$$

For both configurations, the limiting solutions with end-slip restraints only (no distributed bonding) are also considered. The corresponding dimensionless expressions for the point-load configuration are:

$$\frac{\hat{v}(L/2)}{v_\infty(L/2)} = 1 + \frac{1}{2}\left(\frac{EJ_\infty}{EJ_0} - 1\right)\left[2 - \frac{3}{2}\left(\frac{\hat{\alpha}L}{2+\hat{\alpha}L}\right)\right] \tag{70a}$$

$$\frac{\hat{u}_s(x)}{\varphi_0(0)\, d_0} = 2\left(1 - 2\frac{x}{L}\right)\left(\frac{1}{2+\hat{\alpha}L} + \frac{x}{L}\right) \tag{70b}$$

whereas, for the distributed-load configuration, the corresponding quantities are:

$$\frac{\hat{v}(L/2)}{v_\infty(L/2)} = 1 + \frac{4}{5}\left(\frac{EJ_\infty}{EJ_0} - 1\right)\left[\frac{5}{4} - \frac{\hat{\alpha}L}{2+\hat{\alpha}L}\right] \tag{71a}$$

$$\frac{\hat{u}_s(x)}{\varphi_0(0)\, d_0} = 2\left(1 - 2\frac{x}{L}\right)\left(\frac{1}{2+\hat{\alpha}L} + \frac{x}{L} - \left(\frac{x}{L}\right)^2\right) \tag{71b}$$

Fig. 46 compares the dimensionless midspan deflection for the two loading configurations. In particular, Figs. 46a, b show the response versus αL for different values of the end-restraint stiffness $\hat{\kappa}$, whereas Figs. 46c, d show the same quantity versus $\hat{\kappa}$ for αL = 0.5 and 1.0. As already observed for the cantilever cases (Sections 5.8 and 7.1), the midspan deflection decreases with αL, gradually approaching the fully composite condition. For a given αL, the uniformly distributed load yields smaller deflections than the midspan point load. This difference becomes clearer at large $\hat{\kappa}$, when end compatibility is already enforced and the curvature distribution along the beam governs the response.

Fig. 47 shows the dimensionless slip and deflection profiles along the beam length for the two loading configurations and EJ_∞/EJ_0 = 2.5, αL=0.5, normalised by the non-composite and fully composite reference cases, respectively. For $\hat{\kappa}$ = 0, the slip vanishes at midspan and attains its maximum at the supports. Increasing $\hat{\kappa}$ reduces slip at the ends and the maximum shifts towards the interior, with peaks developing around $L/4$ and $3L/4$. The distributed-load case yields lower slip and a vertical-displacement profile closer to the fully composite reference than the midspan point-load case. This is consistent with the trends observed in Fig. 46 and, as shown in Fig. 47, it holds

along the entire beam length. Consistently with the previous cases, the end-only solutions (red marks) provide a good approximation in the low-αL regime: they reproduce the slip distribution well, whereas a small overestimation of vertical displacement remains because curvature compatibility cannot be ensured without distributed shear connection.

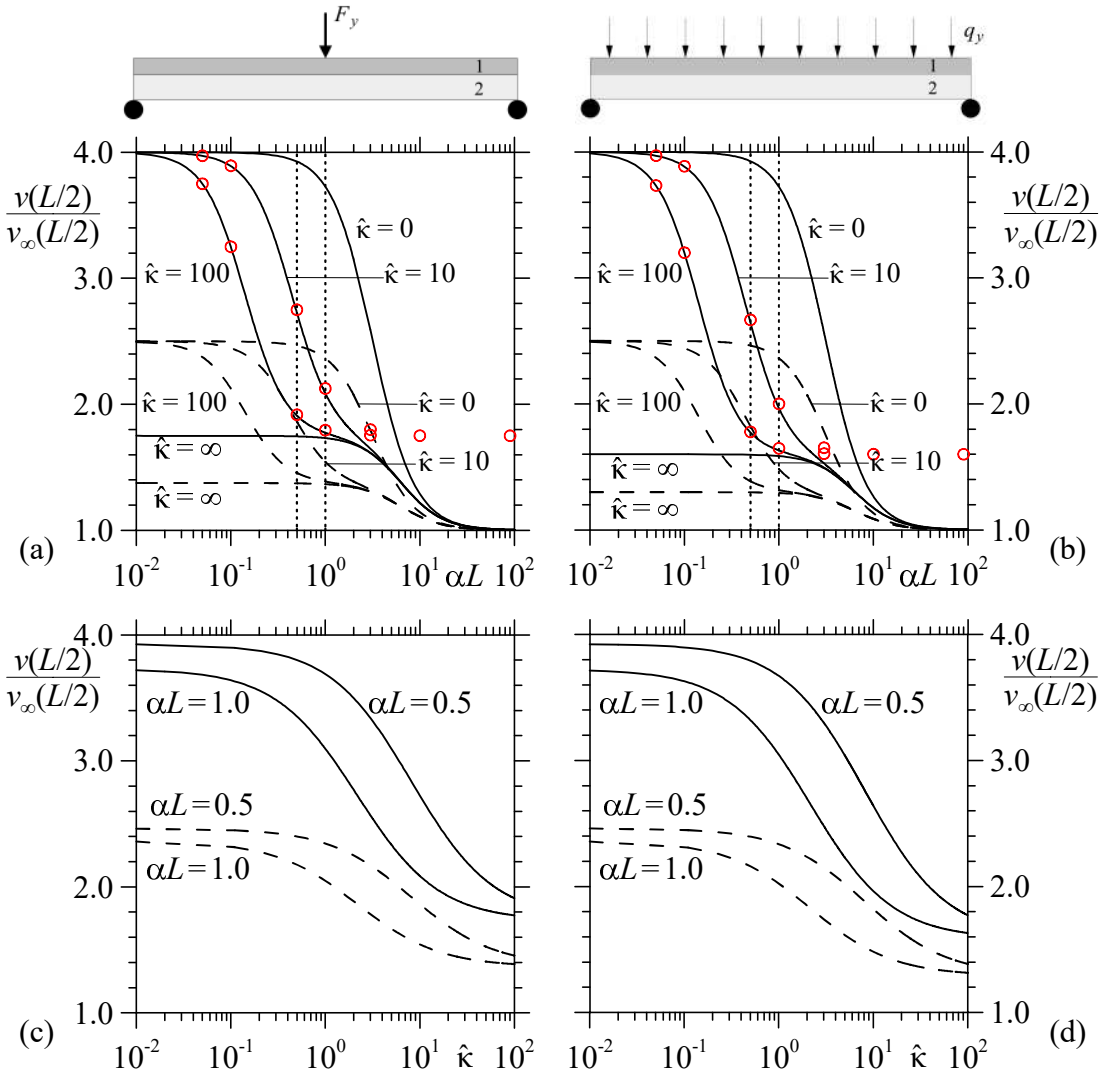


Fig. 21. Maximum vertical displacement for a simply supported two-layer beam subjected to (a, c) a point load F_y at midspan and (b, d) a distributed load q_y versus (a, b) αL for $\hat{\kappa} = 0$, 10, 100, ∞ and (c, d) $\hat{\kappa}$ for $\alpha L = 0.5$ and 1.0. Dashed and solid curves refer to $EJ_\infty/EJ_0 = 2.5$ and 4, respectively. Red marks denote end-slip restraints only configurations.

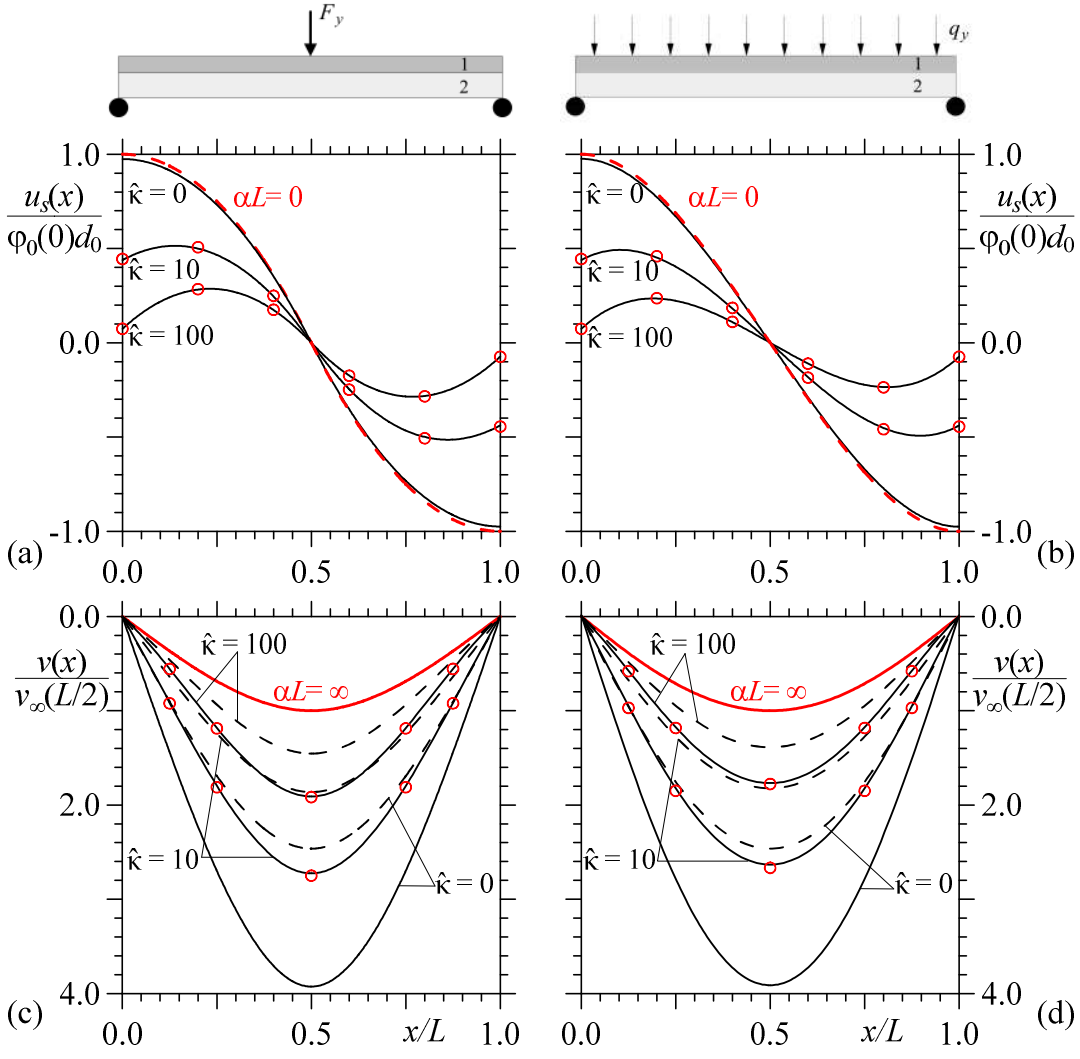


Fig. 22. Simply supported two-layer beam subjected to (a, c) a point load F_y at midspan and (b, d) a distributed load q_y for $EJ_\infty/EJ_0=2.5$ and $\alpha L=0.5$: (a, b) dimensionless interlayer slip and (c, d) dimensionless vertical displacement. Red dashed line indicates the slip for $\alpha L=0$, whereas the solid red line refers to the vertical displacement for $\alpha L=\infty$. Red marks denote end-slip restraints only configurations.

The closed-form solutions for the two loading configurations are validated against established analytical results available in the literature, with emphasis on the limiting case $\hat{\kappa}=0$, for which explicit expressions are reported by several authors.

For the midspan point load (S.10), the present expressions recover the classical solution by Newmark et al. [15] (Table I, where the slip and deflection correspond to γ and y, respectively) and also match Eq. (12) presented in [32]. Agreement is also found with [33], where expressions for vertical displacement w_i, axial force N_i and bending moment M_i along the beam are reported in Table 1, and with [28], which reports closed-form expressions for slip, vertical displacement and axial force. The same limiting solution extends to configurations with finite interlayer thickness

when the parameters are defined as in Eqs. (23a–b), in agreement with the modelling framework adopted in [40].

For the uniformly distributed load (S.15), with $\hat{\kappa} = 0$, the vertical displacement agrees with case (2a) in Table 1a of [25], and the slip expression coincides with Eq. (2.27) in [30] and agrees with Eq. (41) in [21]. Consistency is also found with the results in [33] for vertical displacement, axial force, and bending moment, as well as those in [29] for slip and axial force, and with [28] for the slip, vertical displacement and axial-force fields; the deflection-only expression in [31] is also recovered. For two rectangular equal layer having width b, height $H/2$, Young modulus E and $\hat{k}_h = 0$, the vertical displacement is in agreement with Eq. (A11) proposed in [36]. Finally, in non-composite condition $\alpha L = 0$, Eq. (69) matches the approximate solution in Eq. (61) proposed in [35]. As for the midspan point-load case, analogous agreement is obtained for composite beams with finite interlayer thickness when adopting the definitions in Eqs. (23a–b), in line with the analytical models in [40, 41].

7.3. Simply supported two-layer beam subjected to a vertical distributed load and fixed by rigid anchors at both beam ends

A practically relevant special case of the simply supported two-layer beam under uniformly distributed transverse load is obtained by enforcing rigid end slip restraints at both beam ends ($\hat{\kappa} \to \infty$). This configuration is representative of bonded or end-anchored composite members (e.g., RC–FRP plated beams) in which relative slip is strongly inhibited at the extremities. This limiting case was already examined in [43]; the vertical displacement described matches the corresponding closed-form expression reported therein, and the same remarks apply. For distributed connection and $\hat{\kappa} \to \infty$, the vertical displacement and the interlayer slip reported in the supplementary material (S.15) reduce to:

$$\hat{v}(x) = \frac{q_y L^4}{24 E J_\infty} \left\{ \frac{x}{L} \left[1 - 2\left(\frac{x}{L}\right)^2 + \left(\frac{x}{L}\right)^3 \right] \right.$$

$$+\frac{12}{(\alpha L)^2}\left(\frac{EJ_\infty}{EJ_0}-1\right)\left[\frac{x}{L}\left(1-\frac{x}{L}\right)-\frac{2\sinh[\alpha L/2(1-x/L)]\sinh(\alpha x/2)}{\alpha L\sinh(\alpha L/2)}\right]\Bigg\} \tag{72a}$$

$$\hat{u}_s(x)=\frac{q_y L^3 d_0}{2EJ_0(\alpha L)^2}\left\{1-\frac{2x}{L}-\frac{\sinh[\alpha(L/2-x)]}{\sinh(\alpha L/2)}\right\}$$

$$=\frac{q_y L}{2k_h d_0}\left(1-\frac{EJ_0}{EJ_\infty}\right)\left\{1-\frac{2x}{L}-\frac{\sinh[\alpha(L/2-x)]}{\sinh(\alpha L/2)}\right\} \tag{72b}$$

In particular, the midspan displacement, obtained from Eqs. (67) or (72a), is:

$$\hat{v}(L/2)=v_\infty(L/2)\left[1+\frac{192}{5}\left(\frac{EJ_\infty}{EJ_0}-1\right)\frac{\alpha L/4-\tanh(\alpha L/4)}{(\alpha L)^3}\right] \tag{73}$$

In the frictionless limiting case ($\alpha L = 0$), the midspan displacement can be explicitly evaluated for the two extreme end-restraint conditions, i.e. without end-slip restraints ($\hat{\kappa} = 0$) and with rigid end-slip restraints ($\hat{\kappa} \to \infty$). Accordingly, Eqs. (67) and (73) reduce to:

$$v_0(L/2)=v_\infty(L/2)\frac{EJ_\infty}{EJ_0} \qquad \text{for } \hat{\kappa}=0 \tag{74a}$$

$$\hat{v}(L/2)=\frac{v_\infty(L/2)}{5}\left(4+\frac{EJ_\infty}{EJ_0}\right) \qquad \text{for } \hat{\kappa}\to\infty \tag{74b}$$

A comparison between Eqs. (74a) and (74b) highlights the role of rigid end-slip restraints as effective stiffeners for the whole beam. In fact, the displacement ratio is:

$$\frac{v_0(L/2)}{\hat{v}(L/2)}=5\,\frac{EJ_\infty}{EJ_0}\left(4+\frac{EJ_\infty}{EJ_0}\right)^{-1} \tag{75}$$

For two equal layers ($EJ_\infty/EJ_0 = 4$), Eqs. (74a,b) and (75) give $v_0(L/2) = 4.0\, v_\infty(L/2) = 2.5\, \hat{v}\,(L/2)$.

Eq. (74b) can also be used to characterise the midspan displacement of a concrete beam strengthened with a FRP strip connected by rigid anchors at the beam ends only [18]. For a plated beam with $EJ_\infty = 1.25\, EJ_0$, Eq. (74) gives $\hat{v}(L/2)=1.05 v_\infty(L/2)$, while the end slip in Eq. (72b) reduces, for $\hat{\kappa}\to\infty$ and $\alpha L = 0$, to:

$$\hat{u}_s(x)=\frac{q_y L^3 d_0}{12EJ_0}\frac{x}{L}\left(1-\frac{x}{L}\right)\left(1-\frac{2x}{L}\right) \qquad \text{for } \hat{\kappa}\to\infty \text{ and } \alpha L=0 \tag{76}$$

and becomes zero at the beam ends.

The derivative of Eq. (72b), $\hat{u}_s'(x)$, coincides with Eq. (58) reported in [18] for a FRP strip bonded to a concrete beam and rigidly anchored at both ends. Compared with Eq. (76), Eq. (72b) predicts a markedly smaller slip along the beam length.

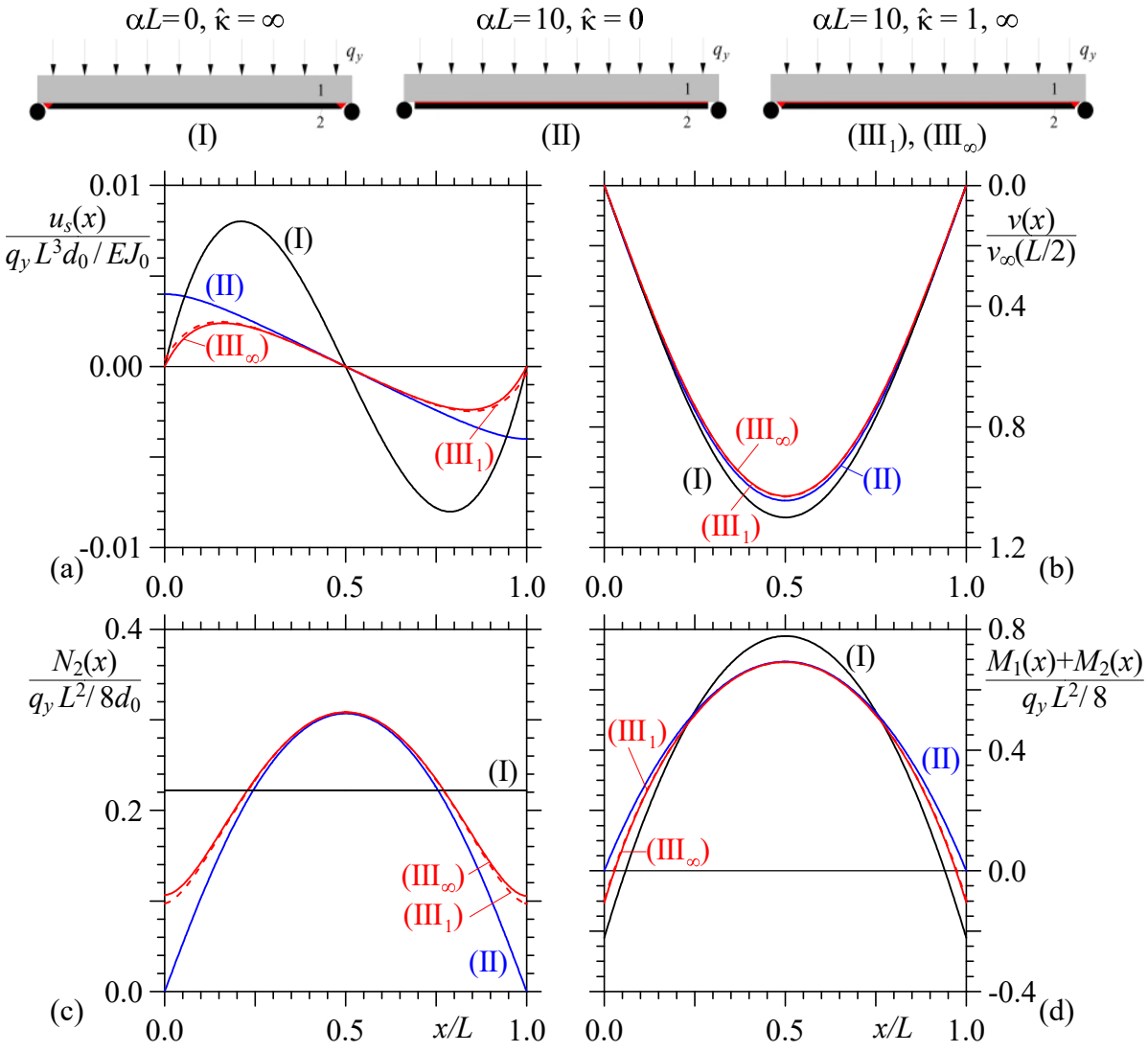


Fig. 23. Simply supported two-layer beam subjected to a distributed vertical load q_y for (I) only end-slip restraints (black solid line); (II) distributed interlayer connection only (blue solid line); (III_1) continuous connection with finite end springs ($\hat{\kappa} = 1$, red dashed line); (III_∞) continuous connection with rigid end springs ($\hat{\kappa} = \infty$, red solid line). Dimensionless (a) interlayer slip, (b) vertical displacement, (c) axial resultant of layer 2, (d) sum of bending moment along the beam. Results refer to $EJ_\infty/EJ_0 = 1.5$ and $\alpha L = 10$.

The comparison with [18] can be further clarified by referring to three representative connection layouts between the two layers, adapted from the configurations discussed therein (Fig. 48). Configuration (I) represents the limiting anchor-only case, where composite action is provided

exclusively by end-slip restraints modelled as infinitely rigid anchors. Configuration (II) corresponds to a fully bonded interface, with continuous adhesion along the entire span. Configuration (III) combines distributed bonding with end-slip restraints, considering both finite end-spring stiffness ($\hat{\kappa} = 1$) and the limiting case of infinitely rigid end restraints. Except for the connection layout, all geometric and mechanical parameters are kept constant. Fig. 48 refers to $EJ_\infty/EJ_0 = 1.5$ and $\alpha L = 10$, which are representative of practical strengthened or hybrid members (e.g., concrete–FRP, timber–steel, and timber–FRP). For these systems, the attainable flexural stiffness increase typically corresponds to $EJ_\infty/EJ_0 \approx 1$–2.

Due to symmetry, the interlayer slip is zero at midspan in all cases (Fig. 48a). Configuration (I) develops its maximum slip in the unbonded region between the anchors, whereas a distributed connection (II) markedly reduces slip along the span; the combined layout (III) further lowers slip, and finite end-restraint stiffness already provides a response close to the rigid-anchor limiting case, indicating that moderately stiff end restraints are sufficient to control slip effectively. The vertical displacement in Fig. 48b shows that configuration (I) provides the most compliant response and the introduction of distributed/combined connection reduces the deflection. The axial-force distribution (Fig. 48c) highlights the different transfer mechanisms: without distributed connection (I) it remains essentially uniform and governed by end compatibility, whereas with distributed connection (II) it evolves from the supports to midspan consistently with the bending demand; adding end restraints (III) mainly affects the boundary region, producing non-zero axial force already at the support while preserving a trend along the beam similar to (II). Accordingly, the bending moment (Fig. 48d) may exhibit a local sign reversal near the supports when end restraints are present (I and III), whereas it remains positive in the purely distributed case (II), reflecting the change in boundary compatibility conditions.

7.4. Simply supported two-layer beam subjected to a sinusoidal load $q_0 \sin(\pi x/L)$

The simply supported two-layer beam subjected to a sinusoidal transverse load $q_y(x) = q_0 \sin(\pi x/L)$ is usually used as a benchmark (S.16), as it corresponds to the reference loading scheme of the

Eurocode 5 γ-method [13], which is formulated for distributed shear connection only. The sinusoidal loading is analytically convenient, as the response of a single-span beam is naturally expressed through sine/cosine functions, leading to compact closed-form expressions for deflection and interlayer slip. For $\hat{\kappa} = 0$, the proposed formulation (S.16) reduces to the classical-distributed connection case and agree with the corresponding closed-form expressions [13, 14, 22]. The same solution is extended to explicitly include end-slip restraints, and the end-only limiting case with no distributed bonding is also reported for comparison.

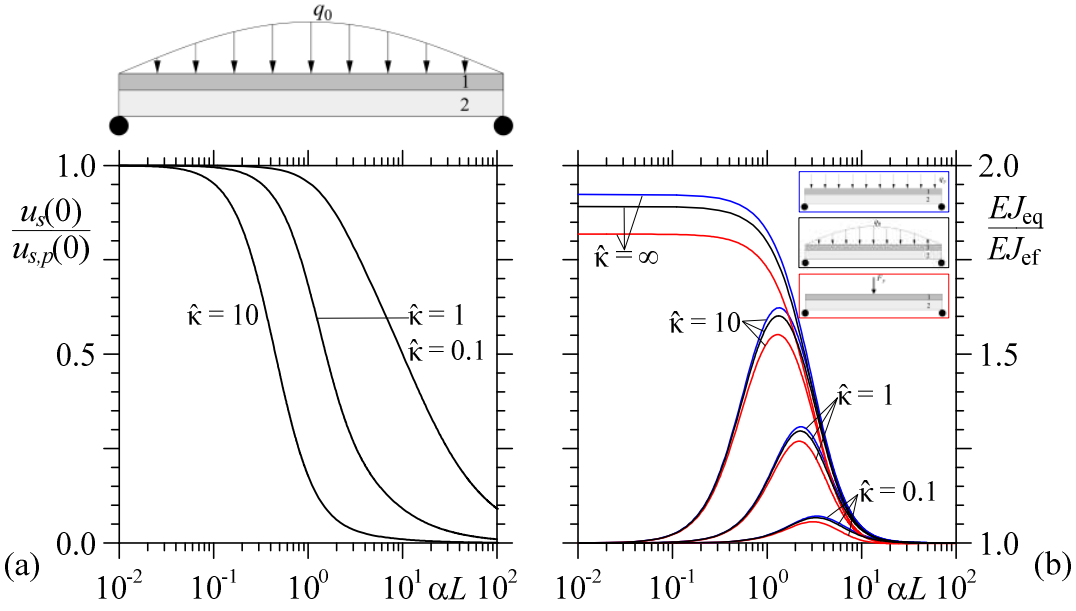


Fig. 24. Simply supported two-layer beam with $EJ_\infty/EJ_0 = 2.5$: (a) dimensionless slip for a sinusoidal load; (b) flexural rigidity ratio EJ_{eq}/EJ_{ef} for three loading schemes: sinusoidal (black line), uniformly distributed load (blue line), and point load applied at midspan (red line).

In Fig. 49a the maximum dimensionless slip of a simply supported two-layer beam under sinusoidal loading considering the extended formulation including end-slip restraints ($\hat{\kappa} > 0$) is compared with the classical configuration with distributed connection only ($\hat{\kappa} = 0$) as a function of the interaction parameter αL. In particular, dimensionless interlayer slip at the support is expressed by:

$$\frac{u_s(0)}{u_{s,p}(0)} = 1 - \alpha L\,\hat{\kappa}\,\frac{\tanh(\alpha L/2)}{1 + \alpha L\,\hat{\kappa}\tanh(\alpha L/2)} \tag{77}$$

where the particular solution for $\hat{\kappa} = 0$ is given by [14]

$$u_{s,p}(0) = \frac{q_0 L^3}{\pi E J_0} \frac{d_0}{(\alpha L)^2 + \pi^2} \tag{78}$$

For $\hat{\kappa} > 0$, the slip reduction becomes progressively more pronounced as αL increases.

The vertical deflection can be interpreted in terms of an equivalent flexural rigidity EJ_{eq}. Fig. 49b shows the stiffness ratio EJ_{eq}/EJ_{ef}, where EJ_{eq} and EJ_{ef} are the flexural rigidities associated with the configuration including the end-slip restraints and the γ-method [13, 14, 22], respectively. For a sinusoidal loading, this ratio is given in closed form as:

$$\frac{EJ_{eq}^{(S.16)}}{EJ_{ef}} = \left[1 - \frac{\pi^3 \hat{\kappa}}{\hat{c}_1^{(S.16)} \beta} \left(\frac{EJ_\infty}{EJ_0} - 1 \right) \left(1 - \frac{1}{\cosh(\alpha L/2)} \right) \right]^{-1} \tag{79}$$

where EJ_{ef} is obtained from the midspan deflection $v_p(L/2)$ of the particular solution with $\hat{\kappa} = 0$:

$$EJ_{ef} = \frac{q_0 L^4}{v_p(L/2)\pi^4} = EJ_\infty \frac{(\alpha L)^2 + \pi^2}{\beta} \tag{80}$$

$\hat{c}_1^{(S.16)}$ coincides with $\hat{c}_1^{(S.10)}$ reported in Eq. (65a) and

$$\beta = (\alpha L)^2 + \pi^2 \frac{EJ_\infty}{EJ_0} \tag{81}$$

In Fig. 49b, $EJ_{eq}/EJ_{ef} > 1$ indicates that the configuration with end-slip restraints exhibits a smaller midspan deflection than the γ-method. Rigid end restraints ($\hat{\kappa} \to \infty$) provide a marked stiffness gain in the low-interaction regime, because they enforce longitudinal compatibility at the boundaries and limit relative slip where it is most effective in reducing the global deformation. For finite $\hat{\kappa}$ the improvement is most evident in an intermediate interaction range ($\alpha L \approx$ 1-10). As αL becomes large, the ratio tends to unity, because both configurations approach the fully composite condition, with vanishing slip and identical midspan deflection.

Making use of Eq. (64a) for point load at midspan (Section 7.2, Solution S.10), the equivalent flexural rigidity takes the following form:

$$EJ_{eq}^{(S.10)} = \frac{F_y L^3}{48 v(L/2)} = \frac{EJ_\infty}{\eta_v} \tag{82}$$

The red curves in Fig. 49b refers to the midspan point-load case. With reference to the stiffness criteria for the floor vibration control prescribed in [13], the equivalent bending rigidity $EJ_{\text{eq}}^{(S.10)}$ can be replaced by EJ_{ef} both for $\hat{\kappa} = 0$ (with any value of αL) and for $\alpha L > 12.5$ (with any value of $\hat{\kappa}$) as the relative error of the ratio $EJ_{\text{eq}}/EJ_{\text{ef}}$ is less than 1%. Vice versa, the relative error increases up to 27% for $\hat{\kappa} = 1$ and $\alpha L = 2.2$ and up to 55% for $\hat{\kappa} = 10$ and $\alpha L = 1.3$.

Analogously, making use of Eq. (67a) for the uniformly distributed load (Section 7.2, Solution S.15), the equivalent flexural rigidity becomes:

$$EJ_{\text{eq}}^{(S.15)} = \frac{5}{384}\frac{q_y L^4}{v(L/2)} = EJ_\infty\left[1+\frac{384}{5}\frac{1}{(\alpha L)^2}\left(\frac{EJ_\infty}{EJ_0}-1\right)\left(\frac{1}{8}-\frac{\hat{c}_1^{(S.15)}}{(\alpha L)^2}\left(1-\frac{1}{\cosh(\alpha L/2)}\right)\right)\right]^{-1} \tag{83}$$

where $\hat{c}_1^{(S.15)}$ is given in Eq. (68a). The response under a uniformly distributed load is reported by the blue curves in Fig. 49b and is nearly coincident with the sinusoidal benchmark. In fact, the relative error is 0.22% for $\hat{\kappa} = 0$ that increases up to 1.7% in the limiting case $\hat{\kappa} \to \infty$. This supports the Eurocode 5 assumption that EJ_{ef} of the sinusoidal load benchmark provides an excellent approximation for the flexural rigidity due to an uniformly distributed vertical load.

8. BUILT-IN TWO-LAYER BEAMS SUBJECTED TO DISTRIBUTED LOADS

Built-in two-layer beams have no slip at both beam ends. Therefore, the influence of boundary constraints on composite interaction is maximised. For completeness, supplementary material S.17 and S.18 report solutions for built-in two-layer beams subjected to vertical and axial distributed loads, respectively.

Fig. 50 shows the dimensionless distributions of interlayer slip and vertical displacement along the beam length. For the vertical distributed load, the adopted dimensionless quantities are:

$$\frac{u_s(x)}{\tau_\infty(0)/k_h} = 2\left(1-\frac{EJ_0}{EJ_\infty}\right)\left(\frac{\cosh\left(\alpha/2(L-x)\right)\sinh\left(\alpha x/2\right)}{\sinh(\alpha L/2)}-\frac{x}{L}\right) \tag{84a}$$

$$\frac{v(x)}{v_\infty(L/2)} = \frac{16(L-x)^2x^2}{L^4}+\frac{192}{\alpha L^3}\left(1-\frac{EJ_\infty}{EJ_0}\right)\left[\alpha x(x/L-1)+(1-\cosh(\alpha x))\coth(\alpha L/2)+\sinh(\alpha x)\right] \tag{84b}$$

where

$$\tau_{\infty}(0)=\frac{q_y L}{2 d_0} \tag{85a}$$

$$v_{\infty}(L/2)=\frac{q_y L^4}{384 E J_{\infty}} \tag{85b}$$

For the axial distributed load, the dimensionless interlayer slip is defined as:

$$\frac{u_s(x)}{\tau_{\infty}(0)/k_h}=-\frac{2\sinh(\alpha/2(L-x))\sinh(\alpha x/2)}{\cosh(\alpha L/2)}\left[1-\frac{12}{\alpha L^3}\left(1-\frac{EJ_{\infty}}{EJ_0}\right)(\alpha L-2\tanh(\alpha L/2))\right]^{-1} \tag{86}$$

where

$$\tau_{\infty}(0)=\frac{C_{\infty}}{d_0} \tag{87a}$$

$$C_{\infty}=q_{x,1}d_{1,\infty}-q_{x,2}d_{2,\infty} \tag{87b}$$

The vertical displacement for the axial-loading case is instead normalised by the reference quantity $C_{\infty}L^3/EJ_0$, as detailed in the solution reported in the supplementary material S.18.

In both loading cases, slip is normalised by the maximum interface shear stress $\tau_{\infty}(0)$ of the fully composite section, Eqs. (85a) and (87a). This choice follows the Jourawski formulation and is consistent with the present kinematics, since d_0 represents the distance between the layer centroids and thus the lever arm associated with the bending couple generated by normal stresses.

For uniformly distributed vertical loading (S.17), the interlayer slip (Fig. 50a) is antisymmetric and vanishes at both built-in ends and at midspan. As αL increases, the slip decreases in magnitude and tends to become more concentrated toward the beam ends. The dimensionless vertical displacement (Fig. 50c) decreases with αL and converges to the fully composite condition, with a more pronounced reduction in the central region. For this built-in configuration, the closed-form expressions recover established results in the literature: the vertical displacement $v(x)$ reduces to case (4a) in Table 1b of [25], while the interlayer slip expression coincides with Eq. (52) in [34].

For uniformly distributed axial loading (S.18), the slip (Fig. 50b) is symmetric and much smaller than in the bending-dominated case: it vanishes at the clamped ends but remains almost uniform along the span. Increasing αL further reduces slip and makes it nearly uniform, indicating that

compatibility is progressively enforced along the entire member. The dimensionless vertical displacement (Fig. 50d), originating from differential axial strains between the layers, drops rapidly with αL and becomes negligible in the fully composite limiting case, being already strongly reduced for relatively small αL.

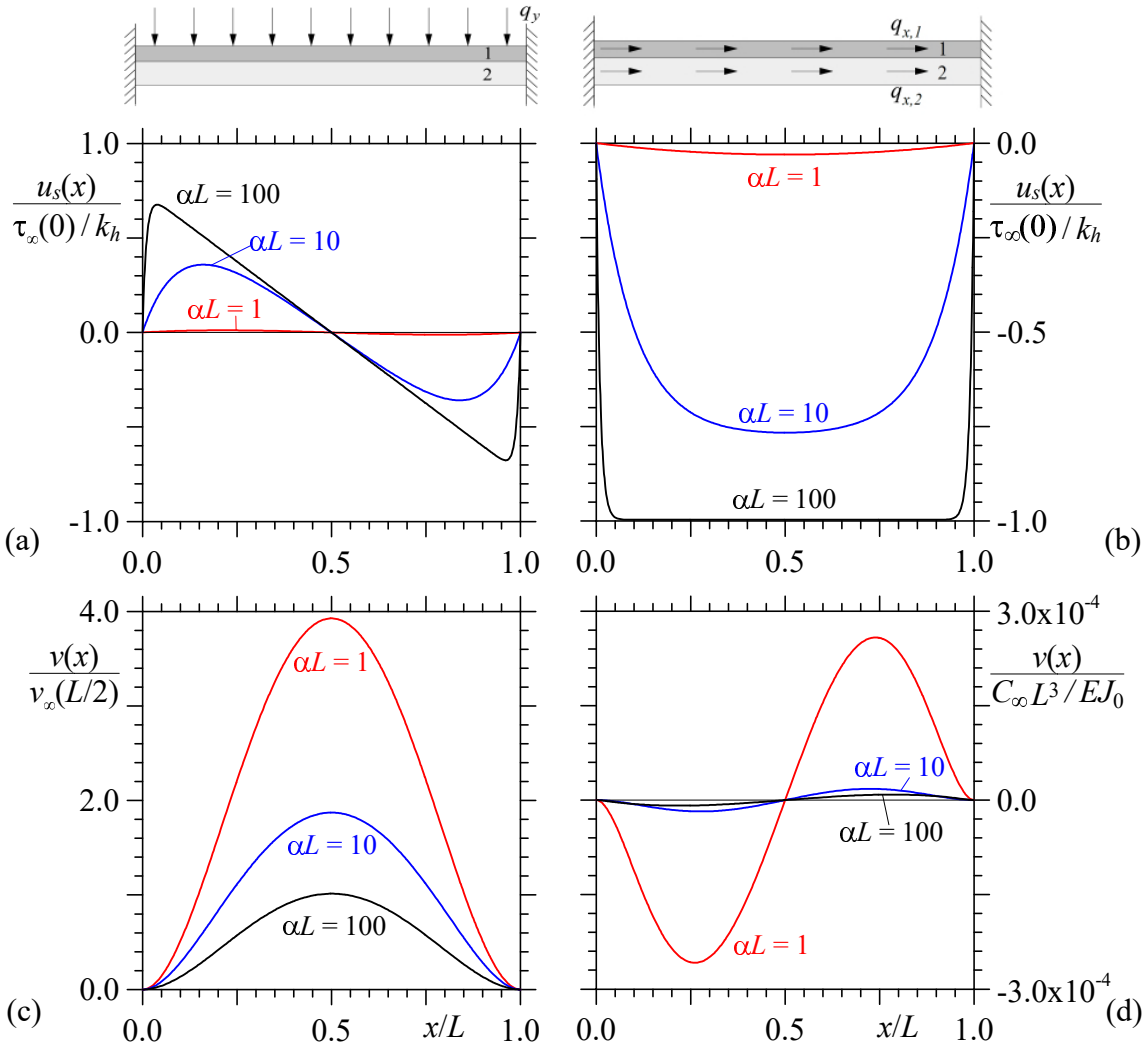


Fig. 25. Built-in two-layer beam subjected to (a, c) a uniformly distributed vertical load and (b, d) axial loads for $\alpha L = 1$ (red line), $\alpha L = 10$ (blue line), $\alpha L = 100$ (black line). Dimensionless (a, c) interlayer slip and (c, d) vertical displacement.

9. CONCLUSIONS

The static behaviour of two-layer beams is significantly affected by load distributions, boundary conditions and interaction parameter αL, but classical end constraints – such as free, simply supported, or clamped ends – may fail in accounting for semi-rigid restraints commonly encountered in practical applications. The presence of end-slip restraints introduces an additional

complexity that must be adequately modelled to ensure accurate predictions of the structural response.

In this work, the effect of end-slip restraints in two-layer composite beams with interlayer slip has been investigated. The proposed closed-form solutions extend classical formulations by explicitly incorporating concentrated restraints at the beam ends, thereby enabling the analysis of semi-rigid end conditions within a unified framework. Moreover, exact solutions for end-slip restraints only configurations were provided. Classical solutions available in the literature – corresponding to fully composite or non-composite beams – are recovered as limiting cases of the present model when the stiffness of either the distributed or concentrated connectors tends to infinity or zero, respectively.

The parametric analyses carried out highlight the pronounced influence of end-slip restraints on both deflections and interlayer slip. In particular, the presence of end-slip restraints effectively reduces interface slip and substantially modifies the displacement field, especially in cases where the stiffness of distributed connectors alone is insufficient to achieve full composite action. It was also observed that, for selected loading and boundary conditions, a near-fully composite behaviour can be obtained even with relatively low stiffness of distributed connectors, due to the additional compatibility enforced at the beam ends. This result has relevant implications for structural design, as it suggests the possibility of reducing the number of distributed connectors required, with potential benefits in terms of cost reduction and ease of construction.

Furthermore, comparing configurations with only end-slip restraints to those combining distributed bonding and end restraints reveals that equivalent stiffness levels can be identified for low αL values. However, this equivalence breaks down at high αL values, where maintaining curvature compatibility along the span becomes critical and boundary restraints alone are no longer sufficient.

The analytical solutions were validated through comparison with simplified models available in the literature, showing full consistency in both fully composite and non-composite limiting conditions, as well as across different loading and support configurations.

ACKNOWLEDGMENTS

Financial support from the University of Ferrara (FAR 2025) is gratefully acknowledged.

DECLARATION OF COMPETING INTEREST

The authors declare that they have no known competing financial interests or personal relationships that could have appeared to influence the work reported in this paper.

DATA AVAILABILITY

All data supporting the findings of this study are contained within the article and its Supplementary Material.

CREDIT AUTHORSHIP CONTRIBUTION STATEMENT

B.T. carried out the investigation, prepared the figures and visualizations, and wrote the original draft. F.M. contributed to the conceptualization of the study and reviewed and edited the manuscript. N.T. contributed to the conceptualization, methodology, and formal analysis, and reviewed and edited the manuscript. All authors reviewed and approved the final manuscript.

Appendix A. Solution of the system of equations (16)

Making use of the differential operator $\mathrm{D}^n(\cdot) = \mathrm{d}^n(\cdot)/\mathrm{d}x^n$, the system of coupled linear differential equations with constant coefficients (16) can be written in matrix form as follows:

$$\mathbf{A}[u_1(x), u_2(x), v(x)]^{\mathrm{T}} = \mathbf{q} \tag{A.1}$$

where

$$\mathbf{A} = \begin{bmatrix} E_1 A_1 \mathrm{D}^2 - k_h & k_h & d_0 k_h \mathrm{D} \\ k_h & E_2 A_2 \mathrm{D}^2 - k_h & -d_0 k_h \mathrm{D} \\ d_0 k_h \mathrm{D} & -d_0 k_h \mathrm{D} & EJ_0 \mathrm{D}^4 - d_0^2 k_h \mathrm{D}^2 \end{bmatrix} \tag{A.2}$$

$$\mathbf{q} = [-q_{x,1}(x), -q_{x,2}(x), q_y(x)]^{\mathrm{T}} \tag{A.3}$$

and the first-order moments S_1 and S_2 in Eq. (10a) are set equal to zero by assuming the reference points with ordinates y_1 and y_2 (Fig. 26) coincident with the centroid of the corresponding layers.

As suggested in [51], Cramer's rule can be applied to the system of equations (A.1). Therefore, the following three uncoupled field equations are obtained

$$\det(\mathbf{A})\,[u_1(x), u_2(x), v(x)]^{\mathrm{T}} = [\det(\mathbf{A}_1), \det(\mathbf{A}_2), \det(\mathbf{A}_3)]^{\mathrm{T}} \tag{A.4}$$

where $\mathbf{A}_i$ (i = 1, 2, 3) are the matrices formed by replacing the i-th column of $\mathbf{A}$ by the column vector $\mathbf{q}$:

$$\mathbf{A}_1 = \begin{bmatrix} -q_{x,1} & k_h & d_0 k_h \mathrm{D} \\ -q_{x,2} & E_2 A_2 \mathrm{D}^2 - k_h & -d_0 k_h \mathrm{D} \\ q_y & -d_0 k_h \mathrm{D} & EJ_0 \mathrm{D}^4 - d_0^2 k_h \mathrm{D}^2 \end{bmatrix} \tag{A.5}$$

$$\mathbf{A}_2 = \begin{bmatrix} E_1 A_1 \mathrm{D}^2 - k_h & -q_{x,1} & d_0 k_h \mathrm{D} \\ k_h & -q_{x,2} & -d_0 k_h \mathrm{D} \\ d_0 k_h \mathrm{D} & q_y & EJ_0 D^4 - d_0^2 k_h \mathrm{D}^2 \end{bmatrix} \tag{A.6}$$

$$\mathbf{A}_3 = \begin{bmatrix} E_1 A_1 \mathrm{D}^2 - k_h & k_h & -q_{x,1} \\ k_h & E_2 A_2 \mathrm{D}^2 - k_h & -q_{x,2} \\ d_0 k_h \mathrm{D} & -d_0 k_h \mathrm{D} & q_y \end{bmatrix} \tag{A.7}$$

Extended solution to Eq. (A.4) is reported in Eqs. (21a, b, c).

REFERENCES

[1] Nie J, Xiao Y, Chen L. Experimental studies on shear strength of steel-concrete composite beams. J Struct Eng 2004;130(8):1206–1213.

[2] Lima JM, Bezerra LM, Bonilla J, Mirambell E. Experimental study on full scale steel-concrete composite beams using truss-type shear connectors. Eng Struct 2024; 303:117490.

[3] Wright HD. The deformation of composite beams with discrete flexible connection. J Construct Steel Res 1990;15:49–64.

[4] Tullini N, Minghini F. Nonlinear analysis of composite beams with concrete-encased steel truss. J Construct Steel Res 2013;91:1–13.

[5] Hosseini R, Valipour H. Timber-Encased-Steel Beams: laboratory experimentation and analytical modeling. J Struct Eng– ASCE 2024;150(7):04024074.

[6] Shehada M, Djamaï ZI, Duprat F. Experimental investigation on adhesively bonded timber-self-compacting concrete composite beams with a thin slab. Eng Struct 2024;309:118108.

[7] Nie Y, Karimi-Nobandegani A, Valipour HR. Experimental behaviour and numerical modelling of Timber-Timber Composite (TTC) joints. Constr Build Mater 2021;290:123273.

[8] Chiniforush A, Valipour H, Ataei A. Timber-timber composite (TTC) connections and beams: An experimental and numerical study. Constr Build Mater 2021;303:124493.

[9] Kožar I, Šuran G. Calculation model for layered glass. Coupled Syst Mech 2023;12(6):519.

[10] Rizzi E, Bedon C, Amadio C. Simplified models to capture the effects of restraints in glass balustrades under quasi-static lateral load or soft-body impact. Buildings 2022;12(10):1664.

[11] Wu T, Wang G, Wang J, Wang Y, Xu R. Variational principles of laminated plates considering interlayer slip. Compos Struct 2022;281:114937.

[12] CNR-DT 203/2006. Guide for the design and construction of concrete structures reinforced with fiber-reinforced polymer bars. National Research Council, Rome, Italy; 2006.

[13] EN 1995:2025. Eurocode 5: design of timber structures – part 1-1: general common rules and rules for buildings. Brussels: European Standard, European Committee for Standardization (CEN); 2025.

[14] Kreuzinger H. Mechanically jointed beams and columns. Timber Eng 1995;1:B11.

[15] Newmark NM, Siess CP, Viest IM. Test and analysis of composite beams with incomplete interaction. Proc Soc Exp Stress Anal 1951;9:75–92.

[16] Newmark NM, Siess CP, Viest IM. Studies of slab and beam highway bridges, Part III–Small scale tests of shear connectors and composite T-beams. Bulletin 396. Urban, Illinois: University of Illinois; 1952.

[17] McCutcheon WJ. Stiffness of framing members with partial composite action. ASCE J. Struct. Eng. 1986;119(7):1623–1637.

[18] Sun Y, Liu W, Li X, Liu X, Bai F. Theoretical analysis of strain incompatibility and slip in a mechanically anchored FRP composite system. J Compos Constr 2022;26(6): 04022075.

[19] Chen S. Load carrying capacity of composite slabs with various end constraints. J. Constr. Steel Res 2003;59:385–403.

[20] Rana MM, Uy B, Mirza O. Experimental and numerical study of end anchorage in composite slabs. J Constr Steel Res 2015;115:372–86.

[21] Smith ST, Teng JG. Interfacial stresses in plated beams. Eng Struct 2001;23(7):857–71.

[22] van der Linden M. Timber–concrete composite floor systems. Doctoral Thesis. *Technical University of Delft*. Netherland; 1999.

[23] Girhammar UA, Gopu VKA. Composite beam-columns with interlayer slip – exact analysis. J Struct Eng– ASCE 1993;119:1265–1282.

[24] Girhammar UA, Pan DH. Exact static analysis of partially composite beams and beam-columns. Int J Mech Sci 2007;49(2):239–255.

[25] Girhammar UA. A simplified analysis method for composite beams with interlayer slip. Int J Mech Sci 2009;51(7):515–530

[26] Challamel N, Girhammar UA. Boundary layer effect in composite beams with interlayer slip. J. Aerospace Eng. ASCE 2011;24(2):199–209.

[27] Challamel N, Girhammar UA. Variationally-based theories for buckling of partial composite beam–columns including shear and axial effects. Eng Struct 2011; 33(8):2297–2319. https://doi.org/10.1016/j.engstruct.2011.04.004

[28] Möhler K. On the load carrying behavior of beams and columns of compound sections with flexible connections. *Technical Univ of Karlsruhe Germany* 1956.

[29] Bärtschi R. Load-bearing behaviour of composite beams in low degrees of partial shear connection. Zurich, Switzerland: Swiss Federal Institute of Technology; 2005.

[30] Johnson RP. Composite structures of steel and concrete: beams, slabs, columns, and frames for buildings. 3rd ed. Hoboken, NJ: Wiley; 2008.

[31] Kyvelou P, Gardner L, Nethercot DA. Design of composite cold-formed steel flooring systems. Structures 2017;12:242–52.

[32] Nie J, Cai CS. Steel–concrete composite beams considering shear slip effects. J Struct Eng 2003;129(4):495–506.

[33] Zhou D, Pahn M, Kurz W, Beitrag zur Berechnung von Verbundträgern mit elastischem Verbund, Stahlbau 2014;83(4):278–288. (In German)

[34] Ranzi G, Bradford MA, Uy B. A general method of analysis of composite beam with partial interaction. Steel Compos Struct 2003;3(3):169–184.

[35] Xu R, Chen D. Variational Principles of Partial-Interaction Composite Beams. J Eng Mech 2012;138(5):542–551.

[36] Peng S, Zhu Z, Wei Y. An analytic solution for bending of multilayered structures with interlayer-slip. Int J Mech Sci 2024;282:109642.

[37] Gustafsson A, The CLT, Handbook. CLT structures – facts and planning. Floor structures. First edition. Stockholm: Swedish Wood 2019:90–109.

[38] Bajzecerová V. Bending stiffness of CLT-concrete composite members-comparison of simplified calculation methods. Procedia Eng 2017;190:15–20.

[39] Christovasilis IP, Brunetti M, Follesa M, Nocetti M, Vassallo D. Evaluation of the mechanical properties of cross-laminated timber with elementary beam theories. Constr Build Mater 2016;122:203–13.

[40] Aşik MZ, Tezcan S. A mathematical model for the behavior of laminated glass beams. Comput Struct 2005;83:1742–53.

[41] Ivanov IV. Analysis, modelling, and optimization of laminated glasses as plane beam. Int J Sol Struct 2006;43:6887–907.

[42] Gjelsvik A. Analog-beam method for determining shear-lag effects. J Eng Mech 1991;117(7):1575–1594.

[43] Betti R, Gjelsvik A. Elastic composite beams. Comput Struct. 1996;59(3): 437–451.

[44] Ellakany AM, Tablia HA. A numerical model for static and free vibration analysis of elastic composite beams with end shear restraint. Meccanica 2010;45:463-474.

[45] He ZQ, Liu Z. Stresses in external and internal unbonded tendons: unified methodology and design equations. J Struct Eng 2010;136(9):1055–65.

[46] Zhang Y, Zhang L, Zhang S. Exact series solutions of composite beams with rotationally restrained boundary conditions: static analysis. Arch Appl Mech 2022;92(12):3999–4015.

[47] Benveniste Y. On the effect of debonding on the overall behavior of composite materials. Mechanics of Materials 1984;3(4):349-358. https://doi.org/10.1016/0167-6636(84)90034-6.

[48] Tullini N, Savoia M, Horgan CO. End effects in multilayered orthotropic strips with imperfect bonding. Mechanics of Materials 1997;26(1):23–34. https://doi.org/10.1016/S0167-6636(97)00016-1.

[49] Timoshenko SP, Goodier JN. *Theory of Elasticity* (3rd Ed.). McGraw Hill; 1970.

[50] Horgan CO, Carlsson LA. Saint-Venant end effects for anisotropic materials. In: Beaumont PW, Zweben CH (Editors). Comprehensive composite materials II. Elsevier; 2018;7:38–55.

[51] Ayres FJ. Differential Equations. McGraw-Hill; 1952.

FIGURE CAPTIONS

Fig. 26. Kinematic representation of a two-layer composite beam segment with zero-thickness interface.

Fig. 27. Geometric parameters of composite beam section: cg,1, cg,2 and cg,∞ are the centroids of layers 1, 2 and of fully composite section, respectively; $d_{1,\infty}$ and $d_{2,\infty}$ are the distances of cg,∞ from cg,1 and cg,2, respectively.

Fig. 28. Shear connection model: distributed springs with stiffness k_h along the interface and end springs with stiffness $\hat{k}_h$. (a) Cantilever beam; (b) Simply supported beam.

Fig. 29. Free body diagram of an infinitesimal two-layer composite beam segment with compliant interface, illustrating the adopted sign convention.

Fig. 30. Kinematic representation of a two-layer composite beam segment with an interlayer of thickness h_a.

Fig. 31. Cantilever two-layer beam subjected to end axial forces $F_{x,1}$ and $F_{x,2}$: dimensionless (a) axial displacement of layer 1 at $x = L$, and (b) interlayer slip at $x = L$. Dashed and solid curves refer to $EJ_\infty/EJ_0 = 2.5$ and 4, respectively. Red marks denote end-slip restraints only configurations, reported at the equivalent αL according to Eq. (20c).

Fig. 32. Cantilever two-layer beam subjected to a clockwise end couple $F_x\, d_0$: dimensionless (a) axial displacement of layer 1 at $x = L$; (b) axial stress resultant of layer 1 at $x = 0$; (c) vertical displacement at $x = L$, and (d) sum of bending moment of the two layers at $x = 0$. Results refer to $EJ_\infty/EJ_0 = 2.5$. Red marks denote end-slip restraints only configurations.

Fig. 33. Cantilever two-layer beam subjected to a clockwise end couple C_L: dimensionless (a) axial displacement of layer 1 at $x = L$; (b) axial stress resultant of layer 1 at $x = 0$; (c) vertical displacement at $x = L$, and (d) sum of bending moment of the two layers $x = 0$. Results refer to $EJ_\infty/EJ_0 = 2.5$. Red marks denote end-slip restraints only configurations.

Fig. 34. Cantilever two-layer beam subjected to clockwise end couples (a, c) $F_x\, d_0$ and (b, d) C_L. Effect of parameter αL on the dimensionless (a, b) axial force and (c, d) bending moment along the beam. Dashed and solid curves refer to $EJ_\infty/EJ_0 = 2.5$ and 4, respectively.

Fig. 35. Cantilever two-layer beam subjected to a self-equilibrated end couple $C_L - F_x\, d_0$, with $C_L = F_x\, d_0$: dimensionless (a) vertical displacement at $x = L$, and (b) stress resultants $R(0)$ in layer 1 at $x = 0$. Red dashed line in (b) corresponds to the asymptotic exponential decay solution proposed in [47, 48].

Fig. 36. Cantilever two-layer beam with $\alpha L = 0$ subjected to: (a) clockwise end couple $F_x\, d_0$; (b) clockwise end couple C_L; (c) self-equilibrated end couple $C_L - F_x\, d_0$, with $C_L = F_x\, d_0$.

Fig. 37. Simply supported two-layer beam subjected to symmetric end axial forces and couples. Dimensionless rotational stiffness K_φ for symmetric end couples: (a) $F_x\, d_0$; (b) C. Dashed and solid curves refer to $EJ_\infty/EJ_0 = 2.5$ and 4, respectively. Red marks denote end-slip restraints only configurations.

Fig. 38. Cantilever two-layer beam subjected to a vertical end point load F_y: dimensionless (a) interlayer slip at $x = L$; (b) axial stress resultant in layer 1 at $x = 0$; (c) vertical displacement at $x = L$, and (d) sum of bending moment of the two layers at $x = 0$. Results refer to $EJ_\infty/EJ_0 = 2.5$. Red marks denote end-slip restraints only configurations.

Fig. 39. Cantilever two-layer beam subjected to a vertical end point load F_y: dimensionless (a) axial displacement of layer i at $x = L$, and (b) rotation at $x = L$; dimensionless (c) axial displacement and (d) rotation along the span for $\alpha L = 0.5$ (solid) and $\alpha L = 1.0$ (dashed) and $\hat{\kappa} = 0$, 10, 100. Vertical red lines at $\alpha L = 0.5$ (solid) and $\alpha L = 1.0$ (dashed) are used as reference for plot in (c, d). Results refer to $EJ_\infty/EJ_0 = 2.5$. Red marks denote end-slip restraints only configurations.

Fig. 40. Simply supported two-layer beam subjected to a point load F_y applied at $x = L/4$ with $EJ_\infty/EJ_0 = 2.5$. Dimensionless axial force distribution in the lower layer along the beam length for (a) $\hat{\kappa} = 0$, (b) $\hat{\kappa} = 10$, (c) $\alpha L = 1$ and (d) $\alpha L = 10$. Red solid line: fully composite limit. Red marks and dashed line: configurations with end-slip restraints only with $\hat{\alpha} L = 100$.

Fig. 41. Simply supported two-layer beam subjected to two point loads F_y applied at $x = L/4$ with $EJ_\infty/EJ_0 = 2.5$: dimensionless (a, b) interlayer slip and (c, d) vertical displacement for (a, c) $\alpha L = 0.1$ and (b, d) $\alpha L = 1$. Red dashed line refer to $\alpha L = 0$ for (a, b) and $\alpha L = \infty$ for (c, d). Red marks denote end-slip restraints only configurations.

Fig. 42. Cantilever two-layer beam subjected to axial distributed loads $q_{x,1}$ and $q_{x,2}$: (a) dimensionless axial displacement of layer 1 at $x = L$; (b) dimensionless vertical displacement at $x = L$. Dashed and solid curves refer to $EJ_\infty/EJ_0 = 2.5$ and 4, respectively. Red marks denote end-slip restraints only configurations.

Fig. 43. Cantilever two-layer beam subjected to axial distributed loads $q_{x,1}$ and $q_{x,2}$ for $EJ_\infty/EJ_0 = 2.5$: (a, b) dimensionless slip; (c, d) dimensionless vertical displacement for (a, c) $\alpha L = 0.1$ and (b, d) $\alpha L = 1$. Red dashed line refers to $\alpha L = 0$ for (a, b) and $\alpha L = \infty$ for (c, d). Red marks denote end-slip restraints only configurations.

Fig. 44. Cantilever two-layer beam subjected to a vertical distributed load q_y for $EJ_\infty/EJ_0 = 4$: dimensionless (a) axial displacement of layer 1 at $x = L$; (b) axial stress resultant of layer 1 at $x = 0$; (c) vertical displacement at $x = L$, and (d) sum of bending moment of the two layers at $x = 0$. Red marks denote end-slip restraints only configurations. The blue lines correspond to the case $\alpha L = 1$.

Fig. 45. Cantilever two-layer beam subjected to a vertical distributed load q_y for $EJ_\infty/EJ_0 = 2.5$: (a) dimensionless slip and (b) vertical displacement along the beam; Red dashed line indicates the slip for $\alpha L = 0$, whereas the solid red line refers to the vertical displacement for $\alpha L = \infty$. Blue lines denote end-slip restraints only configurations for $\hat{\alpha} L = 10, 100$.

Fig. 46. Maximum vertical displacement for a simply supported two-layer beam subjected to (a, c) a point load F_y at midspan and (b, d) a distributed load q_y versus (a, b) αL for $\hat{\kappa} = 0, 10, 100, \infty$ and (c, d) $\hat{\kappa}$ for $\alpha L = 0.5$ and 1.0. Dashed and solid curves refer to $EJ_\infty/EJ_0 = 2.5$ and 4, respectively. Red marks denote end-slip restraints only configurations.

Fig. 47. Simply supported two-layer beam subjected to (a, c) a point load F_y at midspan and (b, d) a distributed load q_y for $EJ_\infty/EJ_0 = 2.5$ and $\alpha L = 0.5$: (a, b) dimensionless interlayer slip and (c, d)

dimensionless vertical displacement. Red dashed line indicates the slip for αL=0, whereas the solid red line refers to the vertical displacement for αL=∞. Red marks denote end-slip restraints only configurations.

Fig. 48. Simply supported two-layer beam subjected to a distributed vertical load q_y for (I) only end-slip restraints (black solid line); (II) distributed interlayer connection only (blue solid line); (III_1) continuous connection with finite end springs ($\hat{\kappa} = 1$, red dashed line); (III_∞) continuous connection with rigid end springs ($\hat{\kappa} = \infty$, red solid line). Dimensionless (a) interlayer slip, (b) vertical displacement, (c) axial resultant of layer 2, (d) sum of bending moment along the beam. Results refer to $EJ_\infty/EJ_0 = 1.5$ and $\alpha L = 10$.

Fig. 49. Simply supported two-layer beam with $EJ_\infty/EJ_0 = 2.5$: (a) dimensionless slip for a sinusoidal load; (b) flexural rigidity ratio EJ_{eq}/EJ_{ef} for three loading schemes: sinusoidal (black line), uniformly distributed load (blue line), and point load applied at midspan (red line).

Fig. 50. Built-in two-layer beam subjected to (a, c) a uniformly distributed vertical load and (b, d) axial loads for $\alpha L = 1$ (red line), $\alpha L = 10$ (blue line), $\alpha L = 100$ (black line). Dimensionless (a, c) interlayer slip and (c, d) vertical displacement.

TABLE CAPTIONS

Table. 2. Case studies S.1–S.18: αL values satisfying condition $|1 - v_{max} / v_{max,\infty}| < 1\%$ for two EJ_∞/EJ_0 ratios and two values of end spring parameter $\hat{\kappa}$.

Supplementary Files

This is a list of supplementary files associated with this preprint. Click to download.

- TMTSupplementarymaterial.pdf